

DYNAMICS OF MACROECONOMICS MODELS WITH HYSTERESIS OPERATORS

by

Eyram Kwame



APPROVED BY SUPERVISORY COMMITTEE:

---

Dmitrii Rachinskii, Chair

---

Wieslaw Krawcewicz

---

Zalman Balanov

---

Maxim Arnold

Copyright © 2017

Eyram Kwame

All rights reserved

*To my parents*

DYNAMICS OF MACROECONOMICS MODELS WITH HYSTERESIS OPERATORS

by

EYRAM KWAME, BS, MS

DISSERTATION

Presented to the Faculty of  
The University of Texas at Dallas  
in Partial Fulfillment  
of the Requirements  
for the Degree of

DOCTOR OF PHILOSOPHY IN  
MATHEMATICS

THE UNIVERSITY OF TEXAS AT DALLAS

August 2017

## ACKNOWLEDGMENTS

I would like to express my profound gratitude to my advisor and mentor Dr. Dmitrii Rachinskii, for guiding and helping me through every step of my dissertation work. He is a loving father who knows when to give corrections and encouragement. Dima as he preferred to be called, is very intelligent, knowledgeable, selfless, dedicated to his work and extremely hardworking. I have learned so much from him these few years of studying under him and working with him. His life is a perfect model of a successful academic. I am grateful to him for teaching me valuable lessons about hard-work, dedication and commitment to a course. I count myself very blessed to be one of his PhD students.

I am grateful to Dr. Maxim Arnold, Dr. Nikita Begun, Dr. Pavel Gurevich, Dr. Pavel Krejčí and Dr. Harbir Lamba for giving me opportunities to work and learn from their rich and diverse academic backgrounds. I am especially grateful to Dr. Pavel Krejčí and Dr. Harbir Lamba for their immense support, which enabled me to work on my dissertation.

I am grateful to my advisory committee members, Dr. Wieslaw Krawcewicz, Dr. Zalman Balanov and Dr. Maxim Arnold, who have all helped and supported me in various ways. I am grateful to the Mathematical Sciences Department of The University of Texas at Dallas for giving me the opportunity for an enriching experience of being a Teaching Assistant. I am grateful to every faculty and staff member of the department for making the years I spent in the department meaningful.

May 2017

# DYNAMICS OF MACROECONOMICS MODELS WITH HYSTERESIS OPERATORS

Eyram Kwame, PhD  
The University of Texas at Dallas, 2017

Supervising Professor: Dmitrii Rachinskii, Chair

We propose a class of DSGE macroeconomics models with the *play* hysteresis operator. The play operator introduces stickiness and path dependence into the response of economic agents to inflation rate variation. The models can be viewed as piecewise linear systems. We show that the systems have an entire line segment of equilibrium states. For a simpler variant of the model, we prove that when there is no exogenous noise, the line segment of equilibrium states is globally stable, and each trajectory converges to one of the states. For more complex versions of the model, other dynamics are possible. In order to understand those, we present a simple prototype 2-dimensional system and obtain a global bifurcation diagram, which includes transitions from the global stability to periodic dynamics, border collision bifurcations, and complex dynamics. We further perform numerical analysis of the DSGE models to study the effects of exogenous noise and shocks, hyperinflation scenarios and other forms of sensitivity of the model to parameters. We interpret our findings in economic context. Finally, we analyze further variations of the model, including the system with multiple agents modeled by the play operators with different thresholds; a model with the sticky Central Bank's policy and a hybrid model in which the inflation rate and output gap are continuous time variables while the interest rate is updated at discrete times.

## TABLE OF CONTENTS

ACKNOWLEDGMENTS . . . . .	v
ABSTRACT . . . . .	vi
LIST OF FIGURES . . . . .	x
CHAPTER 1 INTRODUCTION . . . . .	1
1.1 Systems with Hysteresis operators . . . . .	1
1.2 Economics context . . . . .	5
1.3 Outline of the dissertation . . . . .	11
CHAPTER 2 PRELIMINARIES . . . . .	13
2.1 DSGE models . . . . .	13
2.2 Hysteresis operators . . . . .	14
2.2.1 Stop operator . . . . .	16
2.2.2 Play operator . . . . .	18
2.2.3 The Prandtl–Ishlinskii operator . . . . .	19
2.3 Inversion of PI operators . . . . .	21
2.4 Modeling idea . . . . .	23
CHAPTER 3 DISCRETE TIME SYSTEM WITH STOP OPERATOR . . . . .	27
3.1 System set-up . . . . .	27
3.2 Main results . . . . .	29
3.3 Proofs . . . . .	32
3.3.1 Case (a) . . . . .	36
3.3.2 Case (b), $\lambda \geq 0$ . . . . .	37
3.3.3 Case (c) . . . . .	39
3.3.4 Case (d) . . . . .	42
3.3.5 Case (b), $\lambda < 0$ . . . . .	43
3.3.6 Case (e) . . . . .	46
3.3.7 Case (f) . . . . .	55
3.3.8 Case (g) . . . . .	56

CHAPTER 4	OUTPUT GAP AND INFLATION MODEL	58
4.1	Explicit model with sticky inflation	59
4.2	Line segment of equilibrium points	60
4.3	Local stability analysis	62
4.4	Dynamics far from the line segment of equilibrium states	63
4.5	Global stability (main result)	63
4.6	Proof of Theorem 4.2	63
4.6.1	Preliminary estimates	63
4.6.2	Reformulated equation	66
4.6.3	Estimate 1	67
4.6.4	Estimate 2	68
4.6.5	Lyapunov function	68
4.6.6	Asymptotic behavior	69
4.7	Numerical results	69
4.7.1	Parameter values	69
4.7.2	Lower local volatility due to stickiness	70
4.7.3	Transitions between equilibrium states	71
4.7.4	Response to shocks	71
4.7.5	The possibility of runaway inflation	72
4.7.6	Trade-off between inflation and output gap volatility	73
CHAPTER 5	OUTPUT GAP, INFLATION AND INTEREST RATE MODELS	76
5.1	Discrete time model	76
5.1.1	Equivalent explicit model	76
5.1.2	Line segment of equilibrium points	78
5.1.3	Numerical results	79
5.2	Hybrid model	82
5.3	Multi-agent model	87
5.4	Sticky Central Bank model	91



CHAPTER 6	CONCLUSIONS	95
APPENDIX		97
A.1	Derivation of equations (4.5) – (4.9)	97
A.2	Jury’s stability criterion	98
A.3	Proof of Lemma 4.1 (local stability analysis of system (4.1) – (4.3))	98
A.4	The effect of parameters on stability properties	100
A.5	Derivations of the explicit form for model (5.1), (5.2)	103
A.6	Derivations of the explicit form for system (5.28), (5.29)	104
REFERENCES		105
CURRICULUM VITAE		

## LIST OF FIGURES

2.1	Interpretation of the <i>stop</i> operator with the one-dimensional Moreau sweeping process. . . . .	17
2.2	Illustration of the <i>Stop Operator</i> . Slope of the dashed lines is 1 and movements along these lines are bidirectional. Movement along the upper horizontal line $s = \alpha$ is to the right; movement along the lower horizontal line $s = -\alpha$ is to the left. . . . .	17
2.3	Interpretation of the <i>play</i> operator with a mechanical system. . . . .	18
2.4	Illustration of the <i>Play Operator</i> . . . . .	19
2.5	Interpretation of PI of play type with a mechanical system. . . . .	19
2.6	Discrete time input-output diagram of PI operators with thresholds $\alpha_1 < \alpha_2 < \alpha_3$ . . . . .	20
2.7	Primary response (loading) function $\varphi$ of PI operator (2.21) and primary response function $\varphi^{-1}$ of the inverse PI operator (2.24). . . . .	22
2.8	Multiplicity of equilibrium states from aggregate demand ( <i>AD</i> ) and aggregate supply ( <i>AS</i> ) curves. . . . .	24
3.1	Discrete time representations of the stop and play operators. . . . .	28
3.2	Bifurcation diagram. The segment $EF$ of the fixed points is shown by the blue line. Stable fixed points are denoted by the solid line, unstable fixed points are shown by the dashed line. Stable end-points of $EF$ are shown as filled blue discs; semi-stable points are denoted by empty blue discs; in the unstable case, no special notation is used. The dotted line in case ( <i>b</i> ) corresponds to the set of parameters leading to the infinite slope of the line $EF$ . Periodic points are shown in red. Filled red discs in cases ( <i>c</i> ) and ( <i>d</i> ) correspond to the stable 2-periodic orbit $\pm Q$ ; the red parallelogram in case ( <i>g</i> ) consists of stable 2-periodic orbits. Case ( <i>e</i> ) corresponds to complex dynamics when the system has periodic orbits with arbitrary large periods (see Theorem 3.2). One such orbit is sketched on the diagram. In the critical case ( <i>f</i> ), the segment $EF$ attracts all the trajectories. . . . .	30
3.3	Domains $\Omega_k$ of existence of a (unique) stable periodic orbit of period $2k + 2$ in the coordinates $\beta = \lambda + a > 1$ and $-1/\lambda > 1$ for case ( <i>e</i> ) of Theorem 3.1. . . . .	32
3.4	$\lambda \geq 0, \beta \geq 1$ . A trajectory starting at a point $B$ to the right of the segment $EF$ converges to the fixed point $F$ . Dotted lines have slope 1. . . . .	36
3.5	Theorem 3.1( <i>b</i> ). Case $\lambda \geq 0$ . Dotted lines have slope 1. The shaded area is the parallelogram $\Pi = EE'FF'$ . . . . .	37
3.6	Case $\lambda \geq 0, \beta < -1$ . Each of the red segments $AB$ and $-AB$ is mapped into itself by $f^2$ . . . . .	40

3.7	Case $\lambda < 0, \beta < -1$ . Red half-lines are mapped to themselves by $f^2$ . . . . .	43
3.8	Theorem 3.1(b). Case $\lambda < 0$ . . . . .	45
3.9	The segment $\Xi_k$ and its images $f^k(\Xi_k)$ and $f^{k+1}(\Xi_k)$ . . . . .	48
3.10	Graph of the map $T(x)$ for $x \in (\frac{\alpha}{1-\lambda}, \infty)$ . . . . .	50
3.11	Segment $\Theta_m$ is covered by its image $T^2(\Theta_m)$ under the second iteration of map $T$ . . . . .	51
3.12	Case $\beta = 1, \lambda < 0$ . The parallelogram $\Pi$ degenerates to the segment $EF$ with slope 1. . . . .	56
3.13	Parallelograms $\Sigma$ and $\Pi$ for $\beta = -1$ . . . . .	57
4.1	The projection of the line segment of equilibrium points $EF$ (blue line) onto the $(v, s)$ plane. The segment has a negative slope in (a) and a positive slope in (b). Sample trajectories of system (4.10) are shown in black. . . . .	61
4.2	Volatility of inflation rate $v$ for various $\alpha$ values. . . . .	70
4.3	Transitions between the equilibrium states. Time traces of inflation rate (a-c) and the corresponding plots in the $(v, s)$ space (c,f) exhibiting different transition scenarios. The noise is turned off before and after an interval of time of interest in order to show the equilibrium state at the ends of this interval. (a,d) The sentiment remains within the bounds $ s_t  < \alpha$ , and the system stays in the basin of attraction of one equilibrium point. The inflation rate $v_*(s_*)$ is the same before and after the noisy interval. (b,e) The sentiment reaches the extreme value $-\alpha$ (the highest expectation of inflation), and the trajectory transits from the basin of attraction of an equilibrium state with higher inflation rate and lower output gap (the right slanted segment in (e)) to the basin of attraction of an equilibrium state with a lower inflation rate and higher output gap (the left slanted segment in (e)). (c,f). A transition from the equilibrium with the highest inflation rate (the rightmost point in (f)) to an equilibrium with a more moderate inflation rate through the basins of attraction of several other equilibrium states. . . . .	72
4.4	Response to shocks. (a) The system without stickiness settles to the same unique equilibrium after each shock. (b) The system with stickiness settles on a new equilibrium after a shock is applied. . . . .	73
4.5	Response to shocks of different magnitudes. . . . .	73
4.6	Run-away inflation scenario. Parameters are $\alpha = 1, a = 0.3, b_1 = 0.5, b_2 = 0.05, c_1 = 0.9, c_2 = 0.01$ . The ranges of inflation rate and output gap values at equilibrium states for this set parameter are $v_* \in [-11, 11]$ and $u_* \in [-10, 10]$ , respectively. . . . .	74
4.7	Numerical simulations of $u_t$ and $v_t$ for $\alpha = 1$ and various values of $c_1$ . The remaining parameters values are from Table 4.1. . . . .	75

4.8	Numerical simulations of $u_t$ and $v_t$ for $\alpha = 1$ and various values of $c_2$ . The remaining parameters values are from Table 4.1. . . . .	75
4.9	Measure of the effect of $c_2$ on volatility of $u$ and $v$ with standard deviation (SD).	75
5.1	System (5.9) converges to equilibrium points for parameter regime in Table 5.1. (a) A set of trajectories converging to equilibrium state $z_*(s_*)$ . (b) Projection of trajectories converging to different points of the segment of equilibrium points in the $(v, u)$ plane. . . . .	80
5.2	Projections of various trajectories of system (5.9) onto $(v, u)$ plane. The system contains one stop operator (representing one agent), that is $m = 1$ , $\alpha_1 = 1$ , $\mu_1 = 1$ . Parameters of equations (5.9) are given in the format $a, b = (b_1, b_2), c = (c_1, c_2, c_3)$ . (a) 2-periodic orbit for $a = 0.99, b = (0.76, 0.9), c = (1.4, 9.7, 0.025)$ . (b) 4-periodic orbit for $a = 0.7, b = (0.75, 0.5), c = (4.8, 3.6, 3.45)$ . (c) 8-periodic orbit for $a = 0.9, b = (0.73, 0.9), c = (1.2, 3.15, 1.3)$ . (d) Quasi-periodic orbit for $a = 0.7, b = (0.7, 0.55), c = (4.8, 4.15, 3.8)$ . . . . .	81
5.3	System (5.3) responding to supply shocks for parameter regime in Table 5.1. . .	82
5.4	A set of trajectories of system (5.13) converging to an equilibrium state $z_*(s_*)$ .	85
5.5	Projections of various trajectories (at integer time moments) of the hybrid system (5.13) onto $(v, u)$ plane. The system contains one stop operator (5.14) (representing one agent). Parameters of equations (5.13) are given in the format $a, b = (b_1, b_2), c = (c_1, c_2, c_3)$ . (a) 2-periodic orbit for $a = 0.617, b = (0.429, 2.78), c = (1.16, 5.5, 0.566)$ . (b) 4-periodic orbit for $a = 1.0, b = (0.075, 3.54), c = (0.95, 1.2, 0.15)$ . (c) 14-periodic orbit for $a = 1.0, b = (0.075, 3.54), c = (0.95, 1.2, 0.19)$ . (d) A quasi-periodic orbit of the 4-th iterate of the map for $a = 1.0, b = (0.075, 3.54), c = (0.96, 1.3, 0.18)$ . (e) A quasi-periodic orbit for $a = 1.0, b = (0.075, 3.54), c = (0.95, 1.5, 0.18)$ . (f) A quasi-periodic orbit for $a = 0.61, b = (0.428, 2.78), c = (0.9, 4.2, 0.57)$ . . . . .	86
5.6	Trajectory of system (5.27) with 3 agents near an equilibrium state when none of the agents achieves an extreme sentiment (cf. Figure 4.3(a,d)). . . . .	88
5.7	Trajectory of the system with 3 agents when the most sensitive agent reaches an extreme sentiment and the two less sensitive agents don't (cf. Figure 4.3(b,e)). (a) Time trace of inflation. A change of the equilibrium state occurs. (b) Trajectory in $(v, s)$ -plane for $\alpha = \frac{1}{3}$ . (c) Trajectory in $(v, s)$ -plane for $\alpha = \frac{2}{3}$ and $\alpha = 1$ . . . .	89
5.8	Trajectory of the system with 3 agents with the most sensitive agent and the moderately sensitive agent having an extreme sentiment at the initial (equilibrium) point (cf. Figure 4.3(c,d)). (a) Time trace of inflation. (b) Trajectory in $(v, s)$ -plane for $\alpha = \frac{1}{3}$ . (c) Trajectory in $(v, s)$ -plane for $\alpha = \frac{2}{3}$ . Trajectory of least sensitive agent ( i.e., $\alpha = 1$ ) is similar to Figure 5.7(c). . . . .	89
5.9	Changes of the equilibrium state in the model with 3 agents due to shocks (cf. Figures 4.4, 4.5). . . . .	89

5.10	The run-away inflation scenario in the model with three agents in the case $c_1 < 1$ (cf. Figure 4.6). . . . .	90
5.11	Trade-off between inflation rate and output gap volatility in the model with 3 agents as the inflation targeting parameter $c_1$ in the Taylor rule is varied (cf. Figure 4.7). . . . .	90
5.12	Trade-off between inflation rate and output gap volatility in the model with 3 agents as the output gap targeting parameter $c_2$ in the Taylor rule is varied (cf. Figure 4.8). . . . .	90
5.13	Measure of the effect of $c_2$ on the volatility of $v_t$ and $u_t$ with standard deviation (SD) (cf. Figure 4.9). . . . .	91
5.14	An attractor of system (5.28), (5.29) for several parameter sets. (a-c) A periodic orbit (with period 8, 10, 16, respectively) shown on the $(u, v)$ plane for the system without noise. (d) A quasi-periodic orbit. (e,f) Time trace of $u_t$ and $v_t$ converging to equilibrium points of the system for trajectories with different initial points. (g,h) Time trace of $u_t$ and $v_t$ for trajectories of the system with noise for the same parameters as in (e,f). (i) Trajectories of (e,f) in $(g, s)$ -space; the two equilibrium states correspond to $s_* = \pm\sigma$ . . . . .	93
A.1	Variation of $ \lambda_i $ and $ \lambda_e $ with $a$ . Other parameters are taken from Table 4.1. . .	100
A.2	Dependence of $ \lambda_i $ and $ \lambda_e $ on $b_1, b_2$ . Other parameters are taken from Table 4.1.	101
A.3	Dependence of $ \lambda_i $ and $ \lambda_e $ on $c_1$ and $c_2$ . Other parameters are taken from Table 4.1. . . . .	102
A.4	Cross sections of the plots shown in Figure A.3 for various $c_1$ and (b) $c_2$ values.	102

# CHAPTER 1

## INTRODUCTION

### 1.1 Systems with Hysteresis operators

The term hysteresis was coined by J. A. Ewing in the late 19<sup>th</sup> century referring to “a persistence of previous states” observed when ferric materials are magnetized [33]. The study of hysteresis phenomena produced a number of phenomenological and empirical models and techniques, of which the *play* operator and the Prandtl-Ishlinskii model, introduced by L. Prandtl in [86] and A. Yu. Ishlinskii in [52] as elementary uniaxial constitutive models of elastoplasticity, are of the main interest. A mathematical framework and rigor were first applied to models of hysteresis by a group of mathematicians led by Mark A. Krasnoselskii in their seminal work initiated in the 1970s [58]. The key notion is the hysteresis operator, which satisfies a set of basic properties, of which *rate-independence*, *causality* and *semigroup property* play the main role. Fundamentals of the operator description of hysteresis models and their applications can be found in [16, 59, 74, 110, 111]. Further, various aspects of the methodology, techniques and applications of the theory of hysteresis operators are closely related to the control and systems theory, the theory of switched and piecewise smooth systems [11, 88], variational inequalities [58], differential inclusions [61], Moreau sweeping processes [67, 77, 78], critical phenomena in statistical physics (the Ising model) [101, 102] and phase transitions [16, 97].

The *play* operator is a mathematical description of L. Prandtl’s elastic-ideal plastic element, which can be thought of as a cascade connection of an ideal Hook’s spring with unit stiffness and a Coulomb dry friction element. This simple model accounts for two important effects, saturation of stress with increasing deformation (strain) and hysteresis in the stress-strain relationship. Hysteresis is a manifestation of the fact that stress at a moment  $t$  is not a single-valued function of the concurrent deformation value, but rather a

function of state of the elasto-plastic material, which depends on the history of variations of the deformation prior to the instant  $t$ . The parameter of Prandtl's model is the maximal spring force  $\alpha$ , called the *threshold* (which equals the friction force in the sliding regime for quasistatic deformations). In a different context, the *play* operator also serves as a model of contact force, for example in gear mechanisms, and is known as *backlash* nonlinearity with width  $2\alpha$ .

The Prandtl-Ishlinskii extension of Prandtl's element has been proposed to account for complex constitutive relationships between deformation and stress observed in real elastoplastic materials under uniaxial deformations with multiple yield points (surfaces). In this model, Prandtl's elements with different thresholds and different stiffnesses are superposed to form a weighted parallel connection of play operators. More precisely, a finite or infinite set of Prandtl's elements (characterized by different values of  $\alpha_i$ ) are all subject to the same deformation  $\varepsilon(t)$ , and the total force (or stress)  $\sigma(t)$  is proportional to the sum of all spring forces. The operator that maps the time series  $\varepsilon(t)$  of the deformation (input) to the time series of stress  $\sigma(t)$  (output), given a set of initial stresses of all the springs (initial state), is known as the Prandtl-Ishlinskii (PI) operator in one-dimensional elasto-plasticity [64, 75, 94]. Thanks to the set of very convenient mathematical properties of this operator (see [58, 110]), its equivalent counterparts are also used in several other disciplines including tribology (Maxwell-slip friction model [2, 91, 93]), damage counting and fatigue estimation (the rain flow counting method [32, 96]), and modeling constitutive laws of smart materials such as piezo-electric [54] and magnetostrictive materials [28] and shape memory alloys [16, 98]. One useful property called the composition rule, is that a composition of PI operators is also a PI operator. As a consequence, the inverse operator for a PI operator is another PI operator [16], which can be computed explicitly. Furthermore, a PI operator and its inverse admit an efficient analytic and numerical implementation. This fact is particularly appreciated by engineers as it allows for constructing simple and robust algorithms for inverse control of

technical processes with the goal to eliminate the undesired hysteresis effects. Applications of these compensation-based algorithms include the control of microactuators, sensors and energy harvesters, which use smart materials for energy conversion [4, 27, 46, 66].

The play and PI operators also play a special role in the mathematical theory of hysteresis operators. The Representation Theorem of P. Krejčí [59] and the results of M. Brokate and J. Sprekels [16, Theorem 2.7.7] establish the play operator as the main building block for all hysteresis operators satisfying the Madelung memory rules (also known as *return point memory operators*). In essence, these results say that every return point memory operator (for example, the Preisach operator [58, 87]) can be represented by a functional defined on the space of memory curves generated by the system of play operators; in particular, linear functionals correspond to PI operators.

In addition to traditional applications in engineering and physics, hysteresis operators have been used more recently for modeling biological systems [38, 47–49, 51, 57, 81, 83, 84] and economic systems [23, 24, 45, 89, 90]. In particular, the play operator has been applied to describe dynamics of supply-demand data [43]; the Preisach model was used to analyze hysteresis in unemployment [9, 21, 25, 26]; PI operators were applied to modeling critical phenomena in financial markets with the associated fat tailed distributions of price returns [62, 68] (see also [6, 22–24, 69, 70]). An attempt to use hysteresis operators in the context of models of mathematical economics seems quite natural. Indeed, the phraseology used by economists for describing empirical observations (known as *stylized facts*) often includes such phrases as *path dependence*, *stickiness*, *heterostasis*, *hysteresis*, *remanence*, *thresholds*, *cascades*, which are all directly pertinent to systems with hysteresis. Furthermore, analogies between economics and physics are not unusual for economics thinking [34, 82].

The main challenge of analysis of closed dynamical systems involving hysteresis operators is that these operators are intrinsically non-smooth due to the rate-independence property [60]. In the case of hysteresis operators with a low-dimensional space of states (the states of a



hysteresis operator are also known as memory configurations), this leads to the appearance of switching surfaces in the phase space of the system. The complexity of the structure of these switching surfaces quickly increases with the dimension of the state space [58]. Hysteresis operators with an infinite-dimensional state space are usually obtained as a natural limit of operators with a finite dimensional state space. Their state space is typically a compact metric space, which lacks a local linear structure. Therefore, the analysis of closed systems with such operators relies on non-smooth techniques [15].

Dynamics of continuous time systems with hysteresis operators (operator-differential ODEs and PDEs with hysteresis operators) have been addressed in multiple publications. Discrete time systems with hysteresis have been studied to a significantly lesser extent. At the same time, economic models often use the discrete time setting. In particular, some economic variables are updated only infrequently. A typical example is the interest rate. Naturally, dynamical scenarios in continuous and discrete time systems are not the same.

Hysteresis operators with discrete time inputs and outputs have been considered in [16]. As a matter of fact, due to the rate-independence property, such operators are equivalent to the restriction of the continuous time hysteresis operators to the set of piecewise monotone inputs/outputs. Furthermore, the construction of a hysteresis operator in continuous time setting typically proceeds in two steps. First, the operator is defined on the set of piecewise monotone inputs; then, a continuous extension is used to define the operator in a functional space equipped with an appropriate norm.

In this work, we formulate and study discrete time macroeconomic models involving the hysteresis play operator or a finite sum thereof (a discrete PI operator). These models can be formulated equivalently as piecewise linear (PWL) discrete time dynamical systems. In our analysis, we combine the techniques of the theory of systems with hysteresis and methods of the theory of PWL dynamical systems. In particular, the transition from implicit to explicit models is based on the technique that has been developed for inverting PI operators.

Also, the construction of Lyapunov functions uses the ideas of the theory of systems with hysteresis (energy dissipation due to hysteresis loops). On the other hand, the analysis of dynamics and bifurcations presented in Chapter 3 uses methods of the theory of piecewise smooth dynamical systems.

Economics background that motivates our modeling approach is described in the next subsection.

## 1.2 Economics context

Modern macroeconomics has been dominated by a modeling framework in which the economy is assumed always to be at (or rapidly moving back towards) a unique and stable equilibrium. This has had profound implications both for the way in which the modelers perceive real-world events and their policy prescriptions for dealing with them.

The critiquing of equilibrium models has a long history which we do not attempt to detail here. But many antagonists, see for example [20, 53, 92, 103], have pointed out profound issues concerning the assumed equilibrating processes and the ways in which the ‘aggregation problem’ was being solved. In this work we will focus on one specific pillar of the equilibrium approach which is the assumption of Rational Expectations introduced by Muth in 1961 [79]. This posits that not only are individuals perfectly rational, optimizing, far-sighted and independent of each other but that their expectations about future uncertainties are in agreement with the model itself.

Our mathematical analysis, and the supporting numerics, rigorously show that, when rational expectations about future inflation are replaced by an aggregated ‘sticky’ expectation modeled by the play operator, a simple macroeconomic model changes from a unique equilibrium system to one with an entire continuum of path-dependent equilibria. The form of stickiness that we use is, to our knowledge, new in a macroeconomic setting and differs from, for

example, the stickiness of the Calvo pricing model [17] where hypothetical agents are only allowed to adjust at a fixed rate and the stickiness of [73] where information slowly disseminates.

The way in which we incorporate stickiness into the model will be justified and described more fully below but, briefly, our sticky variables can only be in one of two modes. They are either currently ‘stuck’ at some value or they are being ‘dragged’ along by some other (related) variable because the maximum allowable difference between them has been reached. Each of these modes (which we shall also refer to as the ‘inner’ and ‘outer’ modes respectively) can be analyzed separately as linear systems. However the full PWL system is capable of a much richer range of dynamics.

It must be emphasized right away that our modeling approach and analytical tools are not restricted to inflation expectations or even to macroeconomics. The form of stickiness described above belongs to a class of operators that has well-understood and very desirable properties. These have already been used to develop non-equilibrium asset-pricing models [63] that have (almost-) analytic solutions.

Here, we are able to prove the existence of an entire line interval of feasible equilibrium points, examine their stability, identify some important consequences of path dependence and the effects of exogenous shocks and noise upon the state of the system. Furthermore, these changes are both realistic in that they correspond closely to observed, but potentially puzzling, economic situations and can also be seen numerically in more sophisticated variants of the model. Another useful aspect of this simple model is that the stickiness can be smoothly ‘dialed back’ to zero and the unique equilibrium case is recovered. Or, to put it another way, we can rigorously show that a plausible, boundedly rational *yet fully analyzable*, change to a fully rational model significantly alters the qualitative behaviour of the system in recognizable ways.

Before introducing the model and starting the mathematical analysis, it is worth stepping back to consider the effects of stickiness and friction in physical rather than economic systems.

This helps develop our intuition about the nature of equilibria in such systems but the comparison also offers a high-level explanation of the failure of mainstream economics to foresee the recent economic crisis and help it to recover afterward.

*Economics, Earthquakes and Friction.* In early 2009, Alan Greenspan, former Chairman of the Federal reserve, wrote the following:

“We can model the euphoria and the fear stage of the business cycle. Their parameters are quite different. ... we have never successfully modeled the transition from euphoria to fear” – Alan Greenspan, *Financial Times*, March 27th 2009.

The implication is that Central Bank models work well ‘most of the time’ with suitably calibrated parameters. Occasionally the parameters suddenly change but once these are measured the model again works well in the neighborhood of a new equilibrium.

The above response to models that suddenly fail is only justified when the transitions between euphoria and fear and the changes in parameters are truly exogenously triggered. If they are due to endogenous causes then the model was never really working before the transition and it probably won’t after the transition either.

A useful analogy here is with earthquakes and seismology. Earthquake zones *appear* to be stable (i.e., in an equilibrium) for very long periods of time with only very brief, but violent, ‘transitions’. A tectonic-plate-denying ‘equilibrium seismologist’ might argue that the earthquake-free equilibrium model was essentially correct except for some occasional unpredictable exogenous events that didn’t in any way cast doubt on the modeling assumptions. Of course, earthquakes are almost always endogenously generated and the analogy can be pushed further. An earthquake is a very fast shift from one (meta-)stable internal configuration to another and this leads us to consider the concept of ‘balance-of-forces’ in both physics and economics.

Ever since the time of Walras and Jevons [76] the idea that there should be a complete and unique set of equilibrium prices that exactly balances all of the competing needs and

desires of economic agents has offered a compelling view of a perfectly balanced economy with tâtonnement processes somehow achieving this outcome. But this view is based upon a comparison with physical systems that is misleading. A piece of elastic subjected to competing forces will achieve a unique equilibrium but this is because the elastic has no complex internal structure capable of absorbing any of the stresses without yielding.

A more complicated physical structure such as a tectonic fault line has multiple internal configurations capable of balancing the forces applied to it — up to a point. A particular configuration, which exists at any given moment will depend upon the previous states of the system. When one small part of the fault line suddenly shifts this can transfer excess stress to neighboring parts resulting in a large cascading failure/earthquake. There is a balance of forces before the earthquake and after the earthquake but not *during* the earthquake. These effects have been modeled using the hysteretic Ising model, for example, in [102].

A modern economy is arguably the most complicated man-made system on the planet with an immensely intricate internal structure which cannot simply be averaged away. The analogy is also useful in that the fundamental source of earthquakes is friction. Without it, continental plates would glide rather than stick and then briefly grind. Frictions and stickiness are present in many forms in an economy or financial system and it should not be a surprise if they cause similar qualitative effects.

This brings us to the notion of timescales. In an equilibrium system there is no notion of *any* timescale except for ones imposed exogenously. If one examines an earthquake fault line on a long-enough timescale, maybe tens of thousands of years, then it doesn't look like an equilibrium at all. The mere presence of frictional effects can introduce surprisingly long timescales into a system via the existence of metastable states. If economies feel like they are close to a unique equilibrium maybe that's because most of the time tomorrow does indeed turn out to be a lot like yesterday. Over short timescales unique equilibrium models will appear to be working — especially when their parameters are being frequently updated to match incoming real-world data.

Finally, it must be pointed out that the analogy between earthquakes and the model we analyze below is not perfect. Fault lines are being consistently forced in a single direction while the changes experienced by economies are more random. Also, our main model has a very small number of variables and only one sticky component and so ‘slippage cascades’ aren’t possible. However even the single sticky component allows for the existence of an entire interval of equilibria and complicated transitions between them.

*Permanence and History Dependence.* If the presence of stickiness/frictions in economics does indeed induce a myriad of coexisting equilibria then the phenomena that are not possible (or require a posterior model adjustments) in unique equilibrium models become not just feasible but inevitable. Perhaps the most obvious of these is *Permanence*, also known as remanence, where a system does not revert to its previous state after an exogenous shock is removed. One of the earliest observations of this effect is the Cotton Market before and after the American Civil War [44]. And it is of course of central concern to macroeconomics whether or not economies affected by significant negative shocks can be expected to have permanently reduced productivity levels.

For the models studied in this dissertation, sufficiently small shocks will not change the observed equilibrium and a standard linear stability analysis determines the rate at which the system moves back towards the equilibrium point. Slightly larger shocks will move the system along the line interval of equilibria in the expected direction. But even larger shocks may move the system far enough away from the equilibria interval that the return path and ending point on the interval are very hard to predict. In neither of the last two cases will the system exhibit any tendency to return to its pre-shocked state — the model displays true permanence. And the model parameters alone cannot determine which equilibrium a system is currently in without knowing important information about the prior states of the system — true path dependence.

*Bounded Rationality and the Aggregation Problem.* The standard approach to the problem of aggregating expectations is to introduce a ‘Representative Agent’ whose expectations are fully-informed and rational and consistent with the model itself.

Our approach is similar in spirit to that of De Grauwe [29] in that we will also weaken the assumption of perfect rationality. In [29] both the expectations terms in inflation and output gap are linear combinations of the expectations of two kinds of agent — rational ‘fundamentalists’ and boundedly rational ‘extrapolators’ — with the probability of an agent using each being dictated by discrete choice theory [7, 13]. He then showed numerically that cycles of booms-and-busts occurred with changes in the ‘animal spirits’ and corresponding non-Gaussian ‘fat-tailed’ distributions for the model variables. Discrete choice theory is the aggregating mechanism that De Grauwe uses to avoid ending up with an agent-based model where each agent has to be separately simulated.

We start from the empirical evidence cited above that individual agents’ expectations are often sticky and may lag behind the currently observable values before they start to catch up. We also posit that this gap between future expectations and current reality cannot grow too large. We then imbue our now boundedly rational ‘Representative Agent’ with these same properties. This leads us in a very natural way to the play operator. It seems plausible that stickiness at the micro-level should give macro-stickiness. There is not just empirical evidence for this directly but the New Keynesian school of macroeconomics is even formulated around the idea that sticky wages and prices will be observable at the aggregated macro-level.

The systems that result are both tractable (to a lesser or greater extent) and incorporate an aspect of economic behavior that is missing from Rational Expectations.

### 1.3 Outline of the dissertation

The dissertation is organized as follows. In Chapter 2, we present a brief preview of hysteresis operators, the definition of the play operator (and a dual operator called the *stop*) with discrete time inputs/outputs, and the definition of the discrete PI operator. We then proceed with the inversion formulas for these operators. The inversion is necessary for converting implicit economic models to an explicit form. Further, we present a version of a DSGE macroeconomic model and incorporate the play operator into this model. The play operator accounts for the boundedly rational behavior of the representative economic agent. Then we pass to an equivalent formulation of the model in the form of a 4-dimensional discrete time PWL system. The multi-agent version of the model is also presented.

As we show in the last chapter, the 4-dimensional model has complex dynamics, which are difficult to study analytically in great detail. For this reason, in Chapters 3 and 4, we consider two simplifications of the model. These two chapters contain the main theoretical findings of the dissertation.

The 2-dimensional system considered in Chapter 3 does not have explicit economic interpretation. However, its structure is similar to that of the main model presented in Chapter 2. The purpose of this simpler prototype 2-dimensional system is to help us develop the intuition for possible dynamics of the more complex 4-dimensional model. Chapter 3 presents a detailed analysis of global dynamics of the 2-dimensional system depending on 2 parameters. These dynamics are summarized by a global bifurcation diagram. In particular, for certain parameter values, we describe border collision bifurcations and complex dynamics with infinitely many periodic orbits. The degenerate border collision bifurcation is a feature typical of PWL systems, which is not present in smooth dynamical systems.

In Chapter 4, we consider a particular case of the DSGE model from Chapter 2 obtained by one simplification. Namely, we remove the correlation between the subsequent values of the interest rate from the Central Bank regulatory policy (Taylor rule). This leads



to a 3-dimensional PWL model and allows us to perform a complete analysis of stability depending on parameters. In particular, we construct a family of Lyapunov functions and prove the global stability of the continuum of equilibrium states when a certain parameter of the Central Bank policy satisfies  $c_1 > 1$ . Further, we show the local stability of the equilibrium states combined with *global instability* for  $c_1 < 1$ . We then proceed with a number of numerical simulations testing the response of the model to exogenous noise and shocks and interpret our findings in the economic context.

Chapter 5 presents a numerical study of the 4-dimensional model and a number of its extensions and variations. We consider (a) the 4-dimensional model from Chapter 2; (b) a hybrid version of this model, in which the interest rate is updated at discrete times but the inflation rate and the output gap evolve in continuous time; (c) a model with multiple play operators (a PI operator) representing different types of economic agents; and, (d) a system with the play operator incorporated in the equation for the interest rate, which introduces “stickiness” in the response of the Central Bank to variations of the output gap and inflation (this stickiness is shown to produce a destabilizing effect). Each of these models is shown to be capable of producing a rich set of dynamical scenarios. The simple analysis is performed to find the continuum of equilibrium states and establish their local stability properties. Otherwise we resort to numerical simulations. The dissertation ends with Conclusions and technical Appendices.

## CHAPTER 2

### PRELIMINARIES

#### 2.1 DSGE models

Macroeconomists are responsible for solving practical problems of immense dimensions [71] such as problems posed by the Great Depression of the 1930s. If there are tried and tested resources, which have been used to solve certain classes of problems (either of higher or lesser degree), then it is prudent to develop solution techniques of other problems based on these tried and tested principles. For this reason, macroeconomists over the years have embraced the usefulness of engineering, physics and mathematical tools in solving problems.

The challenge macroeconomists face with adopting problem solving techniques from fields of engineering and other sciences is the availability of laboratories and high-powered computing tools to these fields. Unlike the field of microeconomics, where mechanical systems have been built for demonstrating and teaching consumer demand and producer supply [82], the field of macroeconomics is unable to carry out experiments in laboratories because macroeconomic variables are not independent of humans [108]. For this reason, mathematical models provide the needed experimental tool for satisfying the quest of macroeconomists.

One of the objectives of a system analyst is to understand how a system functions with and without external influences. Macroeconomists are economic system analysts who seek to understand how the system works with and without shocks. To achieve this goal, macroeconomists need to replicate the real world economic system by modeling and analyzing the effects of the endogenous and exogenous variables on the system. Dynamic Stochastic General Equilibrium (DSGE) models have become the crux of modern macroeconomics analysis. It is easy to deduce from the name that all variables are dynamic, thus *ceteris paribus* assumption is annihilated, the system is not necessarily deterministic and the system can be observed in its steady state. Various DSGE models in continuous time, discrete time

and delay differential equations are available [40]. The basic structure of a DSGE model is

$$x_{t+1} = f \left( x_t, E_t[x_{t+1}], y_t, \varepsilon_t \right) \quad (2.1)$$

where  $x$  is a vector of endogenous variables,  $E$  is an expectation operator,  $y$  is a vector of exogenous variables and  $\varepsilon$  is random disturbances (noise) with a well defined density function. The function  $f(\cdot)$  is called economic theory [108]. The number of variables in these models can vary from just a few as in this work to tens and hundreds variables accounting for a variety of participants of the economic process.

Therefore, a typical macroeconomics laboratory is made up of a DSGE model, a computer and an appropriate software. For example, DYNARE is a computational software platform specifically designed for modeling and analyzing a wide class of economic models, in particular DSGE models [1]. DSGE models are *state-of-the-art* models [72] for policy analysis and forecasting by the research departments of Central Banks all over the world [18, 19, 31, 107].

## 2.2 Hysteresis operators

In this section, we state definitions and properties of hysteresis operators. We shall proceed to give examples of hysteresis operators, which shall be used in our models later. We begin by defining certain terminologies, which shall serve as the pillars in our building. We adopt the notations and terminologies of [16].

Denote by  $C_{pm}[0, T]$  the set of continuous piecewise monotone functions  $x : [0, T] \rightarrow \mathbb{R}$ . An admissible time transformation is an increasing continuous function  $\varphi : [0, T] \rightarrow [0, T]$  satisfying

$$\varphi(0) = 0, \quad \varphi(T) = T. \quad (2.2)$$

**Definition 2.1.** (*Rate-Independent Functional*)

A functional  $\mathcal{F} : C_{pm}[0, T] \rightarrow \mathbb{R}$  is called rate-independent if and only if

$$\mathcal{F}[x \circ \varphi] = \mathcal{F}[x] \quad (2.3)$$

holds for all  $x \in C_{pm}[0, T]$  and all admissible time transformations  $\varphi(t)$ .

From Definition 2.1, one can see that  $\mathcal{F}[x]$  is determined by the sequence of values  $\{x(t_0), \dots, x(t_N)\}$ , where  $0 = t_0 < t_1 < \dots < t_N = T$  are the local extrema of  $x$  over  $[0, T]$ .

We denote by  $F_{pm}[0, T]$  the set of all piecewise monotone functions on  $[0, T]$ . Notice that  $C_{pm}[0, T] = F_{pm}[0, T] \cap C[0, T]$ . For any  $x \in F_{pm}[0, T]$ , we define the *standard monotonicity partition* of  $x$  by

$$t_0 = 0, \quad t_{i+1} = \max\{t \in [t_i, T] : x \text{ is monotone on } [t_i, t]\}. \quad (2.4)$$

**Definition 2.2.** (*General Scalar-Valued Hysteresis Operators*)

An operator

$$\mathcal{H} : C_{pm}[0, T] \rightarrow F_{pm}[0, T] \quad (2.5)$$

is called a hysteresis operator on  $C_{pm}[0, T]$  if and only if there exists a rate-independent functional  $\mathcal{F} : C_{pm}[0, T] \rightarrow \mathbb{R}$  such that

$$\mathcal{H}[x](t) = \mathcal{F}[x_t] \quad \text{for all } t \in [0, T], \quad x \in C_{pm}[0, T] \quad (2.6)$$

where  $x_t$  is the truncation of  $x$  at  $t$  given by

$$x_t(\tau) = \begin{cases} x(\tau) & \text{for } 0 \leq \tau \leq t, \\ x(t) & \text{for } t < \tau \leq T. \end{cases} \quad (2.7)$$

Let us set  $t = T$  in the defining equation (2.6). We have

$$\mathcal{H}[x](T) = \mathcal{F}[x_T] = \mathcal{F}[x], \quad x \in F_{pm}[0, T]. \quad (2.8)$$

Hence, for any hysteresis operator  $\mathcal{H}$  on  $C_{pm}[0, T]$ , there exists one and only one rate-independent functional  $\mathcal{F}$ , which satisfies (2.6). We shall call  $\mathcal{F}$  the *generating functional*<sup>1</sup> of  $\mathcal{H}$ .

From Definition 2.2, we make the following consequential observations that

---

<sup>1</sup>Another name for  $\mathcal{H}_f$  is the *final value mapping* because of (2.8).

- (i)  $\mathcal{H}[x]$  shall remain constant on any sub-interval of  $[0, T]$ , whenever  $x$  remains constant;
- (ii)  $\mathcal{H}$  is completely determined by the output values at the end of the evolution;
- (iii)  $\mathcal{H}$  satisfies the *Volterra causality property*, that is, for any  $x, y \in C_{pm}[0, T]$  and  $t \in [0, T]$ , one has  $\mathcal{H}[x](t) = \mathcal{H}[y](t)$  whenever  $x_t = y_t$ .
- (iv)  $\mathcal{H}$  is rate-independent in the sense that for any admissible time transformation  $\varphi$ , one has

$$\mathcal{H}[x \circ \varphi](t) = \mathcal{H}[x](\varphi(t)). \quad (2.9)$$

The above properties have important implications for both discrete and continuous time setting. First, one can consider discrete time input/output sequences  $x = x_t$  and  $(\mathcal{H}[x])_t$ , which can be naturally identified with piecewise monotone inputs/outputs in continuous time setting. Second, in continuous time setting, one can typically construct a continuous extension of  $\mathcal{H}$  to the space  $C[0, T]$  (and other spaces such as  $W^{1,1}[0, T]$ ) from the dense set  $C_{pm}[0, T]$ . We will be mostly concerned with the discrete time setting.

We proceed by considering examples of hysteresis operators, which shall be useful to us later.

### 2.2.1 Stop operator

We begin with the so-called *stop operator*. Before giving the formal definition, let us discuss the following mechanical model associated with the Moreau sweeping process [8, 67, 77]. Consider box  $A_1$  and frame  $B_1$  in Figure 2.1. We control the position  $x(t)$  of the center of the frame by moving the frame; therefore, the position  $x(t)$  serves as the input function while the relative position  $s(t)$  of the center of the frame with respect to the center of box  $A_1$  is the output function of the sweeping process in Figure 2.1. The relative position  $s$  changes at the rate  $\dot{s} = \dot{x}$  when the frame is not in contact with the box. However, the relative position

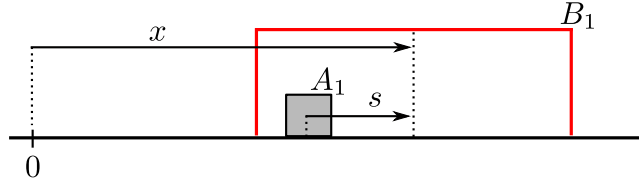


Figure 2.1. Interpretation of the *stop* operator with the one-dimensional Moreau sweeping process.

$s$  remains constant if either the left facet of the frame is in contact with the box and  $\dot{x} > 0$  or the right facet of the frame is in contact with the box and  $\dot{x} < 0$ .

If we take the relative position  $s$  when the box is in contact with the frame to be  $\alpha$ , then the corresponding input-output behavior of the Moreau sweeping process is given by the hysteresis diagram in Figure 2.2.

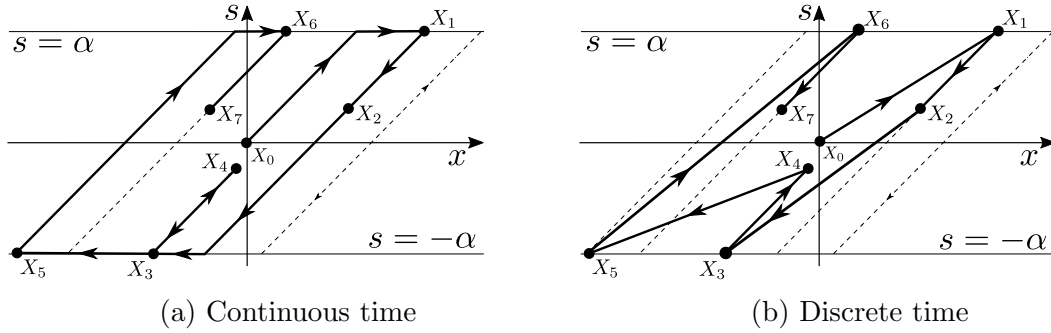


Figure 2.2. Illustration of the *Stop Operator*. Slope of the dashed lines is 1 and movements along these lines are bidirectional. Movement along the upper horizontal line  $s = \alpha$  is to the right; movement along the lower horizontal line  $s = -\alpha$  is to the left.

In discrete time setting, the formal definition is as follows. Let  $x = \{x_t\}$ ,  $t \geq 0$  be a real-valued input sequence and let  $s_0 \in [-\alpha, \alpha]$ . Then the output sequence  $s = \{s_t\}$ ,  $t \geq 0$  of the stop operator is defined by

$$s_t = \Psi_\alpha(x_t - x_{t-1} + s_{t-1}), \quad t \geq 1, \quad (2.10)$$

where the piecewise linear saturation function  $\Psi_\alpha$  is defined by

$$\Psi_\alpha(\tau) = \begin{cases} \alpha & \text{if } \tau > \alpha, \\ \tau & \text{if } |\tau| \leq \alpha, \\ -\alpha & \text{if } \tau < -\alpha. \end{cases} \quad (2.11)$$

We will use the notation

$$s = \mathcal{S}_\alpha[x, s_0] \quad (2.12)$$

for the *stop* operator. Notice that the initial value of the output belongs to the arguments.

### 2.2.2 Play operator

The *play operator*  $\mathcal{P}_\alpha$  is simply defined by the identity

$$\mathcal{P}_\alpha + \mathcal{S}_\alpha = \mathcal{I}d. \quad (2.13)$$

That is, the output sequence  $p = \{p_t\}$ ,  $t \geq 0$  of the play operator is defined by  $p_t = x_t - s_t$ , where  $s = \{s_t\}$ ,  $t \geq 0$  is the output sequence of the stop operator. Equivalently, given an input  $x = \{x_t\}$ ,  $t \geq 0$  and an initial output value  $p_0$  satisfying  $|p_0 - x_0| \leq \alpha$ , the output sequence  $p = \mathcal{P}_\alpha[x, p_0]$  of the play operator is defined by

$$p_t = x_t - \Psi_\alpha(x_t - p_{t-1}), \quad t \geq 1 \quad (2.14)$$

with  $\Psi_\alpha$  given by (2.11). Note that  $|x_t - p_t| \leq \alpha$  at all times.

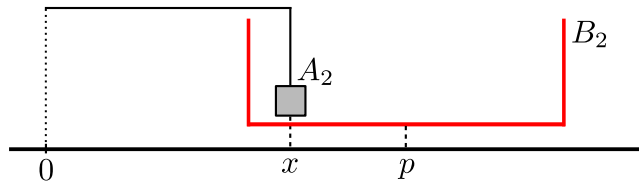


Figure 2.3. Interpretation of the *play* operator with a mechanical system.

A mechanical interpretation of the play operator presented in Figure 2.3 shows two elements  $A_2$  and  $B_2$ . We control the position  $x(t)$  of the center of the box  $A_2$ . Therefore, the

position  $p(t)$  of the center of the frame  $B_2$  remains constant so long as the box only moves within the interior of this frame. However, the position  $p(t)$  changes at the rate  $\dot{p} = \dot{x}$  when the box  $A_2$  touches the boundary of the frame  $B_2$  and proceeds with the velocity  $\dot{x}$  pointing in the outward direction.

If we take the diameter of element  $B_2$  to be  $2\alpha$ , then the corresponding input-output behavior of the mechanical system is given by the hysteresis diagram in Figure 2.4(a).

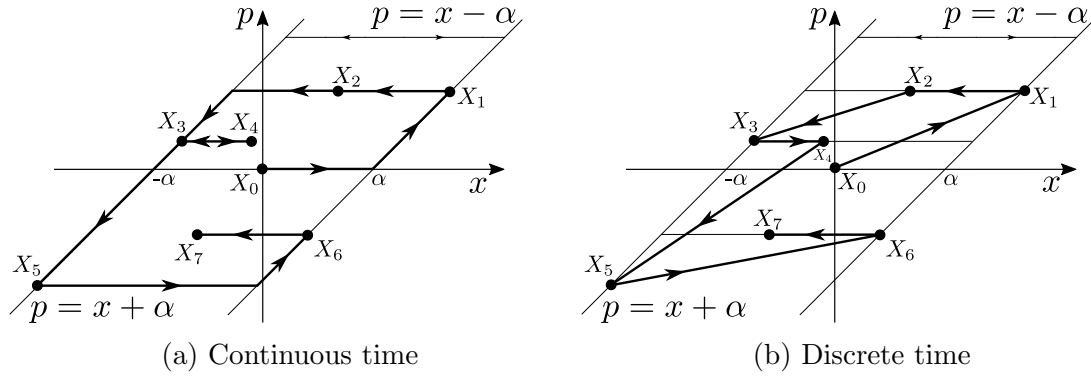


Figure 2.4. Illustration of the *Play Operator*.

### 2.2.3 The Prandtl–Ishlinskii operator

The Prandtl–Ishlinskii (PI) operator is an operator obtained by the superposition of stop operators [5, 95] or play operators [14, 63]. It can therefore be referred to as either the PI operator of play type or the PI operator of stop type [36, 111, 112].

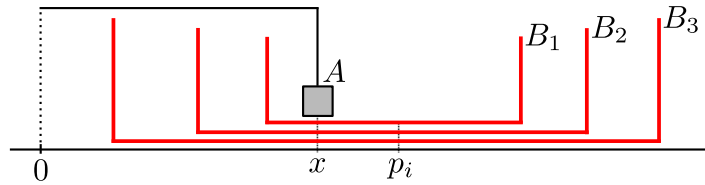


Figure 2.5. Interpretation of PI of play type with a mechanical system.

The PI operator of play type with  $N$  plays is defined by

$$p = \sum_{i=1}^N \mu_i \mathcal{P}_{\alpha_i}[x, p_0^i], \quad (2.15)$$



where a weight  $\mu_i$  is assigned to the  $i$ -th play operator. Similarly, the PI operator of stop type with  $N$  stops is defined by

$$s = \sum_{i=1}^N \mu_i \mathcal{S}_{\alpha_i}[x, s_0^i]. \quad (2.16)$$

Initial values  $p_0^i$  and  $s_0^i$  satisfy

$$s_0^i \in [-\alpha_i, \alpha_i], \quad |p_0^i - x_0| \leq \alpha_i \quad \text{for all } i = 1, \dots, N.$$

Figure 2.5 illustrates the mechanical interpretation of the PI operator of play type with 3 plays. Figure 2.6 shows an input-output diagram for the PI operators of play and stop type.

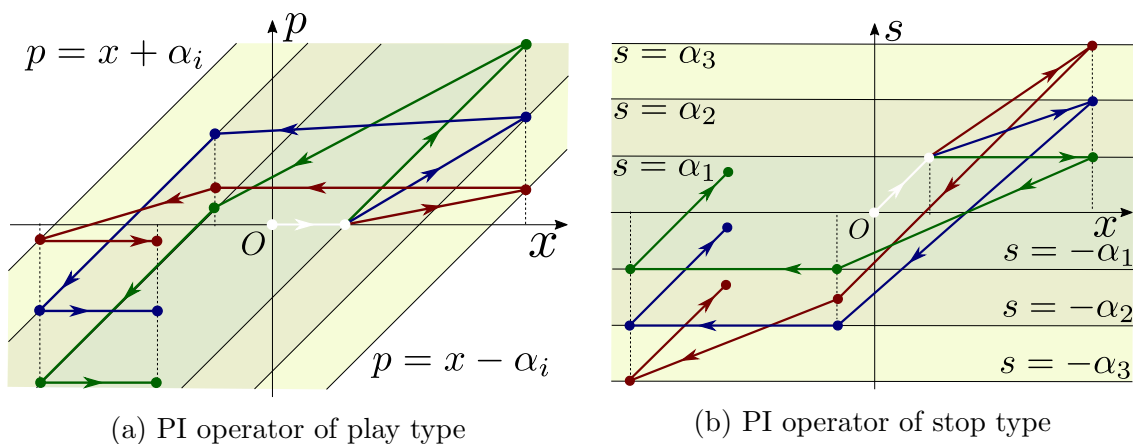


Figure 2.6. Discrete time input-output diagram of PI operators with thresholds  $\alpha_1 < \alpha_2 < \alpha_3$ .

We note that continuous time counterparts of the above operators can be defined using the integrals

$$p = \int_0^\infty \mu(\alpha) \mathcal{P}_\alpha[x, p_0(\alpha)] d\alpha, \quad s = \int_0^\infty \mu(\alpha) \mathcal{S}_\alpha[x, s_0(\alpha)] d\alpha. \quad (2.17)$$

However, this extension is not used in this work.

### 2.3 Inversion of PI operators

In this section, we consider the inverse of a PI operator of the form

$$\mathcal{K}_\varphi[x] = \mu_0 x + \sum_{i=1}^N \mu_i \mathcal{S}_{\alpha_i}[x, 0], \quad (2.18)$$

where

$$0 < \alpha_1 < \cdots < \alpha_N$$

and for simplicity we use the zero initial state for all the stops,  $s_0^i = 0$  (in fact, this is not a restriction). The PWL function  $\varphi$  is known as the *primary response curve* or the *loading curve*. It is defined by

$$\varphi(\rho) = \mu_0 \rho + \begin{cases} (\mu_1 + \mu_2 + \cdots + \mu_N)\rho, & 0 \leq \rho \leq \alpha_1, \\ (\mu_2 + \cdots + \mu_N)\rho, & \alpha_1 < \rho \leq \alpha_2, \\ \vdots & \\ \mu_N \rho, & \alpha_{N-1} < \rho \leq \alpha_N, \\ 0, & \alpha_N < \rho. \end{cases}$$

Notice that the function  $\varphi$  contains all the information about the parameters of the PI operator including the thresholds  $\alpha_i$  and the weights  $\mu_i$ . It is sufficient for identifying the PI operator uniquely.

Under appropriate conditions, operator (2.18) is invertible. Furthermore, the inverse operator is also a PI operator [16]. This fact is based on the following *composition formula*, see [16, Proposition 2.2.15, 2.2.16]:

$$\mathcal{K}_{\varphi_1} \circ \mathcal{K}_{\varphi_2} = \mathcal{K}_{\varphi_1 \circ \varphi_2}, \quad (2.19)$$

which is true if  $\varphi_2$  is monotone. This formula implies that if the primary response curve  $\varphi$  is invertible, then the corresponding PI operator  $\mathcal{K}_\varphi$  is invertible and its inverse is defined

by the formula<sup>2</sup>

$$\mathcal{K}_\varphi^{-1} = \mathcal{K}_{\varphi^{-1}}, \quad (2.20)$$

see Figure 2.7.

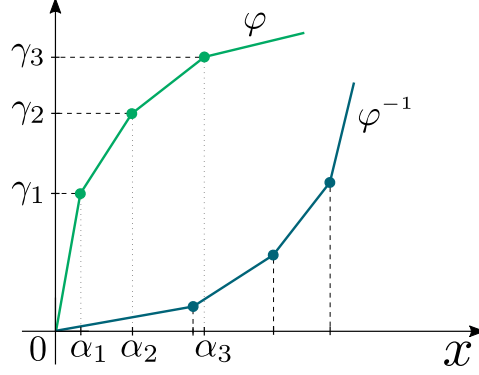


Figure 2.7. Primary response (loading) function  $\varphi$  of PI operator (2.21) and primary response function  $\varphi^{-1}$  of the inverse PI operator (2.24).

This formula for  $N = 1$  will be used in Chapter 4. In this case,  $\mathcal{K}$  and its inverse have the form

$$\mathcal{K}[x] = \mu_0 x + \mu_1 S_\alpha[x, 0], \quad \mathcal{K}^{-1}[x] = \frac{1}{\mu_0} \left( x - \frac{\mu_1}{\mu_0 + \mu_1} S_\gamma[x, 0] \right)$$

with  $\gamma = (\mu_0 + \mu_1)\alpha$ .

Here we also specify the inversion formula (2.20) for  $N = 3$ , the case that will be used in Chapter 5. In this case,

$$\mathcal{K}[x] = \mu_0 x + \sum_{i=1}^3 \mu_i \mathcal{S}_{\alpha_i}[x, 0], \quad \mathcal{K}^{-1}[x] = \frac{1}{\mu_0} \left( x - \sum_{i=1}^3 \kappa_i \mathcal{S}_{\gamma_i}[x, 0] \right), \quad (2.21)$$

where

$$\begin{cases} \kappa_3 = 1 - \frac{\mu_0}{\mu_0 + \mu_3}, \\ \kappa_2 = 1 - \frac{\mu_0}{\mu_0 + \mu_2 + \mu_3} - \kappa_3, \\ \kappa_1 = 1 - \frac{\mu_0}{\mu_0 + \mu_1 + \mu_2 + \mu_3} - \kappa_2 - \kappa_3 \end{cases} \quad (2.22)$$

---

<sup>2</sup>An extension of this formula for PI operators with time dependent thresholds has been recently obtained in [3].

and

$$\begin{cases} \gamma_1 = \alpha_1(\mu_0 + \mu_1 + \mu_2 + \mu_3), \\ \gamma_2 = \gamma_1 + (\alpha_2 - \alpha_1)(\mu_0 + \mu_2 + \mu_3), \\ \gamma_3 = \gamma_2 + (\alpha_3 - \alpha_2)(\mu_0 + \mu_3). \end{cases} \quad (2.23)$$

In general, we can show in a similar fashion that the inverse of the PI operator (2.18) with  $N$  steps is defined by

$$\mathcal{K}^{-1}[x] = \mu_0^{-1} \left( x + \sum_{i=1}^N \kappa_i \mathcal{S}_{\gamma_i}[x, 0] \right), \quad (2.24)$$

where

$$\gamma_i = \gamma_{i-1} + \left( \alpha_i - \alpha_{i-1} \right) \left( \mu_0 + \sum_{j=i}^N \mu_j \right), \quad \gamma_0 = \alpha_0 = 0,$$

$$\kappa_N = 1 - \frac{\mu_0}{\mu_0 + \mu_N}, \quad \kappa_i = 1 - \sum_{j=i+1}^N \kappa_j - \frac{\mu_0}{\mu_0 + \sum_{j=i}^N \mu_j} \quad \text{for } i = 1, \dots, N-1.$$

## 2.4 Modeling idea

In this section, we describe our modeling strategy. We use the play operator to model the economic agents' aggregate expectation of future inflation. Notice that the play operator naturally defines a harmless interval for inflation, corresponding to the 'stuck' mode. The idea of harmless interval and its effect on economic growth is not new in economics [12, 39, 56, 65, 109]. By using the play operator to model expectations of future inflation, an interval of output gap is also obtained for every harmless interval of inflation.

We start from a dynamic stochastic general equilibrium (DSGE) macroeconomics model, which includes aggregate demand and aggregate supply equations and the Taylor rule, which

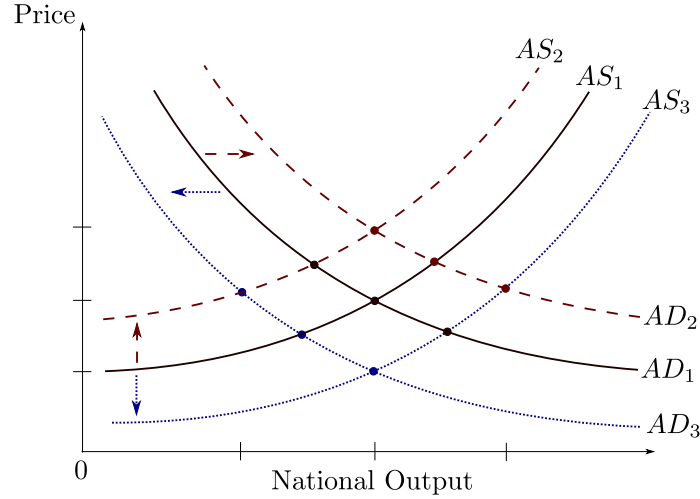


Figure 2.8. Multiplicity of equilibrium states from aggregate demand ( $AD$ ) and aggregate supply ( $AS$ ) curves.

describes the policy strategy of the Central Bank. The model is given by

$$\begin{cases} u_t = u_{t-1} - a(w_t - p_t) + \varepsilon_t, \\ v_t = b_1 p_t + (1 - b_1)v_{t-1} + b_2 u_t + \eta_t, \\ w_t = c_1(v_t - v^*) + c_2 u_t + c_3 w_{t-1} + \zeta_t, \end{cases} \quad (2.25)$$

with  $t = 1, 2, 3, \dots$ , where  $u_t$  is the output gap (or unemployment rate, or another measure of activity of the economy such as the difference between expected and actual gross domestic product),  $v_t$  is the rate of inflation,  $w_t$  is the interest rate,  $p_t$  is the aggregate of economic agents' expectations of the future inflation rate, and  $\varepsilon_t$ ,  $\eta_t$ ,  $\zeta_t$  are exogenous noise terms, see [29, 72] for a very similar model. All the parameters are non-negative,  $b_1 < 1$ , and the parameter  $v^*$ , the inflation target, is for convenience set to zero. More complicated variants, employing many more variables to represent different sectors of the economy, are widely-used by Central Banks to help determine interest rate policy. See [19, 55, 99, 107] for other examples of DSGE models.

In order to close the model, (2.25) must be complemented with an equation defining how the economic agents' expectation of the future inflation rate  $p_t$  is related to the actual inflation rate  $v_t$ . In most standard DSGE models the agents are, put very simply, assumed to have rational expectations about the future. However, there is abundant empirical evidence that, in practice, the process of forming inflation expectations displays hysteresis and in particular stickiness in the sense that many agents will update their expectations only infrequently [73]. Evidence such as this has led to the development of a number of simple *ad hoc* models throughout economics that attempt to account for 'boundedly rational' behavior of economic agents caused by their limited access to information, limited cognitive abilities, emotional behavior, and other human factors. One commonly used modeling heuristic is based around the concept of a threshold — it is postulated that an agent changes its behavior (strategy, opinion) when a variable reaches a certain threshold value (see [100] for example). Play operators may provide a useful alternative to such models because they also incorporate threshold effects and are capable of accounting for the path dependence, hysteresis, and multiplicity of equilibrium states (see Figure 2.8) in an economic model. At the same time they possess a set of useful and well-understood mathematical properties which facilitate the modeling and analysis.

Thus, the novelty of our modeling strategy is in how we define the relationship between the aggregate expectation of inflation  $p_t$  and the inflation rate  $v_t$ . We suppose that the expectation of the future inflation rate  $p^i$  by an agent  $i$  is related to the actual inflation rate  $v$  via the *play* operator see Figure 2.4:

$$p_t^i = v_t - s_t^i, \quad s_t^i = \Psi_{\alpha_i}(v_t - v_{t-1} + s_{t-1}^i), \quad (2.26)$$

where  $\Psi_{\alpha_i}$  is function (2.11) for each  $i$ ,  $\alpha_i$  is a positive threshold parameter; and the sequence  $\{s_t^i\}$  (for fixed  $i$ ) is the output of the *stop* operator with input  $\{v_t\}$ , see Figure 2.2. According to this definition, the expectation of the future inflation rate remains unchanged as long as

the actual current inflation rate deviates from the expected value by less than the value  $\alpha_i$ . In other words, the agent is not responsive to such variations of the inflation rate. However, once the absolute value of the difference between the expected and the actual rates exceeds the threshold  $\alpha_i$ , that is  $|p_{t-1}^i - v_{t-1}| > \alpha_i$  at some time  $t$ , the agent corrects its expectation of the future rate making sure that  $|p_t^i - v_t| \leq \alpha_i$  at all times. It may be considered as a technical assumption of the model that the agent makes the minimal possible correction which ensures that the error between the expectation and the actual inflation rate never exceeds the threshold  $\alpha_i$ , that is  $p_t^i = v_t - \alpha_i$  if  $v_t > p_{t-1}^i + \alpha_i$  and  $p_t^i = v_t + \alpha_i$  if  $v_t < p_{t-1}^i - \alpha_i$ . This rule is similar to some trading strategies based on draw-up and draw-down indicators that are used by momentum traders in financial markets [62].

The aggregate of economic agents' expectation of future inflation rate  $p_t$  in the macroeconomics model (2.25) can be naturally defined as

$$p_t = \sum_{i=1}^m \mu_i p_t^i \tag{2.27}$$

in a model with  $m$  agents, which have different thresholds  $\alpha_i$  and contribute to the aggregate with weights  $\mu_1, \dots, \mu_m > 0$ . Equation (2.25) complemented by relations (2.26) and (2.27) form a closed macroeconomics model with  $m$  agents.

In Chapter 4, we will consider this model with  $m = 1$  representative agent. Multiple agents are considered in Chapter 5.

## CHAPTER 3

### DISCRETE TIME SYSTEM WITH STOP OPERATOR

It will be shown later in chapter 5 that the macroeconomics model (2.25), (2.26), (2.27) can exhibit a variety of complex dynamical scenarios. In order to comprehend some of the possible dynamics, we shall consider a simpler prototype low-dimensional system in this chapter. In the case of one representative agent ( $m = 1$  in (2.27)), our macroeconomics model is a 3-dimensional linear system coupled with the stop operator. Or putting it another way, it is a 4-dimensional PWL system. In this chapter, we consider a 2-dimensional PWL system,<sup>1</sup> which is made up of one linear equation and one piecewise linear equation representing the stop operator. Further, we set the noise terms to zero and consider the autonomous dynamics.

#### 3.1 System set-up

Let  $s_0 \in [-1, 1]$  and let  $\{x_t\}$ ,  $t \in \mathbb{N}_0$ , be a real-valued sequence. The stop operator  $\mathcal{S}_1$  with the unit threshold  $\alpha = 1$  maps a pair  $s_0, \{x_t\}$  to a sequence defined by the formula

$$s_{t+1} = \Psi(s_t + x_{t+1} - x_t), \quad t \in \mathbb{N}_0,$$

where  $\Psi(\tau)$  is given by (2.11) with  $\alpha = 1$  as

$$\Psi(\tau) = \begin{cases} -1 & \text{if } \tau < -1, \\ \tau & \text{if } |\tau| \leq 1, \\ 1 & \text{if } \tau > 1. \end{cases}$$

Let us recall that  $s_0$  is called the initial state,  $\{x_t\}$  is called the input, and  $\{s_t\}$  is called the output (or, the variable state) of the stop operator. The play operator maps the pair  $s_0, \{x_t\}$  to the sequence  $\{p_t\} = \{x_t - s_t\}$ , see Figure 3.1.

---

<sup>1</sup>The main results presented in this chapter also appear in [8]. The 2-dimensional PWL system, all Figures except 3.1, 3.2, 3.9, 3.10, 3.11 and all computations presented in this dissertation are the works of E. Kwame with guidance from D. Rachinskii and oversight from M. Arnold.



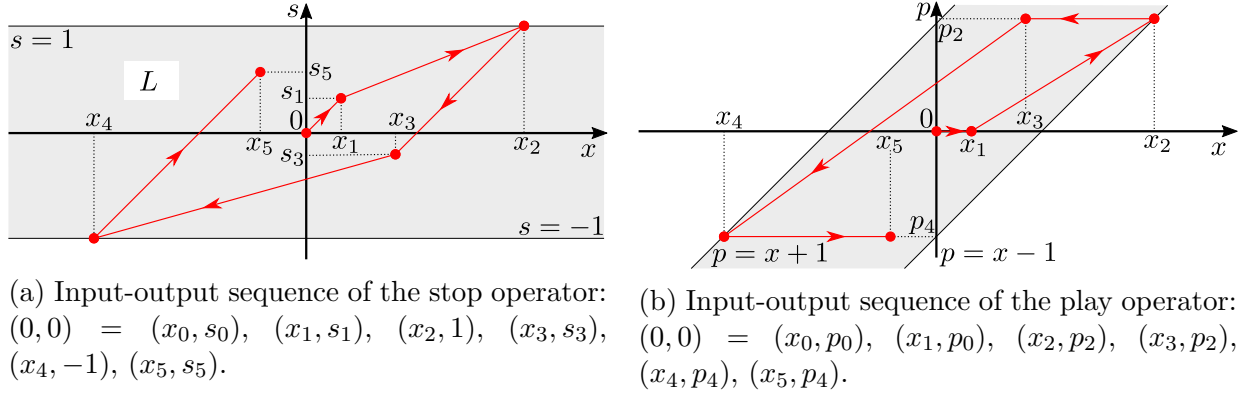


Figure 3.1. Discrete time representations of the stop and play operators.

Coupling the output of the stop operator with the input sequence via a linear transformation with real-valued coefficients  $\lambda$  and  $a$ , we consider the dynamical system

$$\begin{cases} x_{t+1} = \lambda x_t + a s_t, \\ s_{t+1} = \Psi(s_t + x_{t+1} - x_t) \end{cases} \quad (3.1)$$

with  $t \in \mathbb{N}_0$  on the strip  $L = \{(x, s) : x \in \mathbb{R}, s \in [-1, 1]\}$ . From hereon we assume that  $|\lambda| < 1$ . This inequality ensures that all the trajectories of system (3.1) are bounded.

It is easy to see that the equilibrium points of system (3.1) form the segment

$$EF = \left\{ (x, s) : x = \frac{as}{1-\lambda}, -1 \leq s \leq 1 \right\} \quad (3.2)$$

with the end points

$$E = (x^*, 1) = \left( \frac{a}{1-\lambda}, 1 \right), \quad F = (-x^*, -1) = \left( -\frac{a}{1-\lambda}, -1 \right).$$

We use the standard notion of stability, asymptotic stability and instability (in the Lyapunov sense) for equilibria and periodic orbits. We will also say that an equilibrium point  $(x_e, s_e)$  of system (3.1) is *semi-stable* if there are open sets  $U_1, U_2 \subset \{(x, s) : |s| < 1\}$  such that  $(x_e, s_e)$  belongs to their boundaries and simultaneously:

- for every  $\varepsilon > 0$  there is a  $\delta > 0$  such that any trajectory starting from the  $\delta$ -neighborhood of the equilibrium point  $(x_e, s_e)$  in the set  $U_1$  belongs to the  $\varepsilon$ -neighborhood of  $(x_e, s_e)$  for all positive  $t$ ;
- there is an  $\varepsilon_0 > 0$  such that any trajectory starting in  $U_2$  leaves the  $\varepsilon_0$ -neighborhood of the equilibrium  $(x_e, s_e)$  after a finite number of iterations.

### 3.2 Main results

Our main result consists in the classification of the long time behavior for the orbits of system (3.1). Dynamics of system (3.1) depends on the values of the parameters  $\lambda$  and  $\beta = \lambda + a$  as described in Theorem 3.1. The results are summarized in Figure 3.2.

**Theorem 3.1.** *Let  $\beta = \lambda + a$  and  $|\lambda| < 1$ .*

- (a) *If  $\lambda \geq 0$ ,  $\beta \geq 1$ , then the equilibrium points  $E$  and  $F$  are semi-stable and all the other equilibrium points are unstable. Each non-equilibrium trajectory either converges to  $E$  or to  $F$ .*
- (b) *If  $|\beta| < 1$ , then all the equilibrium points are stable and each trajectory of system (3.1) converges to an equilibrium point.*
- (c) *If  $\lambda \geq 0$ ,  $\beta < -1$ , then the points  $E$  and  $F$  are semi-stable, all the other equilibrium points are unstable, and there exists a stable 2-periodic orbit*

$$\pm Q = \left( \mp \frac{a}{1 + \lambda}, \pm 1 \right). \quad (3.3)$$

*Each non-equilibrium trajectory either converges to  $E$  or to  $F$  or to the orbit (3.3).*

- (d) *If  $\lambda < 0$ ,  $\beta < -1$ , then all the equilibrium points are unstable. Each non-equilibrium trajectory converges to the stable 2-periodic orbit (3.3).*

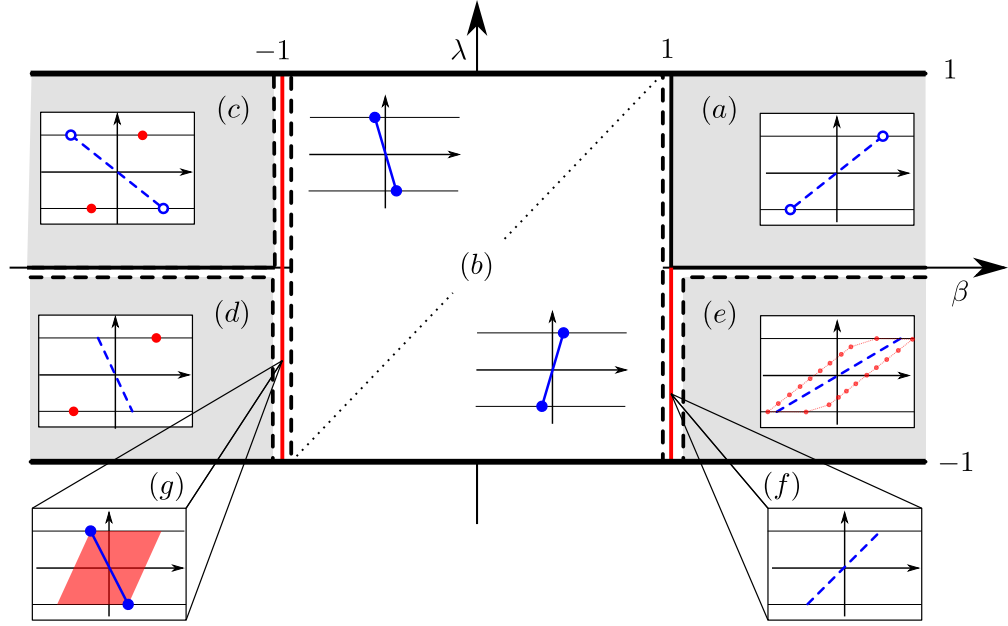


Figure 3.2. Bifurcation diagram. The segment  $EF$  of the fixed points is shown by the blue line. Stable fixed points are denoted by the solid line, unstable fixed points are shown by the dashed line. Stable end-points of  $EF$  are shown as filled blue discs; semi-stable points are denoted by empty blue discs; in the unstable case, no special notation is used. The dotted line in case (b) corresponds to the set of parameters leading to the infinite slope of the line  $EF$ . Periodic points are shown in red. Filled red discs in cases (c) and (d) correspond to the stable 2-periodic orbit  $\pm Q$ ; the red parallelogram in case (g) consists of stable 2-periodic orbits. Case (e) corresponds to complex dynamics when the system has periodic orbits with arbitrary large periods (see Theorem 3.2). One such orbit is sketched on the diagram. In the critical case (f), the segment  $EF$  attracts all the trajectories.

(e) *If  $\lambda < 0$ ,  $\beta > 1$ , then all the equilibrium points are unstable. System (3.1) has periodic orbits of all sufficiently large periods. At most one periodic orbit is stable.*

(f) *If  $\lambda < 0$ ,  $\beta = 1$ , then all the equilibrium points are unstable. Each trajectory either ends up at  $E$  or at  $F$ , or converges to the segment  $EF$ .*

(g) *If  $\beta = -1$ , then all the equilibrium points are stable. The parallelogram*

$$\Sigma = \left\{ (x, s) : 2 \frac{(1-\lambda)x - a}{1-\lambda+a} + 1 \leq s \leq 2 \frac{(1-\lambda)(x-1)}{1-\lambda+a} + 1, |s| \leq 1 \right\} \quad (3.4)$$

with the vertices  $E, F$ ,  $Q = (1, 1)$  and  $-Q = (-1, -1)$  consists of stable 2-periodic orbits and the diagonal  $EF$  of fixed points. Every non-equilibrium trajectory converges either to one of the equilibrium points  $E$  or  $F$ , or to a 2-periodic orbit in the parallelogram  $\Sigma$ .

The existence of infinitely many periodic orbits in case (e) indicates the presence of a global strange attractor or a chaotic attractor co-existing with the stable periodic orbit. More detailed analysis of this case will be a subject of future work.

Theorem 3.1 describes several bifurcation scenarios. In particular, the period doubling scenario (see case (g)) is a type of a border-collision degenerate flip bifurcation, which is typical for piecewise linear systems [35, 41, 104–106]. Specifics of the realization of this scenario in system (3.1) are dictated by the fact that 2-periodic orbits bifurcate from an interval of fixed points.

Let us consider  $\beta$  as a decreasing bifurcation parameter. When this parameter crosses the value  $-1$ , the equilibrium points of the segment  $EF$ , which are stable for  $\beta \in (-1, 1)$  (see case (b)), destabilize and the 2-periodic orbit (3.3) appears away from the segment  $EF$  (see cases (c) and (d)). This transition is accompanied by the creation of the parallelogram  $\Sigma$  filled with 2-periodic orbits at the critical value  $\beta = -1$  (case (g)). This parallelogram is spanned by the 2-periodic orbit  $\pm Q = (\pm 1, \pm 1)$  and the equilibrium points  $E, F$  (case (g)).

Assume that  $\lambda < 0$ . When the parameter  $\beta$  increases and crosses the value 1, the equilibrium points destabilize and infinitely many periodic orbits appear (see case (e)). Dynamics for the critical value  $\beta = 1$  is described by case (f). The following theorem complements case (e) of Theorem 3.1.

**Theorem 3.2.** *Assume that the conditions of case (e) of Theorem 3.1 hold and hence system (3.1) has infinitely many periodic orbits, of which at most one is stable. Then the relation  $(\lambda, \beta) \in \Omega_k$  with*

$$\Omega_k = \left\{ (\lambda, \beta) : \frac{\beta^k - 1}{\beta - 1} \leq -\frac{1}{\lambda} < \beta^k, \beta > 1, -\frac{1}{\lambda} > 1 \right\}, \quad (3.5)$$

where  $k \in \mathbb{N}$ , ensures that system (3.1) has a unique stable  $(2k + 2)$ -periodic orbit. If  $(\lambda, \beta) \notin \bigcup_{k=1}^{\infty} \Omega_k$ , then all the periodic orbits are unstable.

**Remark 3.3.** The domains  $\Omega_k$  of existence of stable periodic orbits with different periods do not intersect (see Figure 3.3).

**Remark 3.4.** It will follow from the proof of Theorem 3.2 that if  $(\lambda, \beta)$  belongs to the interior of  $\Omega_k$  for some  $k$ , then the corresponding stable periodic orbit is asymptotically stable.

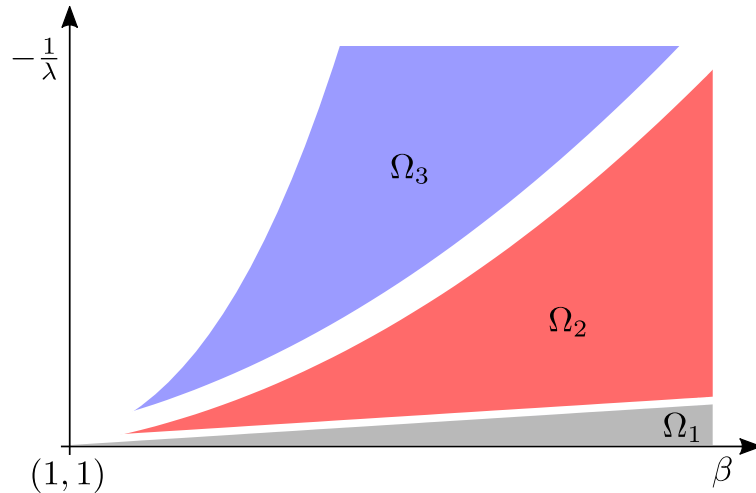


Figure 3.3. Domains  $\Omega_k$  of existence of a (unique) stable periodic orbit of period  $2k + 2$  in the coordinates  $\beta = \lambda + a > 1$  and  $-1/\lambda > 1$  for case (e) of Theorem 3.1.

### 3.3 Proofs

We will prove statements of Theorem 3.1 in the counter-clockwise order along the bifurcation diagram in Figure 3.2. Thus, we prove case (a) in Section 3.3.1, then case (b) for non-negative  $\lambda$  in Section 3.3.2. Proofs for cases (c) and (d) are presented in Sections 3.3.3 and Section 3.3.4, respectively. In Section 3.3.5, we present the proof of the remaining part of case (b)

for negative  $\lambda$ . Proofs of case (e) and of Theorem 3.2 are presented in Section 3.3.6. Finally, Sections 3.3.7 and 3.3.8 contain the proofs for critical cases (f) and (g), respectively.

We use the following notations:  $A_x$  and  $A_s$  will denote the  $x$  and  $s$  coordinates of a point  $A$  in the  $(x, s)$ -plain. Transformation (3.1) will be denoted by  $f$ . Throughout the proofs, we will use the variable  $p = x - s$  (output of the play operator, see Figure 3.1(b)). We will denote by  $A_p = A_x - A_s$  the  $p$ -coordinate of a point  $A$ .

Let us start with a few auxiliary lemmas. First, due to the fact that

$$f(-x, -s) = -f(x, s), \quad (3.6)$$

it is sufficient to present the proofs for a half of the phase space.

**Lemma 3.5.** *For any point  $A$  to the left of the segment  $EF$ , one has  $[f(A)]_x > A_x$ . For any point  $B$  to the right of the segment  $EF$ , one has  $[f(B)]_x < B_x$ .*

*Proof.* Since  $A$  lies to the left of the segment  $EF$ , one has  $(1 - \lambda)A_x < aA_s$ . Thus

$$[f(A)]_x = \lambda A_x + aA_s > \lambda A_x + (1 - \lambda)A_x = A_x.$$

The second statement follows from (3.6). ■

**Lemma 3.6.** *Let  $\beta > 0$ . Then for any two points  $A$  and  $B$  with the same  $p$ -coordinate  $A_p = B_p$ , from  $A_x > B_x$  it follows  $[f(A)]_x > [f(B)]_x$ .*

*Proof.* It suffices to note that  $[f(A)]_x = \lambda A_x + aA_s = \beta A_x - aA_p$ . ■

Denote by  $\Pi \subset L$  the parallelogram with the diagonal  $EF$ , two sides on the lines  $s = \pm 1$ , and two sides with slope 1:

$$\Pi = \left\{ (x, s) : |x - s| \leq \left| \frac{a}{1 - \lambda} - 1 \right|, |s| \leq 1 \right\}. \quad (3.7)$$

**Lemma 3.7.** *Let  $(x_0, s_0) \in \Pi$  and  $p_0 = x_0 - s_0$ . If either  $-1 < \beta < 0$  and  $|\beta x_0 - (a+1)p_0| \leq 1$  or  $0 \leq \beta < 1$ , then the trajectory with the initial point  $(x_0, s_0)$  satisfies  $p_t = p_0$  for all  $t \geq 0$  and  $(x_t, s_t) \rightarrow (x_*, s_*)$  as  $t \rightarrow \infty$ , where*

$$(x_*, s_*) = \left( -\frac{ap_0}{1-\beta}, -\frac{(1-\lambda)p_0}{1-\beta} \right) \quad (3.8)$$

*is a fixed point of  $f$  with  $x_* - s_* = p_0$ .*

*Proof.* Consider a sequence  $(x_t, s_t)$  defined by

$$x_{t+1} = \beta x_t + a(s_t - x_t), \quad s_{t+1} = x_{t+1} - x_t + s_t \quad (3.9)$$

and suppose that  $|s_t| \leq 1$  for all  $t$ . Then, this sequence is a trajectory of (3.1). Equations (3.9) are equivalent to the relations  $x_t - s_t = p_0$ ,  $x_{t+1} = \beta x_t - ap_0$ , which result in the explicit formulas

$$x_t - x_* = s_t - s_* = \beta^t(x_0 - x_*) = \beta^t(s_0 - s_*), \quad (3.10)$$

where we use the notation (3.8). Since  $s_0, s_* \in [-1, 1]$ , equations (3.10) imply  $|s_t| \leq 1$  for all  $t$  if  $0 \leq \beta < 1$ . Similarly, if  $-1 < \beta < 0$  and, in addition,  $|s_* + \beta(s_0 - s_*)| \leq 1$ , then equations (3.10) also imply  $|s_t| \leq 1$  for all  $t$ . By definition of  $s_*$ , we have  $s_* + \beta(s_0 - s_*) = \beta x_0 - (a+1)p_0$ , hence under the assumptions of the lemma, the sequence  $s_t$  defined by (3.10) satisfies  $|s_t| \leq 1$ , and therefore formulas (3.10) explicitly define a trajectory of (3.1). It remains to note that from (3.10), it follows that  $x_t - s_t = x_* - s_* = p_0$  and  $x_t \rightarrow x_*, s_t \rightarrow s_*$  for  $|\beta| < 1$ . ■

**Lemma 3.8.** *For  $0 \leq \lambda < 1$ ,  $\beta \leq 0$  and for  $-1 < \lambda \leq 0$ ,  $-1 \leq \beta \leq 0$  the parallelogram  $\Pi$  is invariant under the map (3.1).*

*Proof.* Let  $(x_t, s_t) \in \Pi$ , i.e.,  $|p_t| \leq \frac{1-\beta}{1-\lambda}$ . Since the upper-right and the lower-left vertices of  $\Pi$  are the points  $E' = \left(-\frac{a}{1-\lambda} + 2, 1\right)$  and  $F' = \left(\frac{a}{1-\lambda} - 2, -1\right)$ , respectively, it suffices to prove that

$$|x_{t+1}| \leq -\frac{a}{1-\lambda} + 2. \quad (3.11)$$

If  $0 \leq \lambda < 1$ ,  $\beta \leq 0$ , then

$$|x_{t+1}| \leq \lambda \frac{1-\beta}{1-\lambda} - \beta = -\frac{a}{1-\lambda},$$

which implies (3.11). If  $-1 < \lambda \leq 0$ ,  $-1 \leq \beta \leq 0$ , then

$$|x_{t+1}| \leq -\lambda \frac{1-\beta}{1-\lambda} - \beta,$$

which yields (3.11) because  $\lambda < 1$  and  $\lambda\beta \leq 1$ .

Using the definition of the saturation function  $\Psi$ , from the second equation of system (3.1) one can see that

$$p_{t+1} = p_t \text{ if } |s_{t+1}| < 1; \quad p_{t+1} \geq p_t \text{ if } s_{t+1} = 1; \quad p_{t+1} \leq p_t \text{ if } s_{t+1} = -1.$$

Combining these relations with (3.11), we obtain

$$p_{t+1} = p_t \text{ if } |s_{t+1}| < 1; \quad p_t \leq p_{t+1} \leq \frac{1-\beta}{1-\lambda} \text{ if } s_{t+1} = 1; \quad \frac{\beta-1}{1-\lambda} \leq p_{t+1} \leq p_t \text{ if } s_{t+1} = -1.$$

Hence, the relation  $|p_t| \leq \frac{1-\beta}{1-\lambda}$  always implies  $|p_{t+1}| \leq \frac{1-\beta}{1-\lambda}$ , which is equivalent to the implication  $(x_t, s_t) \in \Pi \Rightarrow (x_{t+1}, s_{t+1}) \in \Pi$ . ■

**Lemma 3.9.** *System (3.1) has a 2-periodic orbit if and only if  $\beta \leq -1$ . If  $\beta < -1$ , then a 2-periodic orbit is unique and consists of the point  $\pm Q$  defined by (3.3).*

*Proof.* A 2-periodic orbit  $A_1 = (x_1^*, s_1^*)$ ,  $A_2 = f(A_1) = (x_2^*, s_2^*)$  of (3.1) satisfies

$$x_1^* = \lambda x_2^* + a s_2^*, \quad x_2^* = \lambda x_1^* + a s_1^*, \quad (3.12)$$

where we assume without loss of generality that  $s_1^* \leq s_2^*$ . It follows from the definition of the stop operator that if the input sequence  $x_t$  and the output sequences  $s_t$  of this operator are 2-periodic, then either  $x_t - s_t = \text{const}$  or  $s_t$  alternates between the values  $\pm 1$ . Hence, the same is true for a 2-periodic orbit, i.e., either  $x_1^* - x_2^* = s_1^* - s_2^*$  or  $s_1^* = -s_2^* = -1$ . In the former case, dividing the difference of equations (3.12) by  $x_1^* - x_2^*$  gives  $\beta = -1$  and



conversely, it is straightforward to check that if  $\beta = -1$ , then all points of the parallelogram  $\Sigma$  (cf. (3.4)) except for the diagonal  $EF$  are 2-periodic (see case (g) of Theorem 3.1). In the latter case  $s_1^* = -s_2^* = -1$ , formulas (3.12) imply

$$x_1^* = -x_2^* = \frac{a}{1 + \lambda},$$

i.e., points  $A_1, A_2$  coincide with (3.3). The equality  $A_2 = f(A_1)$  is ensured by formulas (3.12) and, additionally, the relations  $s_2^* = \Psi(x_2^* - x_1^* + s_1^*)$ ,  $s_1^* = \Psi(x_1^* - x_2^* + s_2^*)$ , which due to  $A_1 = Q$ ,  $A_2 = -Q$  are equivalent to

$$1 = \Psi\left(-1 - \frac{2a}{1 + \lambda}\right).$$

This last equation is equivalent to  $\beta \leq -1$ . ■

### 3.3.1 Case (a)

In this case,  $\lambda \geq 0$  and  $\beta \geq 1$ . Therefore  $a > 0$  and the slope of the segment  $EF$  of equilibrium points is positive and less than or equal to 1 as shown in Figure 3.4.

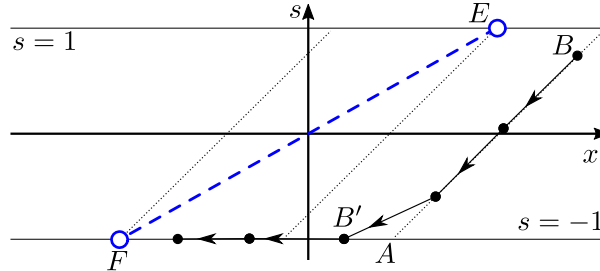


Figure 3.4.  $\lambda \geq 0$ ,  $\beta \geq 1$ . A trajectory starting at a point  $B$  to the right of the segment  $EF$  converges to the fixed point  $F$ . Dotted lines have slope 1.

Consider a point  $B$  which lies to the right of the segment  $EF$ . Denote by  $A$  the intersection point of the lines  $p = B_p$  and  $s = -1$ . Let  $B'$  denote the point at which the trajectory  $\{f^t(B)\}$  hits the line  $s = -1$  for the first time. From Lemma 3.5 it follows that  $[f^{-1}(B')]_x > A_x$ , and  $[f(A)]_x > F_x$  since  $\lambda > 0$ . Thus, from Lemma 3.6 we obtain  $B'_x > F_x$ .

Since  $B'_s = -1$ , it follows that  $[f(B')]_x - F_x = \lambda(B'_x - F_x)$ . Hence, due to  $\lambda \in [0, 1)$ , the trajectory converges to the equilibrium  $F$  along the line  $s = -1$  (see Figure 3.4). We conclude that every trajectory that starts to the right of the segment  $EF$  of equilibrium points, converges to  $F$ . Every trajectory which starts to the left of  $EF$  converges to  $E$  due to (3.6).

### 3.3.2 Case (b), $\lambda \geq 0$

#### 3.3.2.1 First assume that $0 < \beta < 1$ .

In this case, the segment  $EF$  has a positive slope greater than 1 if  $a > 0$  and non-positive if  $a \leq 0$ . Let us consider the trajectory of a point  $A$  that belongs to the parallelogram  $\Pi$  defined by (3.7), see Figure 3.5. Then, by Lemma 3.7, this trajectory converges to the fixed point  $P^*$ , which lies at the intersection of the line  $p = A_p$  with the segment  $EF$ . By Lemma 3.6, all the other trajectories that start to the right of the parallelogram  $\Pi$ , move down along the line  $p = \text{const}$  until they hit the line  $s = -1$  and then monotonically converge to the equilibrium point  $F$  along this line from the right, see Figure 3.5(a).

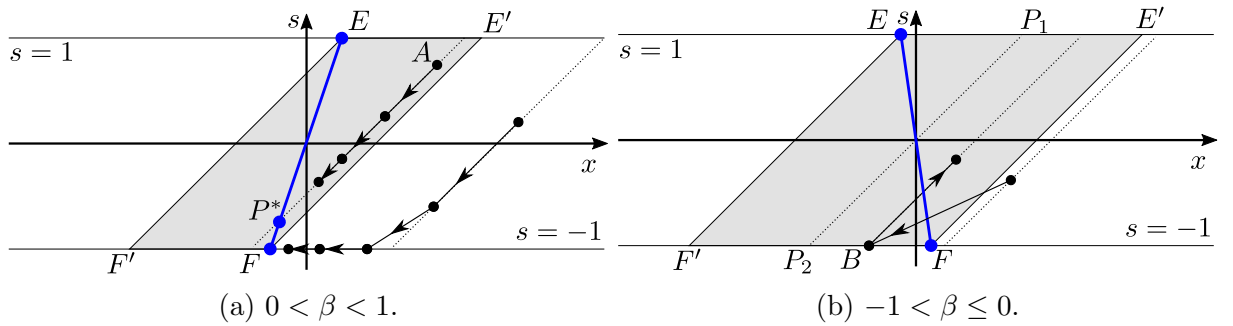


Figure 3.5. Theorem 3.1(b). Case  $\lambda \geq 0$ . Dotted lines have slope 1. The shaded area is the parallelogram  $\Pi = EE'FF'$ .

#### 3.3.2.2 Now assume that $-1 < \beta \leq 0$ .

In this case,  $a < 0$  and the segment  $EF$  has a negative slope as in Figure 3.5(b). If a trajectory starts to the right of the parallelogram  $\Pi$ , then, since  $\beta \leq 0$ , it hits the line

$s = -1$  after one iteration. If it hits the line to the right of the equilibrium  $F$ , then the trajectory converges to this equilibrium along the line  $s = -1$  from the right due to  $\lambda \geq 0$ . On the other hand, if this trajectory hits the line  $s = -1$  at a point  $B$  to the left of the point  $F$ , then  $B$  belongs to the parallelogram  $\Pi$ . In order to show this, we note that for the previous point  $f^{-1}(B) = (x_t, s_t)$ , we have

$$x_t - s_t > -\frac{a}{1-\lambda} + 1,$$

because the point  $(x_t, s_t)$  lies to the right of the parallelogram  $\Pi$ . Therefore,

$$\begin{aligned} x_{t+1} &= \lambda x_t + a s_t > \lambda \left( -\frac{a}{1-\lambda} + 1 + s_t \right) + a s_t \\ &\geq \lambda \left( -\frac{a}{1-\lambda} + 1 \right) + \lambda + a. \end{aligned}$$

This last expression is greater than  $F'_x = \frac{a}{1-\lambda} - 2$ , which is the  $x$ -coordinate of the lower left vertex of the parallelogram  $\Pi$ .

Consider points on the horizontal sides of  $\Pi$ . To be definite, assume that  $s_t = -1$ . Denote by  $P_1 = (1, 1)$  and  $P_2 = (-1, -1)$  the middle points of  $EE'$  and  $FF'$ , respectively. If  $(x_t, s_t) \in P_2F$ , then the conditions of Lemma 3.7 are satisfied, and the trajectory converges to the equilibrium along the line  $p = \text{const}$ . Let  $(x_t, s_t) \in F'P_2$ . If  $s_{t+1} < 1$ , then, again using Lemma 3.7, the trajectory converges to the equilibrium along the line  $p = \text{const}$ . If  $s_{t+1} = 1$ , then  $(x_{t+1}, s_{t+1}) \in EP_1$  because  $x_{t+1} = \lambda x_t - a \leq -\lambda - a < 1$ . Since the segments  $EP_1$  and  $P_2F$  are centrally symmetric, and the function  $f$  is odd, this trajectory also converges to the equilibrium along the line  $p = \text{const}$ .

It remains to consider points in  $\Pi$  that belong to the open band  $|s| < 1$ . A trajectory starting from such a point either converges to an equilibrium along the line  $p = \text{const}$  without hitting the lines  $s = \pm 1$ , or hits one of these lines and then converges to an equilibrium as discussed above.

### 3.3.3 Case (c)

As in the previous case,  $a < 0$  and the segment  $EF$  has a negative slope (see Figure 3.6). In this case, by Lemma 3.9, there is a unique 2-periodic orbit consisting of the points  $\pm Q$  defined by (3.3).

Now we consider dynamics of trajectories starting in different parts of the phase space.

#### 3.3.3.1 Denote

$$A = \left( \frac{a+2}{1-\lambda}, 1 \right), \quad B = \left( \frac{1}{\lambda} \left( -\frac{a+2}{1-\lambda} - a \right), 1 \right). \quad (3.13)$$

If  $\lambda = 0$ , we formally set  $B_x = \infty$  and replace the segment  $AB$  below by the corresponding half-line. Note that  $B_x > A_x$  and  $Q \in AB$ .

The following lemma ensures that if the point  $B$  lies to the right of the point  $E'$ , then any trajectory starting from the segment  $AE'$  converges to a 2-periodic orbit.

**Lemma 3.10.** *Under the hypothesis of Theorem 3.1 (c), the segment  $AB$  is invariant under the second iteration  $f^2$  of the map  $f$  and  $f^2$  is a contraction on  $AB$ .*

*Proof.* First, we note that if a point  $(x_t, s_t)$  lies on the line  $s = 1$  to the right of the point  $A$ , then the image  $(x_{t+1}, s_{t+1}) = f(x_t, s_t)$  of this point under the map (3.1) belongs to the line  $s = -1$ . Indeed,

$$x_{t+1} - x_t = \lambda x_t + a - x_t \leq (\lambda - 1)A_x + a = -2,$$

which implies  $s_{t+1} = -1$ . By (3.6), the points of the line  $s = -1$  lying to the left of  $-A$  are mapped to the line  $s = 1$ . Furthermore, if a point  $(x_t, s_t)$  lies on the line  $s = 1$  between the points  $A$  and  $B$ , then its image  $f(x_t, s_t) = (\lambda x_t + a, s_{t+1})$  lies on the line  $s = -1$  to the left of the point  $-A$ , and therefore the second iteration  $f^2(x_t, s_t)$  belongs to the line  $s = 1$ . Hence, the segment  $AB$  is mapped by the second iteration  $f^2$  to the line  $s = 1$ . Therefore, it remains to show that the scalar function  $\phi(y) = [f^2(y, 1)]_x$  maps the interval  $[A_x, B_x] \ni y$

into itself and is a contraction on this interval. To this end, note that  $\phi(y) = \lambda^2 y + \lambda a - a$  on  $[A_x, B_x]$ , that is  $\phi$  is a linear function with the positive coefficient  $\lambda^2 < 1$ . Thus, we just need to check that  $A_x \leq \phi(A_x)$  and  $\phi(B_x) \leq B_x$ . Indeed, since

$$\phi(A_x) = \frac{-a + 2\lambda^2 + 2a\lambda}{1 - \lambda},$$

the inequality

$$\frac{-a + 2\lambda^2 + 2a\lambda}{1 - \lambda} > \frac{a + 2}{1 - \lambda},$$

which is equivalent to  $(\lambda - 1)(\beta + 1) > 0$ , ensures that  $A_x < \phi(A_x)$ . To show that  $\phi(B_x) \leq B_x$ , it is sufficient to establish the following inequality:

$$\lambda^2 \left( \frac{-2a - 2 + a\lambda}{\lambda(1 - \lambda)} \right) + a(\lambda - 1) < \frac{-2a - 2 + a\lambda}{\lambda(1 - \lambda)}.$$

After a simple manipulation, this inequality follows from  $\beta + 1 < 0$ . ■

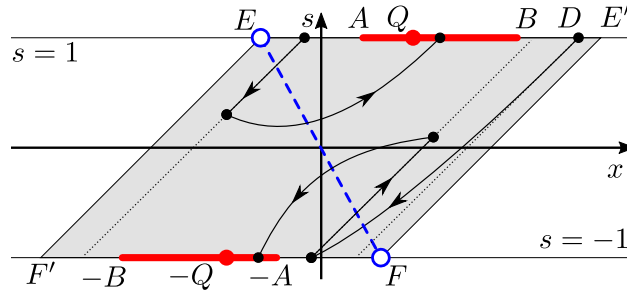


Figure 3.6. Case  $\lambda \geq 0$ ,  $\beta < -1$ . Each of the red segments  $AB$  and  $-AB$  is mapped into itself by  $f^2$ .

**3.3.3.2** Next, we consider the situations where  $B$  lies to the right of  $E'$  and where  $B$  lies between  $A$  and  $E'$ , respectively. In the former case, any trajectory starting between  $A$  and  $E'$  converges to the 2-periodic orbit due to the above argument. Consider the latter case. Let a trajectory start on the upper side of the parallelogram  $\Pi$  to the right of the point  $B$  at a point  $D = (x_t, 1)$ , see Figure 3.6. The image  $f(D) = (x_{t+1}, -1)$  of this point lie on

the line  $s = -1$  to the right of the point  $-A$ . Therefore,  $f^2(D)$  belong to the interior of the strip  $L$ . Since  $\beta < -1$ , further iterations  $f^{t+k}(D)$  belong to the line  $s = -1$  for odd  $k$  and to the interior of  $L$  for even  $k$ , and the  $x$ -coordinate of the odd iterations monotonically decreases until the trajectory reaches the half-line  $\{(x, s) : x \leq -A_x, s = -1\}$ . Without loss of generality, we can assume that  $f(D)$  is the last point of the trajectory, which is still to the right of the point  $-A$  on the line  $s = -1$ . Let us show that the point  $(x_{t+3}, -1)$  lies to the right of the point  $(\frac{a}{1+\lambda}, -1)$ . To this end, we note that

$$\begin{aligned}(x_{t+2}, s_{t+2}) &= (\lambda x_{t+1} - a, -1 + \lambda x_{t+1} - a - x_{t+1}), \\ x_{t+3} &= \lambda^2 x_{t+1} - \lambda a + a(-1 + \lambda x_{t+1} - a - x_{t+1}).\end{aligned}$$

Thus, we need to show that  $x_{t+1} > -\frac{a+2}{1-\lambda}$  implies

$$\lambda^2 x_{t+1} - \lambda a + a(-1 + \lambda x_{t+1} - a - x_{t+1}) > \frac{a}{1+\lambda}, \quad (3.14)$$

i.e.,

$$(\lambda^2 + a\lambda - a)x_{t+1} - a(\beta + 1) > \frac{a}{1+\lambda}.$$

Since  $\lambda^2 + a\lambda - a > 1$ , it suffices to show (3.14) for  $x_{t+1} = -\frac{a+2}{1-\lambda}$ , i.e.,

$$(\lambda^2 + a\lambda - a) \left( -\frac{a+2}{1-\lambda} \right) - a(\beta + 1) > \frac{a}{1+\lambda}.$$

But this is equivalent to

$$\lambda^2(\beta + 1) < 0,$$

which is true in the case we are considering. We see that the point  $(x_{t+3}, -1)$  belongs to the segment connecting the points  $-A$  and  $-B$ , which is invariant for the map  $f^2$  by Lemma 3.10. Hence the trajectory converges to the 2-periodic orbit.

**3.3.3.3** Next, we consider a trajectory which starts at a point  $D'$  on the line  $s = 1$  to the left of the point  $A$  in the parallelogram  $\Pi$ . For this trajectory, further odd iterations  $f^k(D')$

lie in the interior of  $L$ , while the even iterations  $f^k(D')$  belong to the line  $s = 1$ , and the  $x$ -coordinate of the even iterations monotonically increases until the trajectory reaches the segment  $AB$ . (This behaviour is similar to the behaviour that we considered in paragraph 2 of section 3.3.2.2). Hence, such a trajectory also converges to the 2-periodic orbit.

The above cases cover all the initial conditions from the upper side  $EE'$  of  $\Pi$ . Since the map  $f$  is odd, trajectories starting at the lower side  $F'F$  have similar behavior.

Any trajectory that starts in the parallelogram  $\Pi$ , but not on the lines  $s = \pm 1$  and not on the segment of equilibrium points, will stay inside  $\Pi$  because of Lemma 3.8. It reaches one of the lines  $s = \pm 1$  in several iterations due to the condition  $\beta < -1$ . Thus, we see that all the trajectories that start in the parallelogram  $\Pi$  except for the segment of equilibrium points, converge to the 2-periodic orbit.

**3.3.3.4** Finally, let us consider a trajectory that starts to the right of the parallelogram  $\Pi$ . Since  $\beta < 0$ , this trajectory reaches the line  $s = -1$  after one iteration. If it reaches this line to the right of the equilibrium point  $F$ , then it will move to the left along the line  $s = -1$  and converge to the equilibrium point  $F$  from the right. On the other hand, if a trajectory reaches the line  $s = -1$  at a point, which lies to the left of the point  $F$ , then this point belongs to  $\Pi$ . This can be shown exactly in the same way as we did in Section 3.3.2. Therefore, such a trajectory converges to the 2-periodic orbit. We conclude that the 2-periodic orbit is stable and its basin of attraction contains the parallelogram  $\Pi$  with the exception of equilibrium points. However, some trajectories from outside the parallelogram  $\Pi$  are attracted to the semi-stable equilibrium points  $E$  and  $F$ .

### 3.3.4 Case (d)

In this case,  $a < 0$  and the segment  $EF$  has a negative slope (see Figure 3.7). Like in Section 3.3.3, there exists a 2-periodic orbit  $\pm Q$  defined by (3.3). Let  $A$  be as in (3.13).

First, we note that if a point  $(x_t, -1)$  satisfies  $x_t \leq -A_x$ , then  $x_{t+1} > \frac{a+2}{1-\lambda}$ ,  $s_{t+1} = 1$ . Hence the half-line  $\{(x, s) : x \leq -A_x, s = -1\}$  is mapped to itself under  $f^2$ . Since  $x_{t+2} = \lambda^2 x_t - \lambda a + a$  and  $\lambda^2 < 1$ , any trajectory starting at this half-line converges to the 2-periodic orbit  $\pm Q$ .

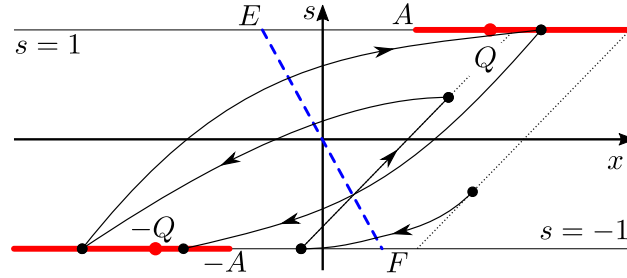


Figure 3.7. Case  $\lambda < 0$ ,  $\beta < -1$ . Red half-lines are mapped to themselves by  $f^2$ .

If a point belongs to the open segment  $\{(x, s) : -A_x < x < \frac{-a}{1-\lambda}, s = -1\}$ , then its trajectory enters the half-line  $\{(x, s) : x \leq -A_x, s = -1\}$  after finitely many iterations because  $\beta < -1$  (like in Section 3.3.3). Hence, the half-line  $\{(x, s) : x < \frac{-a}{1-\lambda}, s = -1\}$  belongs to the basin of attraction of the 2-periodic orbit. If a point belongs to the half-line  $\{(x, s) : x > \frac{-a}{1-\lambda}, s = -1\}$ , then its first iteration is in the half-line  $\{(x, s) : x < \frac{-a}{1-\lambda}, s = -1\}$  because  $\lambda < 0$ . Hence, we conclude that the lines  $s = -1$  and  $s = 1$  (except for the equilibria  $F$  and  $E$ , respectively) belong to the basin of attraction of the 2-periodic orbit.

Finally, all trajectories that start inside the strip  $-1 < s < 1$ , except for the equilibrium points, will reach one of the lines  $s = \pm 1$  after finitely many iterations because  $\beta < -1$ . Therefore, the 2-periodic orbit attracts all the trajectories except for the equilibrium points and their pre-images under the iterations  $f^k$  of the map  $f$ .

### 3.3.5 Case (b), $\lambda < 0$

#### 3.3.5.1 First assume that $-1 < \beta < 0$ .



For the point  $(x_t, s_t)$  to the right of the parallelogram  $\Pi$ , one has

$$x_t - s_t > p^* = 1 - x^* = 1 - \frac{a}{1 - \lambda},$$

and so  $x_{t+1} < \lambda p^* - \beta = -x^*$ , hence the point  $(x_{t+1}, s_{t+1})$  lies to the left of the equilibrium  $F$  on the line  $s = -1$ , see Figure 3.8(a). Due to (3.6), for the point  $(x_t, s_t)$  to the left of  $\Pi$ , its image will lie on the line  $s = 1$  to the right of the point  $E$ .

Now, we prove that every trajectory enters  $\Pi$ . Arguing by contradiction, let us show that if a trajectory never entered  $\Pi$ , then the distance from the trajectory to  $\Pi$  would exponentially decrease. This would imply that such a trajectory converges to a 2-periodic orbit, because, as we have seen, its points belong to the union of the lines  $s = \pm 1$  and the sign of  $s_t$  alternates at every iteration. However, this is impossible as a 2-periodic orbit does not exist in the case we are considering due to Lemma 3.9.

In order to see that the distance from a trajectory to  $\Pi$  exponentially decreases, it is sufficient to establish the inequality

$$q \left( \frac{a}{1 - \lambda} - 2 - x_t \right) > \lambda x_t - a + \frac{a}{1 - \lambda} - 2$$

for  $x_t < \frac{a}{1 - \lambda} - 2$  and some  $q \in (-\lambda, 1)$  independent of  $t$ . This inequality can be written as

$$x_t < \frac{a - \left(\frac{a}{1 - \lambda} - 2\right)(1 - q)}{q + \lambda}.$$

Thus we need to show that

$$\frac{a}{1 - \lambda} - 2 < \frac{a - \left(\frac{a}{1 - \lambda} - 2\right)(1 - q)}{q + \lambda},$$

which is equivalent to  $(1 + \lambda) \left(\frac{a}{1 - \lambda} - 2\right) < a$  and, further, to  $\beta\lambda < 1$ . Since the last inequality is true in the case being considered, we can use any  $q \in (-\lambda, 1)$ . The above argument shows that every trajectory enters the parallelogram  $\Pi$ .

Since  $\beta \in (-1, 0)$  and  $\lambda \in (-1, 0)$ , it follows from Lemma 3.8 that  $\Pi$  is invariant for the map  $f$ . Further, we note that if some iteration of a point from  $\Pi$  is mapped in the interior of  $L$ , then the trajectory converges to an equilibrium due to  $|\beta| < 1$ , see Figure 3.8(a).

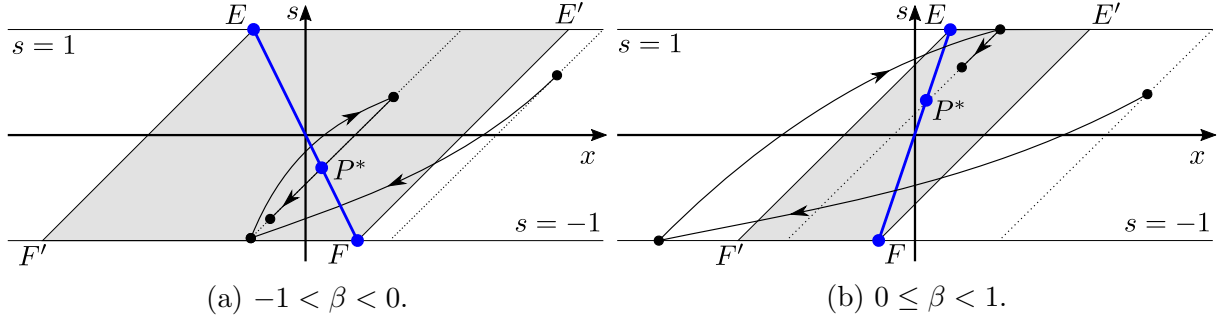


Figure 3.8. Theorem 3.1(b). Case  $\lambda < 0$ .

Finally, let us show that a trajectory cannot jump from the line  $s = 1$  to the line  $s = -1$  and back all the time. Indeed, if this was the case, then a point  $(x_t, 1)$  from this trajectory would satisfy  $x_t > 1$  and the point  $(x_{t+1}, -1)$  would satisfy  $x_{t+1} = \lambda x_t + a < -1$ . But inequalities  $-1 < \beta$  and  $x_t > 1$  imply that  $-1 - (\lambda x_t + a) < x_t - 1$ . In other words,  $0 < -1 - x_{t+1} < x_t - 1$  and, similarly,  $0 < x_{t+2} - 1 < -1 - x_{t+1}$ . Therefore, this trajectory would converge to the 2-periodic orbit, which does not exist in this case due to Lemma 3.9. This contradiction implies that every trajectory converges to an equilibrium point.

### 3.3.5.2 Now assume that $0 \leq \beta < 1$ .

In this case,  $a > 0$  and so the slope of the segment  $EF$  is greater than 1 (see Figure 3.8(b)). If a trajectory starts in  $\Pi$ , then it converges to an equilibrium point  $P^* \in EF$  along the line  $p = \text{const}$ .

A trajectory starting to the right of the parallelogram  $\Pi$  moves along the line  $p = \text{const}$  down and left until it reaches the line  $s = -1$ . At this point, or at the next iteration step, the trajectory reaches a point  $(x_t, -1)$  that lies to the left of the equilibrium point  $F$  because  $\lambda < 0$ . If  $(x_t, -1) \in \Pi$ , then the trajectory converges to an equilibrium due to Lemma 3.7. If the point  $(x_t, -1)$  lies to the left of the parallelogram  $\Pi$ , then let us show that the absolute value  $|x_t - s_t| = -1 - x_t$  of the  $p$ -coordinate of this point is less than the absolute value  $|x_{t-1} - s_{t-1}| = x_{t-1} - s_{t-1}$  of the  $p$ -coordinate of its pre-image  $(x_{t-1}, s_{t-1})$ . Moreover, we

want to show that  $|x_t - s_t| < q|x_{t-1} - s_{t-1}|$  with some  $q \in (-\lambda, 1)$  independent of the point  $(x_{t-1}, s_{t-1})$ . In other words, since  $x_t = \lambda x_{t-1} + a s_{t-1}$  and  $s_t = -1$ , we want to establish that

$$-(\lambda x_{t-1} + a s_{t-1} + 1) < (x_{t-1} - s_{t-1})q, \quad (3.15)$$

which is equivalent to

$$x_{t-1} - s_{t-1} > \frac{-\beta s_{t-1} - 1}{q + \lambda}.$$

Indeed, since the point  $(x_{t-1}, s_{t-1})$  lies to the right of  $\Pi$ , we have  $x_{t-1} - s_{t-1} > \frac{-a}{1-\lambda} + 1$  and it remains to show that

$$\frac{-a}{1-\lambda} + 1 > \frac{-\beta s_{t-1} - 1}{q + \lambda}.$$

This inequality is equivalent to

$$1 + q > -\beta s_{t-1}(1 - \lambda) + \beta(q + \lambda). \quad (3.16)$$

If we set  $q = -\lambda + \varepsilon$  with a sufficiently small  $\varepsilon > 0$ , then  $q \in (0, 1)$  and the inequalities  $|s_{t-1}| \leq 1$  and  $0 \leq \beta < 1$  imply that

$$-\beta s_{t-1}(1 - \lambda) < 1 - \lambda, \quad \beta(q + \lambda) = \varepsilon(\lambda + a) < \varepsilon,$$

hence the relation (3.16) holds.

Since  $q$  in (3.15) does not depend on  $(x_{t-1}, s_{t-1})$  and the segment connecting the points  $P_1 = (1, 1)$  and  $P_2 = (-1, -1)$  belongs to the interior of  $\Pi$ , all trajectories that start outside the parallelogram  $\Pi$  will eventually enter  $\Pi$  and converge to one of the equilibrium points.

### 3.3.6 Case (e)

In this case,  $a > 0$  and the slope of the segment  $EF$  is positive and less than 1 (see Figure 3.9). We divide the proof of this case into five parts.

**3.3.6.1** Denote by  $l_1$  and  $l_2$  the open half-lines starting at the point  $E$  on the upper boundary of the strip  $L$ :

$$l_1 = \left\{ (x, s) : x > \frac{a}{1-\lambda}, s = 1 \right\}, \quad l_2 = \left\{ (x, s) : x < \frac{a}{1-\lambda}, s = 1 \right\}$$

and by  $l_3$  and  $l_4$  the half-lines starting from the point  $F$  on the lower boundary of the strip  $L$ :

$$l_3 = \left\{ (x, s) : x < -\frac{a}{1-\lambda}, s = -1 \right\}, \quad l_4 = \left\{ (x, s) : x > -\frac{a}{1-\lambda}, s = -1 \right\}.$$

From the condition  $\lambda < 0$  it follows that  $f(l_2) \subseteq l_1$  and  $f(l_4) \subseteq l_3$ . Also from Lemma 3.5 it follows that for any point  $(x_t, s_t)$  such that  $x_t > \frac{as_t}{1-\lambda}$  one has  $x_{t+1} < x_t$ . Thus, starting from  $l_1$ , any trajectory arrives after finitely many iterations to the closed half-line  $\bar{l}_3$ . Hence, we can define the first-hitting map  $\mathcal{P} : l_1 \rightarrow \bar{l}_3$  as  $\mathcal{P}(A) = f^k(A)$  where  $f^k(A) \in \bar{l}_3$  and  $f^i(A) \notin \bar{l}_3$  for  $i = 0, \dots, k-1$ . This map can be represented by the scalar function  $T : (\frac{a}{1-\lambda}, \infty) \rightarrow [\frac{a}{1-\lambda}, \infty)$  defined by the formula

$$(-T(x), -1) = \mathcal{P}(x, 1), \quad x \in \left( \frac{a}{1-\lambda}, \infty \right). \quad (3.17)$$

It is convenient to set  $T(\frac{a}{1-\lambda}) = \frac{a}{1-\lambda}$  and consider  $T$  as a map of the half-line  $[\frac{a}{1-\lambda}, \infty)$  into itself.

**3.3.6.2** In this part, we describe the structure of the function  $T(x)$ . We begin with the following observation.

**Lemma 3.11.** *Let  $(x_0, 1) \in l_1$  be a point such that the first  $t-1$  iterations of it under the map  $f$  belong to the line  $p = \text{const}$ . Then for any  $m \leq t$  we have*

$$x_m = \beta^m x_0 - a(x_0 - 1) \sum_{i=0}^{m-1} \beta^i. \quad (3.18)$$

*Proof.* For  $m = 1$  equation (3.18) is obvious. Suppose that (3.18) holds for  $m < t$ . Then

$$x_{m+1} = \lambda x_m + a(1 + x_m - x_0) = \beta^{m+1}x_0 - a(x_0 - 1) \sum_{i=0}^m \beta^i.$$

■

Let us show that for any  $k \in \mathbb{N}$  there exists a unique point  $(r_k, 1) \in l_1$  such that its first  $k - 1$  iterations under the map  $f$  belong to the line  $p = \text{const}$  and its  $k$ -th iteration is  $(r_k - 2, -1)$ . Setting  $m = k$ ,  $x_0 = r_k$ , and  $x_m = r_k - 2$  in (3.18), we obtain

$$r_k = \frac{2 + a \frac{1-\beta^k}{1-\beta}}{1 - \beta^k + a \frac{1-\beta^k}{1-\beta}} \quad (3.19)$$

(it is easy to see that the denominator does not vanish as long as  $f^i(r_k, 1)$  belongs to the interior of  $L$  for  $i = 1, \dots, k - 1$ ).

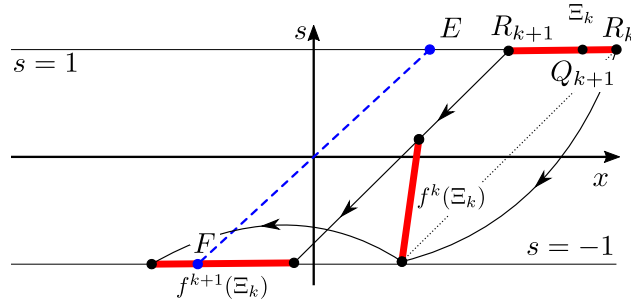


Figure 3.9. The segment  $\Xi_k$  and its images  $f^k(\Xi_k)$  and  $f^{k+1}(\Xi_k)$ .

Next we show that for any  $k \in \mathbb{N}$  there exists a unique point  $Q_k = (q_k, 1) \in l_1$  such that its first  $k - 1$  iterations under the map  $f$  belong to the line  $p = \text{const}$  and its  $k$ -th iteration is  $F$ .

Obviously,  $q_1 = \frac{1}{\lambda}(-a - \frac{a}{1-\lambda})$ . Set  $R_i = (r_i, 1)$  and consider the  $k$ -th iteration of the segment  $\Xi_k = R_{k+1}R_k$ . The point  $R_k$  is mapped to the point  $(r_k - 2, -1)$ , and the image of the point  $R_{k+1}$  belongs to the interior of  $L$ . Hence,  $f^k(\Xi_k)$  is a segment which lies entirely to the right of the segment  $EF$  and all its points except  $f^k(R_k)$  belong to the interior of  $L$ .

Consider the  $(k + 1)$ th iteration of  $\Xi_k$ . The point  $f^{k+1}(R_k)$  lies on the line  $s = -1$  to the left of the point  $F$ , while  $f^{k+1}(R_{k+1}) = (r_{k+1} - 2, -1)$ . Hence,  $f^{k+1}(\Xi_k)$  is a segment on the line  $s = -1$  and  $F \in f^{k+1}(\Xi_k)$ , see Figure 3.9. Hence, there exists a point  $q_{k+1} \in (r_{k+1}, r_k)$  for each  $k \in \mathbb{N}$ . Now  $q_k$  can be found in a unique way using Lemma 3.11 by setting  $m = k$ ,  $x_0 = q_k$ , and  $x_m = \frac{-a}{1-\lambda}$ :

$$q_k = \frac{-\frac{a}{1-\lambda} - a\frac{1-\beta^k}{1-\beta}}{\beta^k - a\frac{1-\beta^k}{1-\beta}}. \quad (3.20)$$

Since  $\lambda < 0$  and  $\beta > 1$ , the denominator does not vanish. Note that

$$q_1 > r_1 > q_2 > r_2 > \cdots > \frac{a}{1-\lambda}, \quad q_k, r_k \rightarrow \frac{a}{1-\lambda} \text{ as } k \rightarrow \infty. \quad (3.21)$$

It follows from the relation  $(r_k - 2, -1) = f^k(R_k)$  that  $f^{k+1}(R_k) = (\lambda(r_k - 2) - a, -1)$ , i.e.,

$$T(r_k) = a - \lambda(r_k - 2). \quad (3.22)$$

Combining (3.21) and (3.22), we see that

$$\begin{aligned} T(r_1) &> T(r_2) > T(r_3) > \cdots, \\ T(r_k) - \frac{a}{1-\lambda} &\rightarrow T_* > 0 \text{ as } k \rightarrow \infty, \end{aligned} \quad (3.23)$$

where

$$T_* = \frac{2\lambda(1-a-\lambda)}{1-\lambda}. \quad (3.24)$$

Furthermore, let us show that the function  $T(x)$  is linear for  $x \in [q_1, \infty)$ ,  $x \in [q_{k+1}, r_k]$ , and  $x \in [r_k, q_k]$ ,  $k = 1, 2, \dots$ . This will imply that  $T(x)$  is continuous for  $x \in (a/(1-\lambda), \infty)$ . Indeed, consider  $x \in [q_{k+1}, r_k]$ , i.e.,  $(x, 1) \in Q_{k+1}R_k \subset \Xi_k$  (see Figure 3.9). By (3.17) it suffices to show that  $\mathcal{P}$  is affine linear on  $Q_{k+1}R_k$ . But  $\mathcal{P}$  is a composition of  $k$  maps each of which is given by

$$\begin{cases} x_{t+1} = \lambda x_t + a s_t, \\ s_{t+1} = s_t + x_{t+1} - x_t \end{cases} \quad (3.25)$$

(see (3.1) with  $\Psi(\tau) = \tau$ ) with the map

$$\begin{cases} x_{t+1} = \lambda x_t + a s_t, \\ s_{t+1} = -1 \end{cases} \quad (3.26)$$

(see (3.1) with  $\Psi(\tau) = -1$ ). Since (3.25) and (3.26) are affine linear, so is  $\mathcal{P}$ . The cases  $x \in [q_1, \infty)$  and  $x \in [r_k, q_k]$  can be treated analogously.

Using (3.19), (3.20), and (3.22), we see that  $T(x)$  increases on the intervals  $(q_1, \infty)$  and  $(q_k, r_{k-1})$ ,  $k = 2, 3, \dots$  with

$$T'(x) = -\lambda, \quad x \in (q_1, \infty), \quad T'(x) = -\left(\beta^k - a \frac{1 - \beta^k}{1 - \beta}\right), \quad x \in (q_k, r_{k-1}), \quad (3.27)$$

respectively, and decreases on the intervals  $(r_k, q_k)$ ,  $k \in \mathbb{N}$ , with

$$T'(x) = -\lambda \left(\beta^k - a \frac{1 - \beta^k}{1 - \beta}\right), \quad x \in (r_k, q_k), \quad (3.28)$$

see Figure 3.10. Every point  $x \in [q_1, \infty)$  possesses the property that  $f(x, 1) \in l_3$ . Every point  $x \in [q_{k+1}, q_k)$ ,  $k \in \mathbb{N}$ , possesses the property that the  $(k + 1)$ th iteration of the point  $(x, 1) \in l_1$  under the map  $f$  reaches the half-line  $l_3$  for the first time.

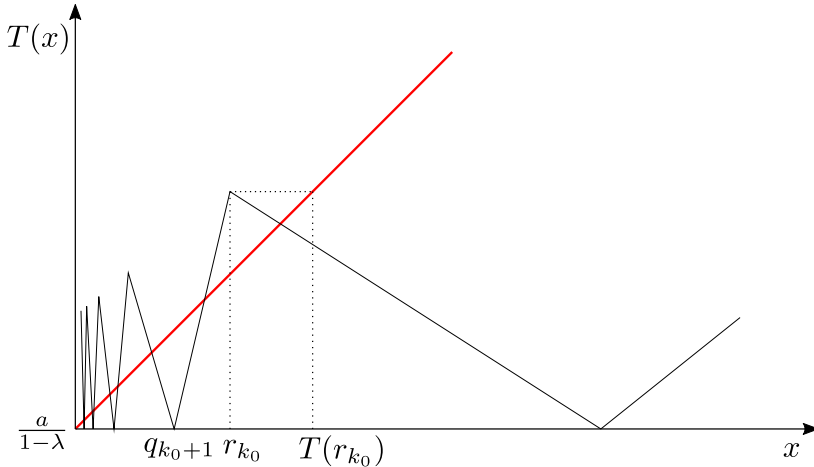


Figure 3.10. Graph of the map  $T(x)$  for  $x \in \left(\frac{a}{1-\lambda}, \infty\right)$ .

**3.3.6.3** Now we show that system (3.1) has periodic orbits of all sufficiently large periods.

Fix  $k_1 \in \mathbb{N}$  such that

$$q_{k_1} - \frac{a}{1-\lambda} < T_*, \quad (3.29)$$

where  $T_* > 0$  is given by (3.24). Note that  $T([r_{k_1}, q_{k_1}]) = [\frac{a}{1-\lambda}, T(r_{k_1})]$ . Fix  $k_2 \in \mathbb{N}$  such that

$$q_{k_2} < T(r_{k_1}).$$

For any  $m \geq k_2$ , denote by  $\Theta_m$  the subsegment of  $[r_{k_1}, q_{k_1}]$  such that  $T(\Theta_m) = [r_m, q_m]$ . It follows from (3.23) and (3.29) that

$$T^2(\Theta_m) \supset \left[ \frac{a}{1-\lambda}, \frac{a}{1-\lambda} + T_* \right] \supset \Theta_m,$$

see Figure 3.11.

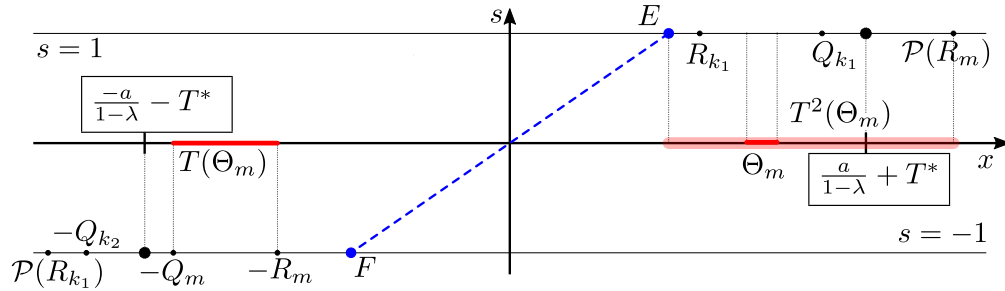


Figure 3.11. Segment  $\Theta_m$  is covered by its image  $T^2(\Theta_m)$  under the second iteration of map  $T$ .

Hence, the map  $T^2$  has a fixed point in  $\Theta_m$ . Due to the argument in part 2 of this section, the corresponding periodic solution of the system (3.1) will be of period  $k_1 + m + 2$ . Hence, for any  $k \geq k_1 + k_2 + 2$ , system (3.1) has a  $k$ -periodic orbit.

**3.3.6.4** To complete the proof of statement (e), it remains to show that system (3.1) has no more than one stable periodic orbit. In this part, we find a necessary and sufficient condition for the map  $T(x)$  to have fixed points in the interval  $(q_{k+1}, q_k)$  (obviously,  $T(x)$  has no fixed points for  $x \geq q_1$  because  $T'(x) = -\lambda \in (0, 1)$  for all  $x > q_1$ ). Then we show that at most



one fixed point of  $T(x)$  can be stable. Finally, in part 5, we prove that all the periodic orbits of  $T(x)$  with period greater than 1 are unstable.

**Lemma 3.12.** *The map  $T(x)$  has a fixed point in the interval  $(q_{k+1}, q_k)$  if and only if*

$$1 + \lambda\beta^k \leq 0. \quad (3.30)$$

*The period of the corresponding orbit of system (3.1) equals  $(2k + 2)$ .*

*Proof.* The interval  $(q_{k+1}, q_k)$  contains a fixed point if and only if

$$T(r_k) \geq r_k, \quad (3.31)$$

see Figure 3.10. Using formulas (3.19) and (3.22), we see that (3.31) is equivalent to

$$\frac{a + 2\lambda}{1 + \lambda} \geq \frac{2 + a\frac{1-\beta^k}{1-\beta}}{1 - \beta^k + a\frac{1-\beta^k}{1-\beta}},$$

which can be rewritten as (3.30). ■

Note that, given  $a$  and  $\lambda$ , inequality (3.30) holds for all sufficiently large  $k$ . We denote by  $k_0 = k_0(\lambda, a)$  the smallest  $k$  with this property.

Now we fix  $a$  and  $\lambda$  and an arbitrary  $k \geq k_0(\lambda, a)$  and study the stability of the fixed points of  $T(x)$  in the interval  $(q_{k+1}, q_k)$ . First, note that if (3.30) holds as an equality, then the interval  $(q_{k+1}, q_k)$  contains a unique fixed point  $r_k$ . It is unstable because the slope of the graph of  $T(x)$ ,  $x \in (q_{k+1}, r_k)$  is positive and greater than one. Assume that (3.30) holds as a strict inequality, i.e.,

$$1 + \lambda\beta^k < 0. \quad (3.32)$$

Then there are two fixed points on the interval  $(q_{k+1}, q_k)$ . The left one belongs to the interval  $x \in (q_{k+1}, r_k)$  and is unstable (as in the previous case). The right one belongs to the interval  $(r_k, q_k)$ . It is stable if and only if

$$T'(x) \in [-1, 0), \quad x \in (r_k, q_k). \quad (3.33)$$

Combining (3.33) and (3.28), we conclude that the fixed point from the interval  $(r_k, q_k)$  is stable if and only if

$$\lambda\beta^k + a - 1 \geq 0. \quad (3.34)$$

**Lemma 3.13.** *Inequalities (3.32) and (3.34) are either incompatible for all  $k \geq k_0$ , or they hold for  $k = k_0$  only.*

*Proof.* In the parameter plane  $(\lambda, \beta)$ , we introduce the regions  $\Omega_k$  (see (3.5)). We proceed by contradiction. Assume that for given  $(\lambda, \beta)$ , inequalities (3.32) and (3.34) hold for  $k_1$  and  $k_2$ ,  $k_1 \neq k_2$ . Then,  $(\lambda, \beta) \in \Omega_{k_1} \cap \Omega_{k_2}$ . But  $\Omega_{k_1}$  and  $\Omega_{k_2}$  do not intersect for  $k_1 \neq k_2$ . Hence, there exists no more than one  $k \geq k_0$  for which inequalities (3.32) and (3.34) hold simultaneously. Now we again proceed by contradiction and assume that both inequalities hold for some  $k > k_0$ . Then inequality (3.32) holds also for  $k_0$  by definition of  $k_0$ , while inequality (3.34) holds for  $k_0$  due to the monotonicity of its left-hand side with respect to  $k$ . However, as we have just seen, both inequalities (3.32) and (3.34) cannot hold for two different values  $k$  and  $k_0$  simultaneously. ■

**3.3.6.5** We denote by  $r_*$  the (unique) fixed point of the map  $T(x)$  in the interval  $[r_{k_0}, q_{k_0})$ , where  $k_0 = k_0(\lambda, a)$  was introduced in part 4. Recall that the map  $T(x)$  has no fixed points for  $x > r_*$ , see Figure 3.10. In particular, this implies that

$$T(x) < x \quad \text{for all } x > r_*. \quad (3.35)$$

Now, let us show that the segment  $[\frac{a}{1-\lambda}, T(r_{k_0})]$  is mapped onto itself under  $T(x)$ . Indeed,  $[q_{k_0+1}, r_{k_0}] \subset [\frac{a}{1-\lambda}, T(r_{k_0})]$  and  $T([q_{k_0+1}, r_{k_0}]) = [\frac{a}{1-\lambda}, T(r_{k_0})]$ . Hence,  $[\frac{a}{1-\lambda}, T(r_{k_0})] \subset T([\frac{a}{1-\lambda}, T(r_{k_0})])$ . On the other hand,  $T(x) \leq T(r_{k_0})$  for  $x \leq r_*$  due to the monotonicity of  $T(r_k)$  (see (3.23)) and  $T(x) < x \leq T(r_{k_0})$  for  $x \in [r_*, T(r_{k_0})]$  due to (3.35). Thus,

$$T\left(\left[\frac{a}{1-\lambda}, T(r_{k_0})\right]\right) = \left[\frac{a}{1-\lambda}, T(r_{k_0})\right].$$

Second, we note that the fixed points of any iteration belong to the segment  $[\frac{a}{1-\lambda}, T(r_{k_0})]$ . Indeed, assume to the contrary that a fixed point  $x$  of some iteration of  $T(x)$  satisfies  $x > T(r_{k_0}) \geq r_*$ . If  $T^j(x) \in [\frac{a}{1-\lambda}, T(r_{k_0})]$  for some  $j$ , then all the subsequent iterations of  $T^j(x)$  remain in the segment  $[\frac{a}{1-\lambda}, T(r_{k_0})]$  due to the invariance of this segment. If  $T^j(x) > T(r_{k_0})$  for all  $j$ , then (3.35) implies that  $T^{j+1}(x) < T^j(x)$  for all  $j$ . In both cases, we obtain a contradiction with the fact that  $x$  is a fixed point of some iteration of  $T(x)$ .

**3.3.6.6** We consider two cases: the fixed point  $r_*$  is stable or unstable.

Assume that the fixed point  $r_*$  is stable. Let us show that

$$T(r_{k_0}) \in [r_*, q_{k_0}). \quad (3.36)$$

Obviously  $T(r_{k_0}) \geq r_*$ . On the other hand, since

$$|T'(x)| \leq 1 \quad \text{for all } x \in (r_{k_0}, q_{k_0}), \quad (3.37)$$

it follows that

$$q_{k_0} - r_{k_0} \geq T(r_{k_0}) - \frac{a}{1-\lambda} > T(r_{k_0}) - r_{k_0},$$

i.e.,  $T(r_{k_0}) \leq q_{k_0}$ .

Next, we show that the segment  $[r_{k_0}, T(r_{k_0})]$  is invariant under  $T$ , i.e.,

$$T([r_{k_0}, T(r_{k_0})]) \subset [r_{k_0}, T(r_{k_0})]. \quad (3.38)$$

Since  $T(x)$  is linear on this segment, we need to check the images  $T(r_{k_0})$  and  $T^2(r_{k_0})$  of the end points only. Obviously,  $T(r_{k_0})$  belongs to this segment. Moreover, relations (3.36) and (3.37) show that all the iterations of  $r_{k_0}$  under the map  $T$  belong to the segment  $[r_{k_0}, T(r_{k_0})]$  (and converge to  $r_*$ ). In particular,  $T^2(r_{k_0})$  belongs to this interval.

Now we are ready to prove that the fixed points of any iteration of  $T(x)$ , except for  $r_*$ , are unstable. Assume, to the contrary, that  $x_* \in (\frac{a}{1-\lambda}, T(r_{k_0})]$  is a stable fixed point of  $T^{j_*}(x)$

for some  $j_* \geq 2$  and  $x_* \neq r_*$ . We have seen in part 4 of this section that  $|T'(x)| > 1$  for all  $x \in (r_{k+1}, q_{k+1}) \cup (q_{k+1}, r_k)$ ,  $k \geq k_0$ . Therefore, the only possibility for  $x_*$  to be stable is that  $T^j(x_*) \in [r_{k_0}, T(r_{k_0})]$  for some  $j \in \mathbb{N}$ . However, all the trajectories entering this segment converge to  $r_*$  due to (3.37) and (3.38).

Finally, assume that the fixed point  $r_*$  is unstable. Then  $k_0 > 1$  (otherwise,  $|T'(r_*)| = \lambda^2 < 1$ ). It follows from the monotonicity of  $T(r_k)$  (see (3.23)) and (3.35) that  $T(r_{k_0}) < T(r_{k_0-1}) < r_{k_0-1}$ , i.e.,

$$\left[ \frac{a}{1-\lambda}, T(r_{k_0}) \right] \subset \left[ \frac{a}{1-\lambda}, r_{k_0-1} \right]. \quad (3.39)$$

But  $|T'(x)| > 1$  for all  $x \in (q_{k+1}, r_k) \cup (r_k, q_k)$ ,  $k \geq k_0$ , due to part 4 of this section, and  $|T'(x)| = |\lambda^{-1}T'(r_*)| > 1$  for all  $x \in (q_{k_0}, r_{k_0-1})$  due to (3.27) and (3.28). This and (3.39) imply that the absolute values of all the slopes of the graph of  $T(x)$  on the interval  $[\frac{a}{1-\lambda}, T(r_{k_0})]$  are greater than 1. Hence, the same is true for any iteration of  $T(x)$  on this interval. Therefore, all the fixed points of any iteration of  $T$  are unstable. This completes the proof of statement (e) of Theorem 3.1.

## Proof of Theorem 3.2

If  $(\lambda, \beta) \in \Omega_k$  for some  $k \in \mathbb{N}$ , then, according to Lemmas 3.12 and 3.13, the map  $T$  has a stable fixed point in the interval  $[r_k, q_k)$  and  $k = k_0(\lambda, a)$ . It corresponds to the stable  $(2k+2)$ -periodic orbit of system (3.1). According to part 3.3.5.1 of this section, all the other periodic orbits are unstable.

If  $(\lambda, a) \notin \bigcup_{k \in \mathbb{N}} \Omega_k$ , then, according to Lemma 3.13, the map  $T$  has no stable fixed points. Therefore, due to part 3.3.5.2 of this section, all the periodic orbits are unstable.

### 3.3.7 Case (f)

In this case, the parallelogram  $\Pi$  degenerates into the segment of the equilibrium points  $EF$  with the slope 1 (see Figure 3.12).

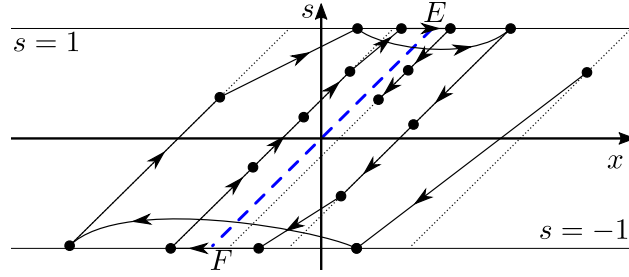


Figure 3.12. Case  $\beta = 1$ ,  $\lambda < 0$ . The parallelogram  $\Pi$  degenerates to the segment  $EF$  with slope 1.

Let us consider a point  $(x_t, s_t) \notin EF$ . To be definite, assume that  $p_t = x_t - s_t > 0$ . Denote by  $(x_{t+k}, s_{t+k})$  the first iteration that reaches the line  $s = -1$  after the moment  $t$ , i.e.,  $s_{t+i} > -1$  for  $i = 0, \dots, k-1$  and  $s_{t+k} = -1$  (if  $s_t = -1$  we agree that  $k = 0$ ). If  $p_{t+k} = 0$ , then the trajectory ends at the point  $F$ . If  $p_{t+k} > 0$ , then  $0 < p_{t+k} \leq p_{t+k-1} = \dots = p_t$  and

$$p_{t+k+1} = \lambda x_{t+k} + a s_{t+k} - s_{t+k+1} = \lambda x_{t+k} - a + 1 = \lambda x_{t+k} + \lambda = \lambda p_{t+k}, \quad (3.40)$$

where we use  $a = 1 - \lambda$ . If  $p_{t+k} < 0$ , then  $p_{t+k} < 0 < p_{t+k-1} = \dots = p_t$  and

$$p_{t+k} = \lambda x_{t+k-1} + a s_{t+k-1} - s_{t+k} = \lambda p_{t+k-1} + s_{t+k-1} - s_{t+k} \geq \lambda p_{t+k-1},$$

hence

$$|p_{t+k}| \leq |\lambda| |p_{t+k-1}|. \quad (3.41)$$

Inequalities (3.40) and (3.41) and similar inequalities that hold for ascending parts of trajectories, due to (3.6), show that the trajectory either ends up at  $E$  or  $F$ , or converges to the segment  $EF$ . In the latter case, the distance from the point  $(x_t, s_t)$  to the segment  $EF$  tends to zero as  $n \rightarrow \infty$ .

### 3.3.8 Case (g)

For  $\beta = -1$  it is straightforward to see that the parallelogram  $\Sigma$ , which is contained in  $\Pi$ , consists of 2-periodic orbits and the segment  $EF$  of equilibrium points.

If  $\lambda \geq 0$  (see Figure 3.13(a)), then from Lemma 3.8 it follows that the parallelogram  $\Pi$  is invariant under the map  $f$  and if  $(x_t, s_t) \in \Pi \setminus \Sigma$ , then either  $(x_{t+1}, s_{t+1}) \in \Sigma$  or  $x_{t+1} < -1$ ,  $s_{t+1} = -1$  or  $x_{t+1} > 1$ ,  $s_{t+1} = 1$ . But, since  $\lambda \geq 0$ , relations  $x_{t+1} < -1$ ,  $s_{t+1} = -1$  and  $f(-1, -1) = (1, 1)$  imply  $x_{t+2} < 1$ ,  $s_{t+2} = 1$  and, similarly, relations  $x_{t+1} > 1$ ,  $s_{t+1} = 1$  and  $f(1, 1) = (-1, -1)$  imply  $x_{t+2} > -1$ ,  $s_{t+2} = -1$ . In both cases,  $(x_{t+2}, s_{t+2}) \in \Sigma$ . Thus,  $f^2$  maps  $\Pi$  into  $\Sigma$ . On the other hand, the argument presented in Section 3.3.3 shows that a trajectory starting outside  $\Pi$  either converges to the point  $F$  along the line  $s = -1$  from the right or to the point  $E$  along the line  $s = 1$  from the left or meets the boundary of the strip  $L$  inside  $\Pi$ .

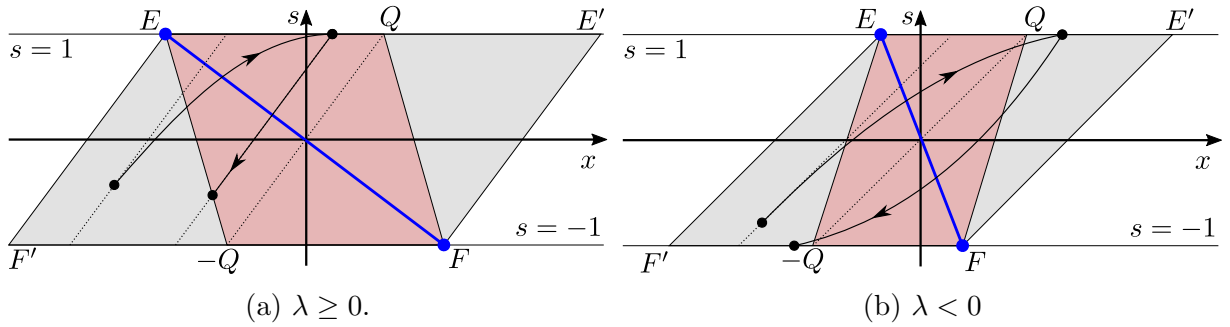


Figure 3.13. Parallelograms  $\Sigma$  and  $\Pi$  for  $\beta = -1$ .

If  $\lambda < 0$  (see Figure 3.13(b)), then the argument used in Section 3.3.4 shows that the set  $M = \{(x, s) : x \leq -1, s = -1\} \cup \{(x, s) : x \geq 1, s = 1\}$  is invariant under the map  $f$  and all the trajectories starting in  $M$  converge to the 2-periodic orbit  $(-1, -1), (1, 1)$ . If  $(x_t, s_t) \in \Pi \setminus \Sigma$ , then  $(x_{t+1}, s_{t+1}) \in M \cup \Sigma$  because  $\beta = -1$ . Finally, if  $(x_t, s_t) \notin \Pi$ , then  $(x_{t+k}, s_{t+k}) \in M \cup \Sigma$  for some  $k \in \mathbb{N}$ . This completes the proof of Theorem 3.1.

## CHAPTER 4

### OUTPUT GAP AND INFLATION MODEL

In this chapter, we consider a simpler version of the DSGE model (2.25). For this simplified version, we are to obtain a complete characterization of the stability properties of the system.

Namely, we remove the correlation between the successive interest rate values from the Taylor rule by setting  $c_3 = 0$ . The aggregate demand and aggregate supply equations remain unchanged:

$$\begin{cases} u_t = u_{t-1} - a(w_t - p_t) + \varepsilon_t, \\ v_t = b_1 p_t + (1 - b_1)v_{t-1} + b_2 u_t + \eta_t. \end{cases} \quad (4.1)$$

However, the Taylor rule simply has the form

$$w_t = c_1 v_t + c_2 u_t. \quad (4.2)$$

Substituting (4.2) into (4.1) gives the system with two macroeconomic variables, the output gap  $u$  and the inflation rate  $v$ , and the additional variable  $p$ , the expectation of inflation.

To maintain the simplicity of model (2.25) in this chapter, we consider a single representative economic agent by setting  $i = 1$  in equation (2.26) so that

$$p_t = v_t + \Psi_\alpha(p_{t-1} - v_t) \quad (4.3)$$

with the piecewise linear saturation function  $\Psi_\alpha(\cdot)$  defined by (2.11):

$$\Psi_\alpha(x) = \begin{cases} \alpha & \text{if } x \geq \alpha, \\ x & \text{if } -\alpha < x < \alpha, \\ -\alpha & \text{if } x \leq -\alpha. \end{cases} \quad (4.4)$$

Equation (4.3) describes the play operator  $p = \mathcal{P}_\alpha[v, p_0]$ .

#### 4.1 Explicit model with sticky inflation

Equations (4.1), (4.2) complemented by formula (4.3) form a complete model for the evolution of the aggregated variables  $u_t, v_t, p_t$ . However, the dependence of these quantities at a moment  $t$  on their values at the moment  $t - 1$  is implicit. In order to numerically implement the model, we proceed by solving equations (4.1)–(4.3) with respect to the variables  $u_t, v_t$ . As shown in Appendix A.1, the model can be written in the following equivalent explicit form:

$$z_t = Az_{t-1} + s_t d + N\xi_t \quad (4.5)$$

where  $z_t = (u_t, v_t)^\top$ ,  $\xi_t = (\varepsilon_t, \eta_t)^\top$ , the superscript  $\top$  denotes transposition, the matrices  $A$ ,  $N$  and the column vector  $d$  are defined by

$$A = \begin{pmatrix} \frac{1-b_1}{(1-b_1)(1+ac_2)+ab_2(c_1-1)} & \frac{a(1-b_1)(1-c_1)}{(1-b_1)(1+ac_2)+ab_2(c_1-1)} \\ \frac{b_2}{(1-b_1)(1+ac_2)+ab_2(c_1-1)} & \frac{(1-b_1)(1+ac_2)}{(1-b_1)(1+ac_2)+ab_2(c_1-1)} \end{pmatrix}, \quad (4.6)$$

$$N = \begin{pmatrix} \frac{1-b_1}{(1-b_1)(1+ac_2)+ab_2(c_1-1)} & \frac{a(1-c_1)}{(1-b_1)(1+ac_2)+ab_2(c_1-1)} \\ \frac{b_2}{(1-b_1)(1+ac_2)+ab_2(c_1-1)} & \frac{1+ac_2}{(1-b_1)(1+ac_2)+ab_2(c_1-1)} \end{pmatrix},$$

$$d = \begin{pmatrix} \frac{a(b_1c_1-1)}{(1-b_1)(1+ac_2)+ab_2(c_1-1)} \\ -\frac{ab_2+b_1(1+ac_2)}{(1-b_1)(1+ac_2)+ab_2(c_1-1)} \end{pmatrix},$$

and  $s_t = v_t - p_t$  is defined by the equation

$$s_t = \frac{1}{1+\beta} \Psi_{(1+\beta)\alpha}(f_t - f_{t-1} + s_{t-1}) \quad (4.7)$$

with

$$\beta = \frac{(1-b_1)(1+ac_2) + ab_2(c_1-1)}{b_1(1+ac_2) + ab_2}, \quad (4.8)$$

$$f_t = \frac{b_2}{b_1(1+ac_2) + ab_2} u_{t-1} + \frac{(1-b_1)(1+ac_2)}{b_1(1+ac_2) + ab_2} v_{t-1} + \frac{b_2\varepsilon_t + (1+ac_2)\eta_t}{b_1(1+ac_2) + ab_2}. \quad (4.9)$$

Equations (4.5), (4.7) express  $u_t, v_t, s_t = v_t - p_t$  explicitly in terms of the previous values  $u_{t-1}, v_{t-1}, s_{t-1}$  of the same variables and the noise values  $\varepsilon_t, \eta_t$ . We use these equations for



all the simulations in this chapter. Note that (4.7) defines a stop operator with the input  $f_t$  and the threshold  $(1 + \beta)\alpha$ , which is different from  $\alpha$  (cf. (4.3)), hence (4.7) can be written as

$$s_t = \frac{1}{1 + \beta} \mathcal{S}_{(1+\beta)\alpha}[f_t, s_0]$$

by using the notation (2.12). It is also important to note that the transition from the implicit model to the explicit 3-dimensional PWL system (4.5), (4.7) is justified under the condition that  $\beta$  is positive, and we assume this constraint to hold in the rest of the dissertation. Particularly in this chapter,  $\beta > 0$  whenever  $c_1 > 1$ , cf. Section 4.4.

The transition from the implicit model to equations (4.5), (4.7) is based on the inversion formulas presented in Section 2.3.

## 4.2 Line segment of equilibrium points

We begin the analysis of model (4.5), (4.7) by looking at how the model behaves if we shut off the exogenous noise, i.e., we set  $\xi_t = 0$  and consider the equation

$$z_t = Az_{t-1} + s_t d, \quad z_t = (u_t, v_t)^\top \quad (4.10)$$

instead of (4.5) with  $s_t$  defined by (4.7), (4.8) and

$$f_t = \frac{b_2}{b_1(1 + ac_2) + ab_2} u_{t-1} + \frac{(1 - b_1)(1 + ac_2)}{b_1(1 + ac_2) + ab_2} v_{t-1}. \quad (4.11)$$

This model produces a segment of equilibrium points which explains multiplicity of equilibrium states of the economy as a function of expectations (sentiments) of economic agents. Indeed, equation (4.10) implies

$$z_* = s_*(\mathbb{I} - A)^{-1}d = s_* \left( \frac{b_1}{b_2}, \frac{b_2 + b_1 c_2}{b_2(1 - c_1)} \right)^\top, \quad -\alpha \leq s_* \leq \alpha, \quad (4.12)$$

for an equilibrium point  $z_* = (u_*, v_*)^\top$ , where  $\mathbb{I}$  is a  $2 \times 2$  identity matrix. Hence one obtains a different equilibrium for any admissible value of the sentiment variable  $s_*$ , which are limited

to the interval  $-\alpha \leq s_* \leq \alpha$ . Thus, the set of all equilibrium points, which can be denoted as  $z_*(s_*)$  for different  $s_*$ , can be naturally thought of as a line segment in the phase space of the system, see Figure 4.1 for the projection of this line segment onto the  $(v, s)$  plane. In particular, the value of the output gap at an equilibrium,  $u_*(s_*)$ , ranges over the interval

$$u_*(s_*) = s_* \frac{b_1}{b_2} \quad \text{with} \quad -\alpha \leq s_* \leq \alpha,$$

and the equilibrium value of inflation belongs to the range

$$v_*(s_*) = s_* \frac{b_2 + b_1 c_2}{b_2(1 - c_1)} \quad \text{with} \quad -\alpha \leq s_* \leq \alpha.$$

One can notice that the range of equilibrium values of the output gap is unaffected by the controls  $c_1, c_2$  applied by the regulator through Taylor's rule (4.2). However, these controls affect the range of possible values of equilibrium of the inflation rate.

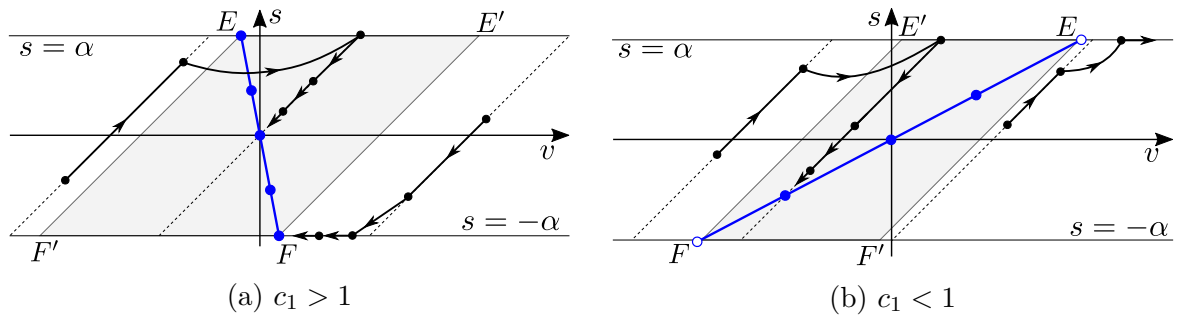


Figure 4.1. The projection of the line segment of equilibrium points  $EF$  (blue line) onto the  $(v, s)$  plane. The segment has a negative slope in (a) and a positive slope in (b). Sample trajectories of system (4.10) are shown in black.

Equation (4.12) indicates the difference between the cases when  $c_1 > 1$  and  $c_1 < 1$ . In the case of  $c_1 > 1$ , the equilibrium  $z_*(\alpha)$  corresponding to the lowest expectation of inflation has the highest value of the output gap and the lowest inflation of all the equilibrium points. Similarly, the equilibrium  $z_*(-\alpha)$  with the highest expectation of inflation has the lowest value of the output gap and the highest inflation. On the other hand, in the case of  $c_1 < 1$ ,

the equilibrium  $z_*(\alpha)$  with the highest output gap value has simultaneously the highest inflation rate.

The difference between the cases  $c_1 > 1$  and  $c_1 < 1$  forms the basis for the main results of this chapter. This difference will be further highlighted in Section 4.7.

### 4.3 Local stability analysis

System (4.5), (4.7) is locally linear in some neighborhood of any equilibrium point from the line segment (4.12) with the exception of the two end points of this segment,  $z_*(\pm\alpha)$ , corresponding to extreme sentiment. In other words, for small deviations of the vector  $z_t = (u_t, v_t)^\top$  from an equilibrium  $z_*(s_*)$ , system (4.10) is equivalent to

$$z_t - z_*(s_*) = B(z_{t-1} - z_*(s_*)), \quad (4.13)$$

where

$$B = \begin{pmatrix} \frac{1}{1+a(b_2c_1+c_2)} & \frac{a(b_1-1)c_1}{1+a(b_2c_1+c_2)} \\ \frac{b_2}{1+a(b_2c_1+c_2)} & \frac{(1-b_1)(1+ac_2)}{1+a(b_2c_1+c_2)} \end{pmatrix}. \quad (4.14)$$

**Lemma 4.1.** *For any admissible set of parameters, every equilibrium  $z_*(s_*)$  of system (4.10) with  $-\alpha < s_* < \alpha$  is asymptotically stable.*

We prove this lemma in Appendix A.3 by using Jury's stability criterion (see Appendix A.2) to show that matrix  $B$  is stable. This local stability ensures that if a small perturbation is applied to the system residing at an equilibrium  $z_*(s_*)$ , the system returns to the equilibrium after the perturbation is removed.

The analysis of the effect of large perturbations as well as stability of the two extreme equilibrium  $z_*(\pm\alpha)$  is more subtle as discussed in the following sections of this chapter. In particular, the basin of attraction of the equilibrium decreases and finally vanishes as one approaches either of the extreme equilibrium points along the line segment (4.12). The extreme points are stable but not asymptotically stable.

## 4.4 Dynamics far from the line segment of equilibrium states

System (4.10) without stickiness ( $\alpha = 0$ ) simply has the form

$$z_t = Az_{t-1}. \quad (4.15)$$

As shown in Appendix A.3, its unique zero equilibrium is globally stable if  $c_1 > 1$  and is unstable if  $c_1 < 1$ .

For system (4.10) with stickiness ( $\alpha > 0$ ), equation (4.15) approximates dynamics far from equilibrium points (in a neighborhood of infinity) because the term  $s_t$  in (4.10) is bounded in absolute value by  $\alpha$ . In particular, since (4.15) is unstable for  $c_1 < 1$ , so is system (4.10). This creates a possibility of run-away inflation for such values of  $c_1$  (see Section 4.7.5).

## 4.5 Global stability (main result)

Interestingly, the same condition  $c_1 > 1$  that ensures the global stability of system (4.15), also guarantees the global stability of the set of equilibrium states for the sticky nonlinear system (4.10). The main result of this chapter is the following theorem.

**Theorem 4.2.** *If  $c_1 > 1$ , then*

- (i) *The segment of equilibrium states (4.12) of system (4.10) is globally stable.*
- (ii) *Every trajectory of system (4.10) converges to one of the equilibrium states (4.12).*

## 4.6 Proof of Theorem 4.2

### 4.6.1 Preliminary estimates

We provide the proof of the main result in several steps. To this end, we first summarize some properties of the discrete stop operator  $s_t = \mathcal{S}_\alpha[v_t, s_0]$  and the discrete play operator

$p_t = \mathcal{P}_\alpha[v_t, p_0]$ , which are needed in the sequel. These properties should seem natural to a reader who is familiar with the continuous time play and stop operators.

For brevity, we shorten the notation and write

$$p_t = \mathcal{P}_\alpha[v_t], \quad s_t = \mathcal{S}_\alpha[v_t]$$

whenever this does not cause confusion.

**Lemma 4.3.** *Let  $\{v_t\}$  be a given sequence. Then  $p_t, s_t$  satisfy (4.3) if and only if  $|s_t| \leq \alpha$  for all  $t \in \mathbb{N}$  and the variational inequality*

$$(p_t - p_{t-1}, s_t - x) \geq 0 \quad \forall t \in \mathbb{N}. \quad (4.16)$$

holds for every  $x \in [-\alpha, \alpha]$ .

*Proof.* Relation (4.3) is equivalent to the series of implications

$$p_t - p_{t-1} > 0 \Rightarrow p_t = v_t - \alpha \Rightarrow s_t = \alpha, \quad p_t - p_{t-1} < 0 \Rightarrow p_t = v_t + \alpha \Rightarrow s_t = -\alpha,$$

which is in turn equivalent to (4.16) under the condition  $|s_t| \leq \alpha$  for all  $t \in \mathbb{N}$ . ■

For a generic sequence  $\{x_t\}$ , we introduce the notation

$$\nabla_t x := x_t - x_{t-1} \quad \text{for } t \in \mathbb{N}. \quad (4.17)$$

Choosing in (4.16) the value  $x = s_{t-1}$ , we obtain that  $\nabla_t p \nabla_t s \geq 0$ , hence

$$\nabla_t v \nabla_t s \geq (\nabla_t s)^2. \quad (4.18)$$

Furthermore, summing up the inequalities

$$\begin{aligned} (p_t - p_{t-1})(s_t - s_{t-1}) &\geq 0, \\ (p_{t-1} - p_{t-2})(s_{t-1} - s_t) &\geq 0, \end{aligned}$$

which follow from (4.16) by the choice  $x = s_{t-1}$  and  $x = s_t$ , respectively, we obtain that  $\nabla_t^2 p \nabla_t s \geq 0$ , hence

$$\nabla_t^2 v \nabla_t s \geq \nabla_t^2 s \nabla_t s = \frac{1}{2}((\nabla_t s)^2 - (\nabla_{t-1} s)^2) + \frac{1}{2}(\nabla_t^2 s)^2, \quad (4.19)$$

and similarly

$$\nabla_t^2 v \nabla_t v = \frac{1}{2}((\nabla_t v)^2 - (\nabla_{t-1} v)^2) + \frac{1}{2}(\nabla_t^2 v)^2, \quad (4.20)$$

which is a special case of the identity

$$\nabla_t x x_t = \frac{1}{2}((x_t)^2 - (x_{t-1})^2) + \frac{1}{2}(\nabla_t x)^2 \quad (4.21)$$

for every sequence  $\{x_t\}$ .

**Lemma 4.4.** *For a given sequence  $\{v_t\}$ , put  $s_t = v_t - p_t$ ,  $p_t = \mathcal{P}_\alpha[v_t]$  with some given initial condition  $p_0$ . Let  $q_t = v_t + \delta s_t = (1 + \delta)v_t - \delta p_t$  for some  $\delta > -1$ . Then*

$$v_t = \frac{1}{1 + \delta} (q_t + \delta \mathcal{P}_{(1+\delta)\alpha}[q_t]). \quad (4.22)$$

*Proof.* We have  $q_t - p_t = (1 + \delta)s_t$ , hence  $|q_t - p_t| \leq (1 + \delta)\alpha$ , and

$$(p_t - p_{t-1}, q_t - p_t - (1 + \delta)\alpha v) \geq 0 \quad \forall t \in \mathbb{N} \quad \forall |v| \leq 1. \quad (4.23)$$

By Lemma 4.3, this implies that  $p_t = \mathcal{P}_{(1+\delta)\alpha}[q]_t$  and the assertion follows.  $\blacksquare$

**Lemma 4.5.** *For a given sequence  $\{v_t\}$ , put  $p_t = \mathcal{P}_\alpha[v_t]$  with some given initial condition  $p_0$ . Then for every  $t, j \in \mathbb{N}$  we have*

$$|p_{t+j} - p_t| \leq \max_{i=1, \dots, j} \{|v_{t+i} - v_t|\}. \quad (4.24)$$

*Proof.* We fix  $t, J \in \mathbb{N}$  and for  $j = 0, 1, \dots, J$  set

$$P_j = \max\{|p_{t+j} - p_t|^2, \max_{i=1, \dots, j} \{|v_{t+i} - v_t|^2\}\}.$$

The proof will be complete if we prove that the sequence  $\{P_j\}$  is non-increasing for  $j = 0, 1, \dots, J$ . Indeed, then  $P_J \leq P_0$ , which is precisely the desired statement.

Assume for contradiction that  $P_j > P_{j-1}$  for some  $j = 1, \dots, J$ . Then

$$|p_{t+j} - p_t| > \max_{i=1, \dots, J} \{|v_{t+i} - v_t|\}, \quad (4.25)$$

$$(p_{t+j} - p_t)^2 > (p_{t+j-1} - p_t)^2. \quad (4.26)$$

Inequality (4.26) can be equivalently written as

$$(p_{t+j} - p_{t+j-1})(p_{t+j} - p_t) > \frac{1}{2}(p_{t+j} - p_{t+j-1})^2 > 0. \quad (4.27)$$

We now replace in (4.16) written for  $t + j$  instead of  $t$  the element  $x$  by  $s_t$  and obtain

$$(p_{t+j} - p_{t+j-1})(s_{t+j} - s_t) \geq 0, \quad (4.28)$$

hence, combining (4.27) with (4.28), we have

$$(p_{t+j} - p_t)(s_{t+j} - s_t) \geq 0,$$

which implies that

$$(p_{t+j} - p_t)^2 \leq (p_{t+j} - p_t)(v_{t+j} - v_t)$$

in contradiction with (4.25). This completes the proof of Lemma 4.5. ■

#### 4.6.2 Reformulated equation

With the notation (4.17), we rewrite (4.1), (4.2) in the form

$$\begin{aligned} \nabla_t u + ac_2 u_t + a(c_1 - 1)v_t + as_t &= \varepsilon_t, \\ (1 - b_1)\nabla_t v + b_1 s_t - b_2 u_t &= \eta_t. \end{aligned} \quad (4.29)$$

Using the identity

$$(1 - b_1)\nabla_t^2 v + b_1 \nabla_t s - b_2 \nabla_t u = \nabla_t \eta,$$

which follows from (4.29) and where we denote

$$\nabla_t^2 v = v_t - 2v_{t-1} + v_{t-2},$$

we can eliminate  $u_t$  from system (4.29) and reformulate it as a second order finite difference equation

$$\nabla_t^2 v + D_1 \nabla_t v + D_2 \nabla_t s + D_3 v_t + D_4 s_t = h_t \quad (4.30)$$

with positive constants

$$D_1 = ac_2, \quad D_2 = \frac{b_1}{1-b_1}, \quad D_3 = \frac{ab_2(c_1-1)}{1-b_1}, \quad D_4 = \frac{b_1ac_2 + ab_2}{1-b_1}$$

(recall that  $c_1 > 1$ ) and with the right hand side

$$h_t = \frac{1}{1-b_1} (\nabla_t \eta + b_2 \varepsilon_t + ac_2 \eta_t). \quad (4.31)$$

We proceed by setting  $\eta_t = \varepsilon_t = 0$ , which implies  $h_t = 0$ .

### 4.6.3 Estimate 1

We let

$$q_t = D_3 v_t + D_4 s_t, \quad (4.32)$$

multiply equation (4.30) with  $\nabla_t q = D_3 \nabla_t v + D_4 \nabla_t s$  and using the relations (4.18)–(4.21) we obtain

$$V_t^1 - V_{t-1}^1 + \frac{D_3}{2} (\nabla_t^2 v)^2 + D_1 D_3 (\nabla_t v)^2 + (D_2 D_3 + D_1 D_4 + D_2 D_4) (\nabla_t s)^2 + \frac{1}{2} (\nabla_t q)^2 \leq 0, \quad (4.33)$$

where

$$V_t^1 = \frac{1}{2} (D_3 (\nabla_t v)^2 + D_4 (\nabla_t s)^2 + q_t^2). \quad (4.34)$$



#### 4.6.4 Estimate 2

With  $h_t = 0$ , we rewrite (4.30) in the form

$$\nabla_t^2 v + \frac{D_1}{D_3} \nabla_t q + \left( D_2 - \frac{D_1 D_4}{D_3} \right) \nabla_t s + q_t = 0, \quad (4.35)$$

where  $q_t$  given by (4.32), and multiply this equation by  $q_t$ . We use (4.21) again and find constants  $D_5 > 0$ ,  $D_6 > 0$  depending on  $D_1, D_2, D_3, D_4$  such that

$$\begin{aligned} \nabla_t v q_t - \nabla_{t-1} v q_{t-1} + \frac{D_1}{2D_3} (q_t^2 - q_{t-1}^2) + \frac{1}{2} q_t^2 &\leq \nabla_t v \nabla_t q - \nabla_t^2 v \nabla_t q + D_5 \nabla_t s^2 \\ &\leq \frac{1}{2} (\nabla_t^2 v)^2 + D_6 (\nabla_t v)^2. \end{aligned} \quad (4.36)$$

We now set

$$V_t^2 = \nabla_t v q_t + \frac{D_1}{2D_3} q_t^2 \quad (4.37)$$

so that (4.36) has the form

$$V_t^2 - V_{t-1}^2 + \frac{1}{2} q_t^2 \leq \frac{1}{2} (\nabla_t^2 v)^2 + D_6 (\nabla_t v)^2. \quad (4.38)$$

#### 4.6.5 Lyapunov function

We now choose  $\gamma > 0$  such that  $\gamma \leq D_3$ ,  $\gamma D_5 < D_1 D_3$ , and  $\gamma V_t^2 \geq -\frac{1}{2} V_t^1$  for all  $t \in \mathbb{N}$ . Then there exists a constant  $\mu > 0$  such that

$$V_t - V_{t-1} + \mu V_t \leq 0 \quad (4.39)$$

for all  $t \in \mathbb{N}$  as a consequence of (4.34), (4.33), and (4.38) with

$$\begin{aligned} V_t &= V_t^1 + \gamma V_t^2 \\ &= \frac{1}{2} \left( D_3 (\nabla_t v)^2 + D_4 (\nabla_t s)^2 + (D_3 v_t + D_4 s_t)^2 \right) \\ &\quad + \gamma \left( (D_3 v_t + D_4 s_t) \nabla_t v + \frac{D_1}{2D_3} (D_3 v_t + D_4 s_t)^2 \right). \end{aligned} \quad (4.40)$$

### 4.6.6 Asymptotic behavior

Formulas (4.39) and (4.40) ensure that  $V_t$  is a non-negative Lyapunov function of the system which decays exponentially to 0 along every trajectory. Further, this function is zero only on the line segment of equilibrium states. In particular,  $q_t$  defined by (4.32) converges exponentially to  $q_\infty = 0$ . It follows from Lemmas 4.4 and 4.5 that  $v_t$  converges to some value  $v_\infty$  and  $s_t = \mathcal{S}_\alpha[v_t]$  converges to some  $s_\infty$  such that  $D_3v_\infty + D_4s_\infty = 0$ , *i.e.*, any trajectory converges to an equilibrium state<sup>1</sup>. This completes the proof of the main result.

We note that for  $h_t \neq 0$  that is when noise is present in system (4.5), the trajectories tend to return towards the segment of equilibrium points after large fluctuations and hover in a vicinity of equilibrium states for extended periods of time.

## 4.7 Numerical results

In this section, we explore numerically the behavior of system (4.1)–(4.3) with exogenous noise and shocks.

### 4.7.1 Parameter values

A typical parameter set that we use for numerical simulation is the same as in [29], see Table 4.1. We will explore the parameter space to some extent using this set as a reference point.

Table 4.1. The set of parameter values.

Parameters	$a$	$b_1$	$b_2$	$c_1$	$c_2$
Values	0.2	0.5	0.05	1.5	0.5

The components of the equilibrium points  $z_*(s_*) = (u_*(s_*), v_*(s_*))^\top$  for this parameter set

---

<sup>1</sup> Due to the multi-valued character of the stop, the values  $v_\infty$  and  $s_\infty$ , *i.e.*, the equilibrium to which a trajectory converges, will be different for different initial conditions.

and  $\alpha = 1$  range over the intervals

$$u_*(s_*) \in [-10, 10], \quad v_*(s_*) \in [-12, 12].$$

#### 4.7.2 Lower local volatility due to stickiness

The range of equilibrium points of the system is directly proportional to the threshold value  $\alpha$  of the play operator because the equilibrium sentiment  $s_*$  in (4.12) can take any value from the interval  $-\alpha \leq s_* \leq \alpha$ . In particular,  $\alpha = 0$  corresponds to the system without stickiness in which the expectation of inflation coincides with the current inflation rate,  $p = v$ . This system is simply described by the equation

$$z_t = Az_{t-1} + N\xi_t \tag{4.41}$$

(cf. (4.5)). In the absence of noise, it has a unique equilibrium at  $u = v = 0$ .

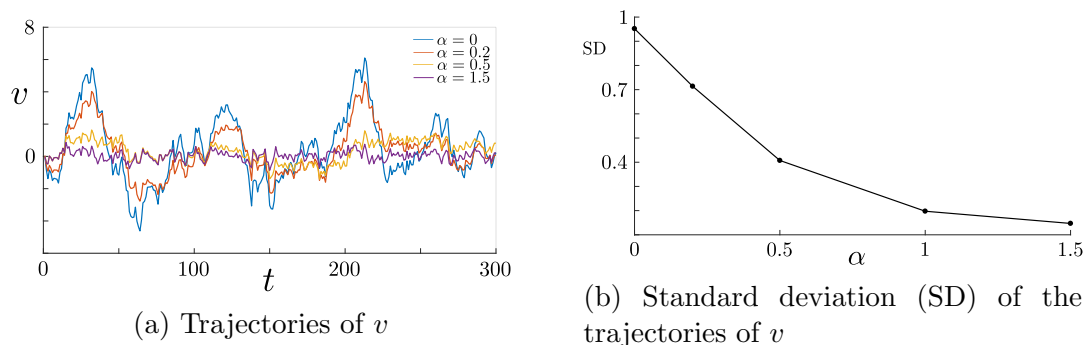


Figure 4.2. Volatility of inflation rate  $v$  for various  $\alpha$  values.

The sticky system exhibits lesser volatile inflation rate than the system without stickiness, see Figure 4.2. This can be explained by the stability properties of matrices  $A$  and  $B$  where  $B$  is the matrix of linearization (4.7) of the sticky system at an equilibrium. For parameter values of Table 4.1, the spectral radius of the matrix  $B$  is smaller than the spectral radius of  $A$  (see Appendix A.4), hence the sticky system is less volatile within the basin of attraction of individual equilibrium states, i.e., as long as the sentiment does not become extreme.

Figure 4.2 shows that the volatility decreases with  $\alpha$ . For large (compared to  $\alpha$ ) deviations of  $z_t$  from the set of equilibrium points, system (4.5) behaves as (4.41).

### 4.7.3 Transitions between equilibrium states

As long as the system remains within the basin of attraction of a particular equilibrium state  $z_*(s_*)$ , the sentiment  $s_t$  does not reach any of the extreme values  $\pm\alpha$  and remains confined to the interval  $|s_t| < \alpha$ , see Figure 4.3(a,d). On the other hand, during a transition to the basin of attraction of another equilibrium state, the sentiment is extreme (Figure 4.3(b,e)). By this reason, the system stays near equilibrium states which correspond to mix sentiments for longer periods of time than near the equilibrium states with a sentiment  $s_*$  close to extreme. Figure 4.3(c,f) illustrate a transition from the equilibrium state with the extreme sentiment,  $z_*(\alpha)$ , to the state with a more moderate sentiment.

### 4.7.4 Response to shocks

We test the system by applying supply shocks through the term  $\eta_t$ .

System (4.41) without stickiness, which has a unique globally stable equilibrium state  $u_* = v_* = 0$ , returns to the equilibrium (and hovers near it due to noise) after each shock, see Figure 4.4(a). Shocks applied to the sticky system (4.5), (4.7) result in transitions from one to another equilibrium state due to the presence of multi-equilibrium points (multiplicity of equilibria) [10, 30], see Figure 4.4(b). Numerical simulation show that shocks of small magnitude typically move the system in the direction of the shock (see Figure 4.5(a)). For example, after a shock that pushes up the inflation rate the system settles to a new equilibrium state, which has higher inflation rate (and lower output gap) than the equilibrium occupied prior to the shock. On the other hand, shocks of large magnitude cause a transition to an equilibrium state, which is hard to predict because such shocks cause a longer and more complex excursion far from equilibrium in the phase space. In Figure 4.5(b), the system

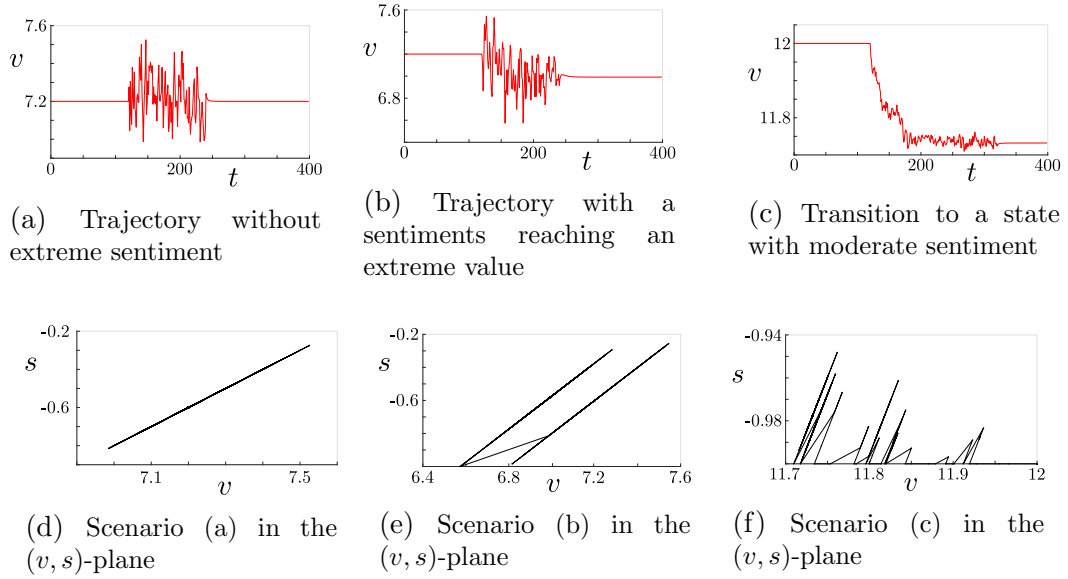


Figure 4.3. Transitions between the equilibrium states. Time traces of inflation rate (a-c) and the corresponding plots in the  $(v, s)$  space (c,f) exhibiting different transition scenarios. The noise is turned off before and after an interval of time of interest in order to show the equilibrium state at the ends of this interval. (a,d) The sentiment remains within the bounds  $|s_t| < \alpha$ , and the system stays in the basin of attraction of one equilibrium point. The inflation rate  $v_*(s_*)$  is the same before and after the noisy interval. (b,e) The sentiment reaches the extreme value  $-\alpha$  (the highest expectation of inflation), and the trajectory transits from the basin of attraction of an equilibrium state with higher inflation rate and lower output gap (the right slanted segment in (e)) to the basin of attraction of an equilibrium state with a lower inflation rate and higher output gap (the left slanted segment in (e)). (c,f). A transition from the equilibrium with the highest inflation rate (the rightmost point in (f)) to an equilibrium with a more moderate inflation rate through the basins of attraction of several other equilibrium states.

resides near an equilibrium with high inflation rate before a shock is applied. Although the shock pushes the inflation even higher, the system eventually settles to an equilibrium with nearly zero inflation rate after the shock is removed.

#### 4.7.5 The possibility of runaway inflation

According to Section 4.4 the system is globally stable for  $c_1 > 1$ , but becomes unstable for  $c_1 < 1$ . The latter case creates a possibility of the run-away inflation scenario. It is interesting that as shown in Section 4.3 all the equilibrium points are *locally* stable even if  $c_1 < 1$ . As

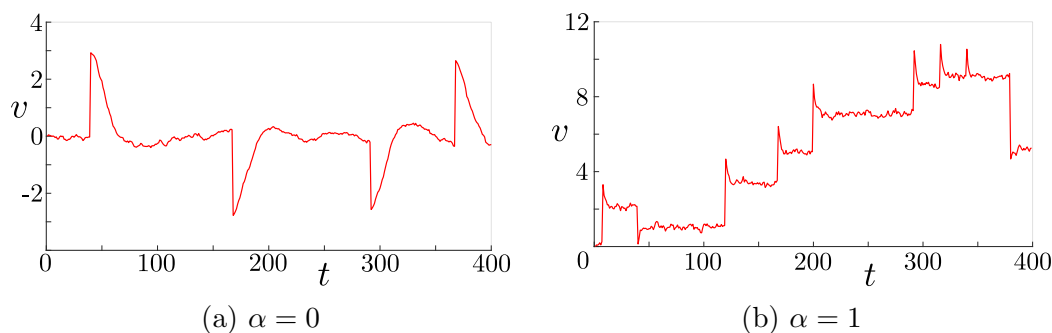


Figure 4.4. Response to shocks. (a) The system without stickiness settles to the same unique equilibrium after each shock. (b) The system with stickiness settles on a new equilibrium after a shock is applied.

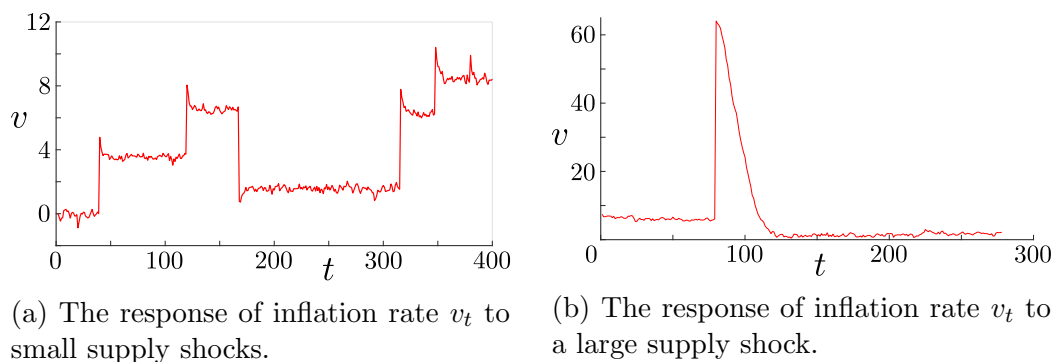


Figure 4.5. Response to shocks of different magnitudes.

a result, dynamics appear to be stable as long as the trajectory is confined to the basin of attraction of an equilibrium state. However, when noise or a shock or another fluctuation drives the trajectory outside this bounded stability domain, the run-away scenario may and is likely to start, see Figure 4.6. Stable dynamics are associated with moderate sentiment, while during the run-away the sentiment is extreme.

#### 4.7.6 Trade-off between inflation and output gap volatility

Parameters  $c_1$  and  $c_2$  of Taylor's rule (4.2) control the volatility level of inflation and output gap near an equilibrium state. Numerical simulations of the model with sticky inflation expectation show that when  $c_1$  increases (which corresponds to stronger inflation targeting

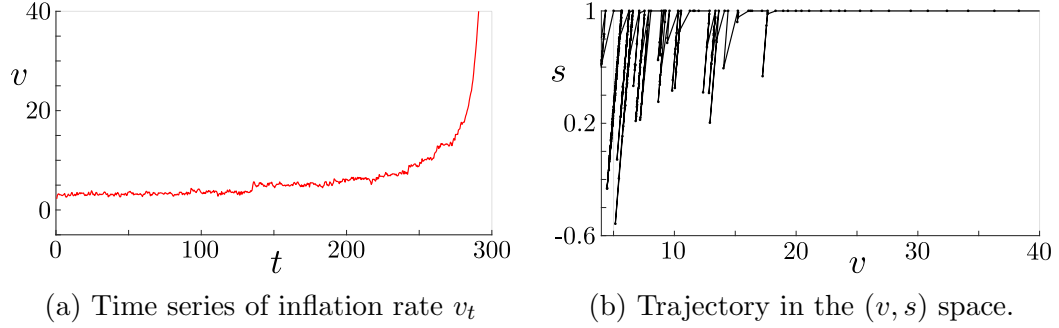
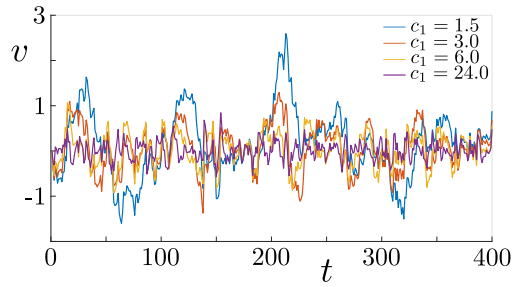


Figure 4.6. Run-away inflation scenario. Parameters are  $\alpha = 1$ ,  $a = 0.3$ ,  $b_1 = 0.5$ ,  $b_2 = 0.05$ ,  $c_1 = 0.9$ ,  $c_2 = 0.01$ . The ranges of inflation rate and output gap values at equilibrium states for this set parameter are  $v_* \in [-11, 11]$  and  $u_* \in [-10, 10]$ , respectively.

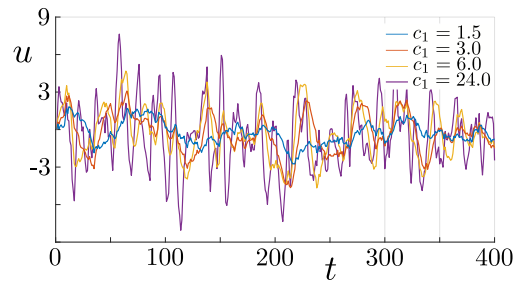
by the Central Bank), the volatility of inflation rate decreases, see Figure 4.7(a). However, at the same time, the output gap becomes highly volatile with increasing  $c_1$ , see Figure 4.7(b).

When  $c_2$  increases (stronger output gap targeting), the output gap volatility decreases, see Figure 4.8(b). In particular, the case  $c_2 = 0$  corresponding to pure inflation targeting in Taylor's rule is characterized by the highest volatility of the output gap. However, from Figure 4.8(a), it appears that the inflation rate volatility exhibits a non-monotone behavior with  $c_2$ . This is confirmed by Figure 4.9, which shows the dependence of the standard deviation of  $u_t$  and  $v_t$  on  $c_2$  for the trajectories presented in Figure 4.8. The inflation rate volatility reaches its minimum for  $c_2 \approx 0.8$  for parameter values  $a, b_1, b_2, c_1$  from Table 4.1 and  $\alpha = 1$ .

All the above results are in agreement with [29]. In addition,  $c_1$  and  $c_2$  affect the range of inflation rate value at the equilibrium states for the model (4.5). According to (4.12), this range increases with  $c_2$  and decreases with  $c_1 - 1$  (for  $c_1 > 1$ ). At the same time, the range of output gap equilibrium values is unaffected by the parameters of the Taylor's rule.

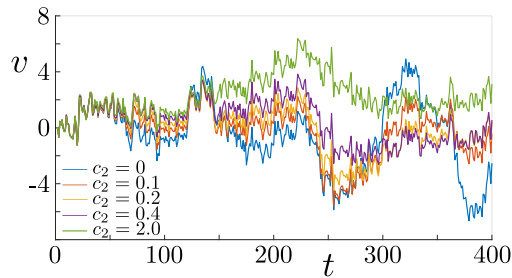


(a) Trajectory of  $v_t$  for various values of  $c_1$

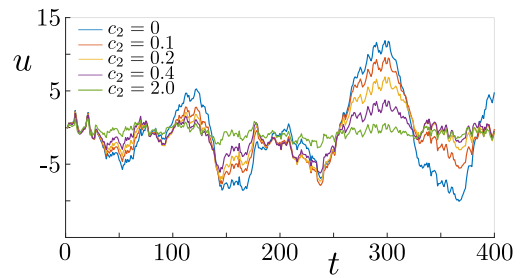


(b) Trajectory of  $u_t$  for various values of  $c_1$

Figure 4.7. Numerical simulations of  $u_t$  and  $v_t$  for  $\alpha = 1$  and various values of  $c_1$ . The remaining parameters values are from Table 4.1.

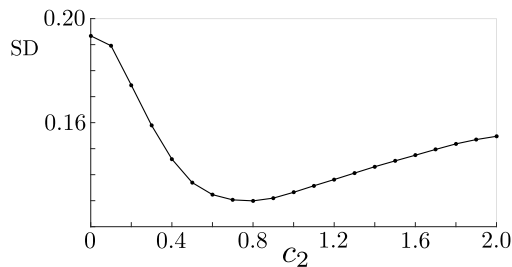


(a) Trajectory of  $v_t$  for various values of  $c_2$

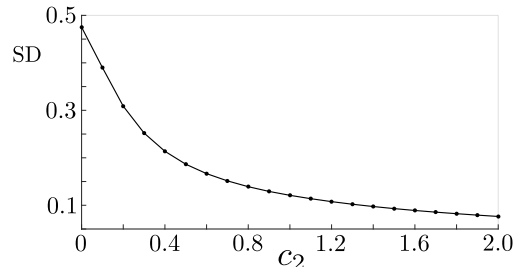


(b) Trajectory of  $u_t$  for various values of  $c_2$

Figure 4.8. Numerical simulations of  $u_t$  and  $v_t$  for  $\alpha = 1$  and various values of  $c_2$ . The remaining parameters values are from Table 4.1.



(a) Effect of  $c_2$  on the volatility of  $v$



(b) Effect of  $c_2$  on the volatility of  $u$

Figure 4.9. Measure of the effect of  $c_2$  on volatility of  $u$  and  $v$  with standard deviation (SD).



## CHAPTER 5

### OUTPUT GAP, INFLATION AND INTEREST RATE MODELS

In this section we consider the model (2.25) – (2.27) and a number of its variations and extensions. Through a simple analysis of equilibrium points and their local stability properties complemented by a few observations based on numerical simulations, we develop some understanding of these models and their connection with the simpler models studied in Chapters 3 and 4 above.

#### 5.1 Discrete time model

Having exhaustively studied a simpler model consisting of (4.1) – (4.3), we are in a better position to consider the originally proposed discrete time macroeconomic model (2.25) – (2.27), which for the reader's convenience, we shall state again as

$$\begin{cases} u_t = u_{t-1} - a(w_t - p_t) + \varepsilon_t \\ v_t = b_1 p_t + (1 - b_1)v_{t-1} + b_2 u_t + \eta_t \\ w_t = c_1(v_t - v^*) + c_2 u_t + c_3 w_{t-1} + \zeta_t. \end{cases} \quad (5.1)$$

In order to keep model (5.1) simple, we consider only a single economic agent by setting  $i = 1$  in (2.26) so that

$$p_t = v_t + \Psi_\alpha(p_{t-1} - v_t) \quad (5.2)$$

with the piecewise linear saturation function  $\Psi_\alpha(\cdot)$  given in (4.4).

##### 5.1.1 Equivalent explicit model

Equations (5.1), (5.2) form a complete PWL model for the evolution of the aggregated variables  $u_t$ ,  $v_t$ ,  $w_t$  and  $p_t$ . However, this is again an implicit model in the sense that the dependence of the variables at a moment  $t$  on their values at the moment  $t - 1$  is implicit.

In order to implement the model numerically, we proceed by solving equations (5.1), (5.2) with respect to the variables  $u_t$ ,  $v_t$ ,  $w_t$  and  $p_t = v_t - \mathcal{S}_\alpha[v_t, p_0]$ . As shown in Appendix A.5, the model can be written in the following equivalent form:

$$z_t = Az_{t-1} + s_t d + N\xi_t, \quad (5.3)$$

where  $z_t = (u_t, v_t, w_t)^\top$ ,  $\xi_t = (\varepsilon_t, \eta_t, \zeta_t)^\top$ , the matrices  $A$ ,  $N$  and the vector  $d$  are defined by

$$A = \begin{pmatrix} \frac{1-b_1}{\Delta} & \frac{a(1-b_1)(1-c_1)}{\Delta} & \frac{a(b_1-1)c_3}{\Delta} \\ \frac{b_2}{\Delta} & \frac{(1-b_1)(1+ac_2)}{\Delta} & -\frac{ab_2c_3}{\Delta} \\ \frac{(1-b_1)c_2+b_2c_1}{\Delta} & \frac{(1-b_1)(c_1+ac_2)}{\Delta} & \frac{(1-b_1-ab_2)c_3}{\Delta} \end{pmatrix}, \quad (5.4)$$

$$N = \begin{pmatrix} \frac{1-b_1}{\Delta} & \frac{a(1-c_1)}{\Delta} & \frac{a(b_1-1)}{\Delta} \\ \frac{b_2}{\Delta} & \frac{1+ac_2}{\Delta} & -\frac{ab_2}{\Delta} \\ \frac{b_2c_1+(1-b_1)c_2}{\Delta} & \frac{c_1+ac_2}{\Delta} & \frac{1-b_1-ab_2}{\Delta} \end{pmatrix},$$

$$d = \begin{pmatrix} \frac{a(b_1c_1-1)}{\Delta} \\ -\frac{ab_2+b_1(1+ac_2)}{\Delta} \\ -\frac{(ab_2+b_1)c_1+ac_2}{\Delta} \end{pmatrix},$$

where  $\Delta = (1-b_1)(1+ac_2) + ab_2(c_1-1)$ . The difference between the inflation rate and the expectation of an agent  $s_t = v_t - p_t$  is defined by the equation

$$s_t = \frac{1}{1+\beta} \Psi_{(1+\beta)\alpha}(f_t - f_{t-1} + s_{t-1}) \quad (5.5)$$

with

$$\beta = \frac{(1-b_1)(1+ac_2) + ab_2(c_1-1)}{b_1(1+ac_2) + ab_2} \quad (5.6)$$

and

$$f_t = \frac{b_2}{b_1(1+ac_2) + ab_2} u_{t-1} + \frac{(1-b_1)(1+ac_2)}{b_1(1+ac_2) + ab_2} v_{t-1} - \frac{ab_2c_3}{b_1(1+ac_2) + ab_2} w_{t-1} \\ + \frac{b_2}{b_1(1+ac_2) + ab_2} \varepsilon_t + \frac{1+ac_2}{b_1(1+ac_2) + ab_2} \eta_t - \frac{ab_2}{b_1(1+ac_2) + ab_2} \zeta_t. \quad (5.7)$$

Equations (5.3) – (5.7) express the variables  $u$ ,  $v$ ,  $w$ ,  $s = v - p$  at the moment  $t$  explicitly in terms of their values at the previous moment  $t - 1$  and the noise terms  $\varepsilon_t$ ,  $\eta_t$ ,  $\zeta_t$ . We use these equations for all the simulations of this section. Note that (5.5) defines a stop operator with the input  $f_t$  and the threshold  $(1 + \beta)\alpha$ , which is different from  $\alpha$  (cf. (5.2)), hence (5.5) can be written as

$$s_t = \frac{1}{1 + \beta} \mathcal{S}_{(1+\beta)\alpha}[f_t, s_0] \quad (5.8)$$

using the notation (2.12). It is important to remember that the transition to equations (5.3) – (5.7) is justified under the condition that  $\beta$  (cf. (5.6)) is positive. Notice that  $\beta$  is the same in (5.6) and (4.8). In particular,  $c_1 > 1$  implies  $\beta > 0$ .

### 5.1.2 Line segment of equilibrium points

Let us set  $\xi_t = 0$  in (5.3) – (5.7) and consider the autonomous system

$$z_t = Az_{t-1} + s_t d, \quad z_t = (u_t, v_t, w_t)^\top \quad (5.9)$$

with  $s_t$  defined by (5.5) and

$$f_t = \frac{b_2}{b_1(1 + ac_2) + ab_2} u_{t-1} + \frac{(1 - b_1)(1 + ac_2)}{b_1(1 + ac_2) + ab_2} v_{t-1} - \frac{ab_2 c_3}{b_1(1 + ac_2) + ab_2} w_{t-1}. \quad (5.10)$$

This is a system without exogenous noise. As seen in the previous chapter, the model produces a segment of equilibrium points, which re-emphasizes the multiplicity of equilibrium states of the economy (cf. Figure 2.8) as a function of expectations (sentiments) of economic agents. Indeed, equation (5.9) implies

$$z_* = s_*(\mathbb{I} - A)^{-1}d = s_* \left( \frac{b_1}{b_2}, \frac{b_1 c_2 + b_2(1 - c_3)}{b_2(1 - c_1 - c_3)}, \frac{b_1 c_2 + b_2 c_1}{b_2(1 - c_1 - c_3)} \right)^\top \quad (5.11)$$

for an equilibrium point  $z_* = (u_*, v_*, w_*)^\top$ , where  $\mathbb{I}$  is the  $3 \times 3$  identity matrix. Once again, one obtains a different equilibrium for any admissible value of the sentiment variable  $s_*$ ,

which are limited to the interval  $-\alpha \leq s_* \leq \alpha$ . In particular, the equilibrium values of output gap, inflation rate and interest rate belong to the ranges

$$u_*(s_*) = \frac{b_1}{b_2} s_*, \quad v_*(s_*) = \frac{b_1 c_2 + b_2(1 - c_3)}{b_2(1 - c_1 - c_3)} s_*, \quad w_*(s_*) = \frac{b_1 c_2 + b_2 c_1}{b_2(1 - c_1 - c_3)} s_*,$$

with  $-\alpha \leq s_* \leq \alpha$ .

As in Chapter 4, one can notice that the range of equilibrium values of the output gap is unaffected by the controls  $c_1, c_2, c_3$  applied by the regulator through the Taylor rule (see the last equation in (5.1)). However, these controls affect the range of possible values of equilibrium states of the inflation rate  $v_*$  and interest rate  $w_*$ .

### 5.1.3 Numerical results

**Equilibria of the autonomous equation.** Due to the presence of  $c_3$  in the Taylor rule, we use the entire parameter set in [29] by extending the parameter set in Table 4.1 to Table 5.1. The components of the equilibrium points  $z_*(s_*) = (u_*(s_*), v_*(s_*), w_*(s_*))^\top$  for this parameter set and  $\alpha = 1$  range over the intervals

$$u_*(s_*) \in [-10, 10], \quad v_*(s_*) \in [-5.5, 5.5], \quad w_*(s_*) \in [-6.5, 6.5].$$

Fortuitously, numerical simulations give an evidence that the segment of equilibrium states

Table 5.1. The set of parameter values.

Parameters	$a$	$b_1$	$b_2$	$c_1$	$c_2$	$c_3$
Values	0.2	0.5	0.05	1.5	0.5	0.5

of system (5.9) is globally asymptotically stable for this parameter regime. Each simulated trajectory converged to an equilibrium point on the segment of equilibrium points (cf. Figure 5.1(a)). Simulations from different initial conditions result in trajectories converging to different equilibrium points on the segment of equilibrium points (cf. Figure 5.1(b)<sup>1</sup>). This

---

<sup>1</sup>This figure was first published in [8]

result re-emphasizes the path dependence characteristic of the play operator, which is used to model expectations of future inflation.

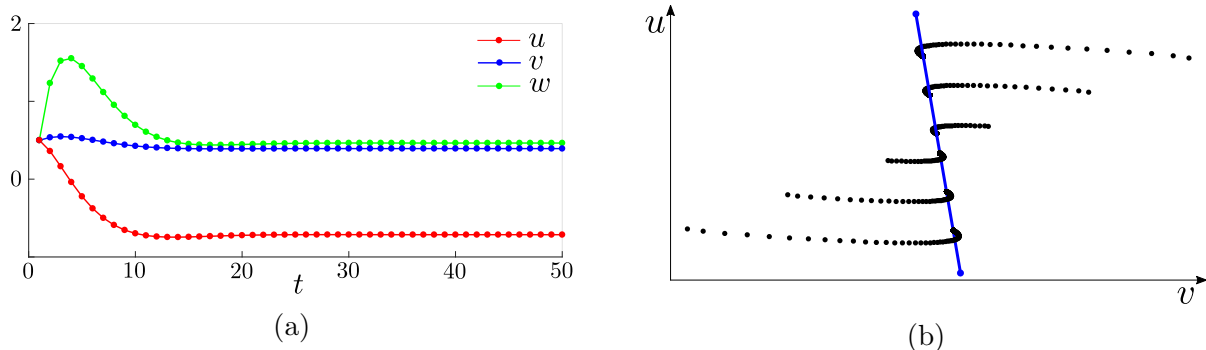


Figure 5.1. System (5.9) converges to equilibrium points for parameter regime in Table 5.1. (a) A set of trajectories converging to equilibrium state  $z_*(s_*)$ . (b) Projection of trajectories converging to different points of the segment of equilibrium points in the  $(v, u)$  plane.

**Periodic dynamics.** Let us write (5.10) in the form  $f_t = b^\top z_{t-1}$ , with

$$b^\top = \left( \frac{b_2}{b_1(1+ac_2) + ab_2}, \frac{(1-b_1)(1+ac_2)}{b_1(1+ac_2) + ab_2}, -\frac{ab_2c_3}{b_1(1+ac_2) + ab_2} \right).$$

For  $|s_t| < (1+\beta)\alpha$ , equation (5.8) becomes

$$s_t - s_{t-1} = \frac{1}{1+\beta} b^\top (z_t - z_{t-1}).$$

Therefore, linearizing (5.9) at an equilibrium state  $z_*(s_*)$  with  $|s_*| < \alpha$  gives

$$z_t - z_*(s_*) = B(z_{t-1} - z_*(s_*)),$$

where matrix  $B \in \mathbb{R}^{3 \times 3}$  is defined by

$$B = \frac{1}{1+\beta} \left( (1+\beta)A + db^\top \right). \quad (5.12)$$

Interestingly, parameter regimes exist for which the matrix  $A$  defined by (5.4) is stable but the matrix  $B$  is unstable. Figure 5.2<sup>2</sup> presents different periodic scenarios that we observed

<sup>2</sup>These figures were first published in [8]

for such parameter regimes (cf. Theorems 3.1 and 3.2 for similar scenarios in the prototype system (3.1)).

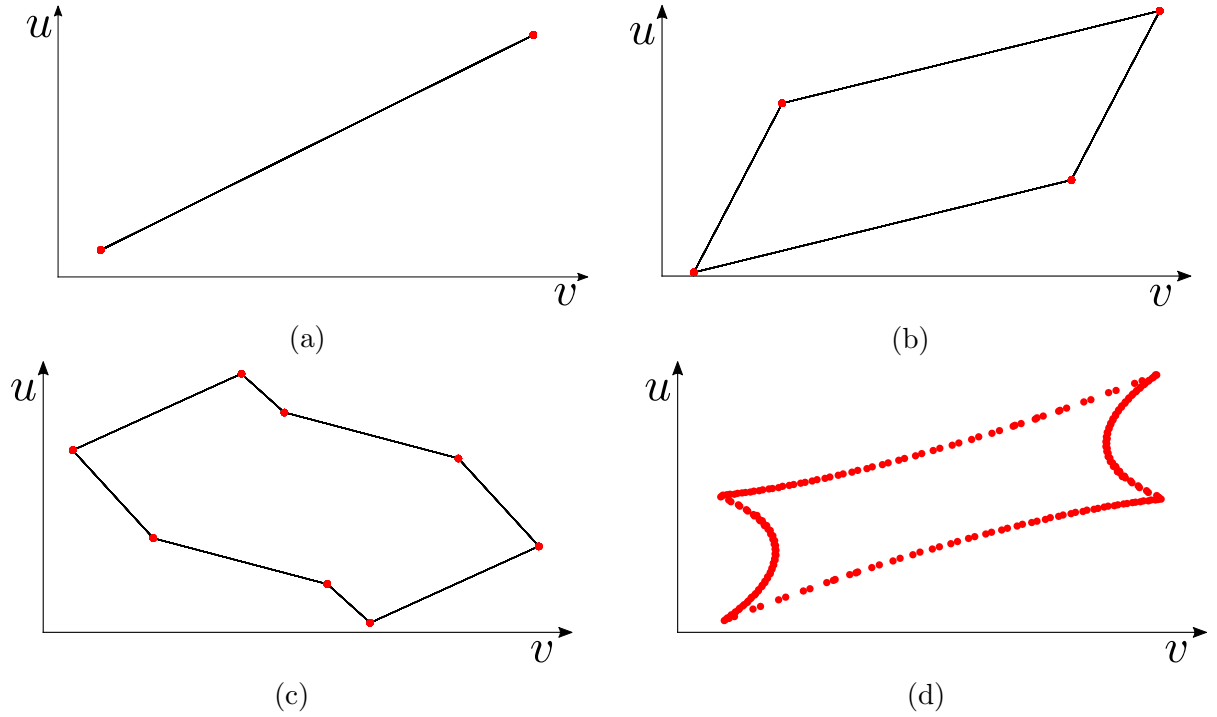


Figure 5.2. Projections of various trajectories of system (5.9) onto  $(v, u)$  plane. The system contains one stop operator (representing one agent), that is  $m = 1$ ,  $\alpha_1 = 1$ ,  $\mu_1 = 1$ . Parameters of equations (5.9) are given in the format  $a, b = (b_1, b_2), c = (c_1, c_2, c_3)$ .

- (a) 2-periodic orbit for  $a = 0.99, b = (0.76, 0.9), c = (1.4, 9.7, 0.025)$ .
- (b) 4-periodic orbit for  $a = 0.7, b = (0.75, 0.5), c = (4.8, 3.6, 3.45)$ .
- (c) 8-periodic orbit for  $a = 0.9, b = (0.73, 0.9), c = (1.2, 3.15, 1.3)$ .
- (d) Quasi-periodic orbit for  $a = 0.7, b = (0.7, 0.55), c = (4.8, 4.15, 3.8)$ .

Though the parameter regimes for which these periodic dynamics are obtained may not make sense economically, these results confirm the claims of [42] that economic systems have inherent tendencies to produce periodic and even frequent systemic crisis (tranquility). According to this theory, busts and booms in economic activities are not only the results of human behaviour [29], but intrinsic to the economic system.

**Response to shocks.** We test system (5.3) – (5.7) by applying shocks to the aggregate supply equation through the  $\eta_t$  term. The results are similar to the results observed in the previous chapter. The shocks generate a transition from one equilibrium state to another.

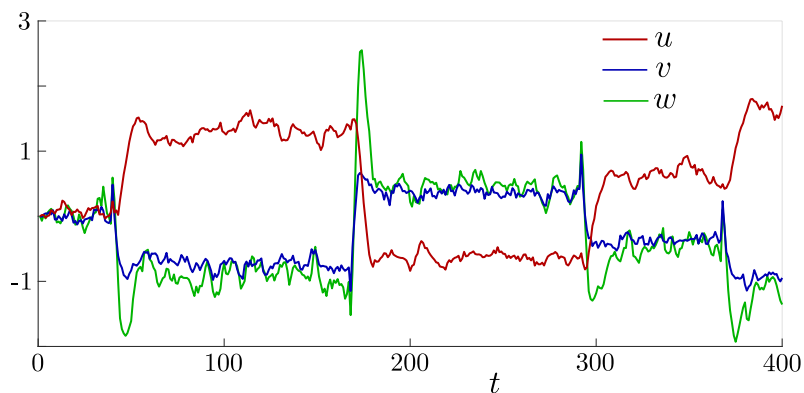


Figure 5.3. System (5.3) responding to supply shocks for parameter regime in Table 5.1.

It is not surprising that, as a result of a shock, trajectories of the interest rate  $w_t$  and the inflation rate  $v_t$  shift in the same direction, while the trajectories of output gap  $u_t$  shifts in the opposite direction, see Figure 5.3. This occurs because a shock to inflation generates a proportional shock to interest rate through the Taylor rule. However, a shock to the interest rate generates an opposite shock to the output gap through the demand equation thereby shifting the trajectories of the output gap in the opposite direction of the other two trajectories.

## 5.2 Hybrid model

Every consumer makes demands for specific goods and services at least once everyday either in response to an advertisement or for the purposes of restocking. These individual demands result in firms or manufacturers supplying the goods and services. The daily demands of consumers and supplies of suppliers results in daily (hourly) changes in prices and in (un)employment. These demands and supplies give the national (federal) statistical services (system or office) the needed data to enable them inform the populace of the average monthly

inflation. However, Central Banks (federal reserves) only review and update (maintain) the interest rate  $w$  quarterly (bi-annually or yearly) after reviewing the economy (market) over a period for the purposes of regulating and steering the economy in the direction deemed to be in the best interest of the nation.

Motivated by these considerations, we modify the model assuming that the output gap  $u$  and the inflation rate  $v$  are continuous time variables but the interest rate  $w$  is a discrete time variable. Reformulating (5.1) along these lines and setting the noise terms for simplicity to zero gives a hybrid system [37, 50, 80, 85] of the form

$$\begin{cases} \dot{u}(t) = a(v(t) - w_{n-1} - s(t)), \\ \dot{v}(t) = \frac{b_2}{1-b_1}u(t) - \frac{b_1}{1-b_1}s(t), \\ w_n = c_1v(n) + c_2u(n) + c_3w_{n-1}, \end{cases} \quad (5.13)$$

where  $t \in \mathbb{R}_+$ ,  $n \in \mathbb{N}_0$  and

$$s(t) = \mathcal{S}_\alpha[v, s_0](t) \quad (5.14)$$

is the stop operator with the continuous time input  $v = v(t)$  and output  $s = s(t)$ . As described in Chapter 2, this operator can be obtained as a continuous extension of the stop operator with discrete time inputs if such an input is identified with the sequences of extremum values of a piecewise monotone continuous time input. The continuous extension can be performed using the sup-norm or  $W^{1,1}$  norm. The operator (5.14) obtained by this procedure is globally Lipschitz continuous [16].

**Equilibrium points.** Equilibrium solutions of the hybrid system (5.13), (5.14) form line segments

$$u_*(s_*) = \frac{b_1}{b_2} s_*, \quad v_*(s_*) = \frac{b_1c_2 + b_2(1-c_3)}{b_2(1-c_1-c_3)} s_*, \quad w_*(s_*) = \frac{b_1c_2 + b_2c_1}{b_2(1-c_1-c_3)} s_*, \quad (5.15)$$

where  $s_* \in [-\alpha, \alpha]$ . These are the same line segments of equilibrium states that the discrete time system (5.3) has (cf. (5.11)).



In order to evaluate dynamics far from equilibrium states, we linearize the system at infinity by setting  $s \equiv 0$  in (5.13) and solving the resulting linear system on a unit time interval:

$$u(t) = \cosh\left(\sqrt{ab_2}t\right) u_o + \sqrt{\frac{a}{b_2}} \sinh\left(\sqrt{ab_2}t\right) v_o - \sqrt{\frac{a}{b_2}} \sinh\left(\sqrt{ab_2}t\right) w_o, \quad (5.16)$$

$$v(t) = \sqrt{\frac{b_2}{a}} \sinh\left(\sqrt{ab_2}t\right) u_o + \cosh\left(\sqrt{ab_2}t\right) v_o + \left(1 - \cosh\left(\sqrt{ab_2}t\right)\right) w_o, \quad (5.17)$$

$$\begin{aligned} w_1 = & \left( c_2 \cosh\left(\sqrt{ab_2}\right) + c_1 \sqrt{\frac{b_2}{a}} \sinh\left(\sqrt{ab_2}\right) \right) u_o \\ & + \left( c_1 \cosh\left(\sqrt{ab_2}\right) + c_2 \sqrt{\frac{a}{b_2}} \sinh\left(\sqrt{ab_2}\right) \right) v_o \\ & + \left( c_1 + c_3 - c_1 \cosh\left(\sqrt{ab_2}\right) - c_2 \sqrt{\frac{a}{b_2}} \sinh\left(\sqrt{ab_2}\right) \right) w_o, \end{aligned} \quad (5.18)$$

where  $u_o$ ,  $v_o$  and  $w_o$  are initial values and  $0 \leq t \leq 1$ . Setting  $t = 1$  in (5.16) – (5.18) gives the transition matrix  $P$  so that

$$z_n = Pz_{n-1}, \quad z_n = (u(n), v(n), w_n)^\top, \quad P \in \mathbb{R}^{3 \times 3}. \quad (5.19)$$

Since the output of the stop operator,  $s(t)$  is bounded, solutions of system (5.13), (5.14) will converge to a bounded set for parameter regimes for which matrix  $P$  is stable.

Now, let us consider dynamics near an equilibrium point. For  $|s_*| < \alpha$ , system (5.13) is described by the linear system

$$\begin{cases} \dot{u} = -a(w_{n-1} + v_*(s_*) - s_*), \\ \dot{v} = \frac{b_2}{1-b_1}u(t) - \frac{b_1}{1-b_1}\left(v(t) + s_* - v_*(s_*)\right), \\ w_n = c_1v(n) + c_2u(n) + c_3w_{n-1}. \end{cases} \quad (5.20)$$

Shifting the equilibrium to zero, we obtain the explicit solution

$$u(t) = u_o - atw_o, \quad (5.21)$$

$$v(t) = \frac{b_2}{b_1} (1 - e^{-b_1 t}) u_o + v_o e^{-b_1 t} + \frac{1}{b_1^2} (ab_2 (1 - e^{-b_1 t}) - ab_1 b_2 t) w_o, \quad (5.22)$$

$$w_1 = \left( \frac{b_2 c_1}{b_1} (1 - e^{-b_1}) + c_2 \right) u_o + c_1 v_o e^{-b_1} + \left( \frac{c_1}{b_1^2} (ab_2 (1 - e^{-b_1}) - ab_1 b_2) - ac_2 + c_3 \right) w_o \quad (5.23)$$

on the interval  $0 \leq t \leq 1$ . This defines the transition matrix  $Q$  for the local discrete time dynamics:

$$z_n - z_*(s_*) = Q \left( z_{n-1} - z_*(s_*) \right). \quad (5.24)$$

Hence stability of the equilibrium points is defined by the stability properties of  $Q$ .

**Numerical results.** We performed numerical simulations and observed that for the parameter values of Table 5.1 and  $\alpha = 1$ , the segments of equilibrium points (5.15) are globally stable and each trajectory convergence to an equilibrium state  $z_*(s_*)$ ; see Figure 5.4. However,

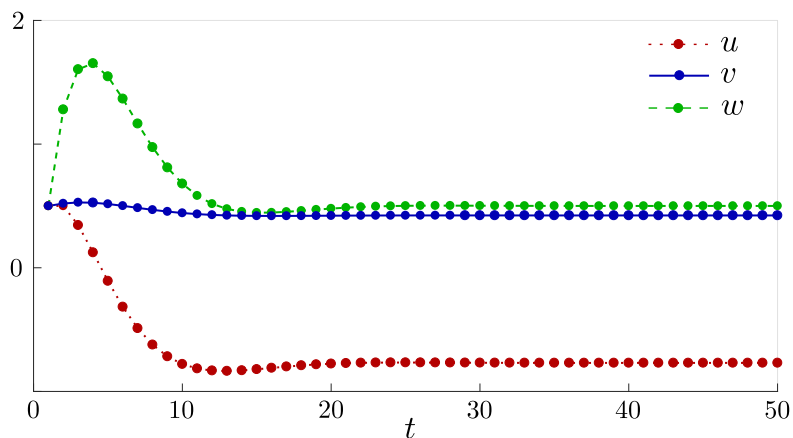


Figure 5.4. A set of trajectories of system (5.13) converging to an equilibrium state  $z_*(s_*)$ .

when we tested parameter regimes for which the transition matrix  $P$  in (5.19) is stable but

the transition matrix  $Q$  in (5.24) is unstable, we observed various periodic and quasi-periodic scenarios.

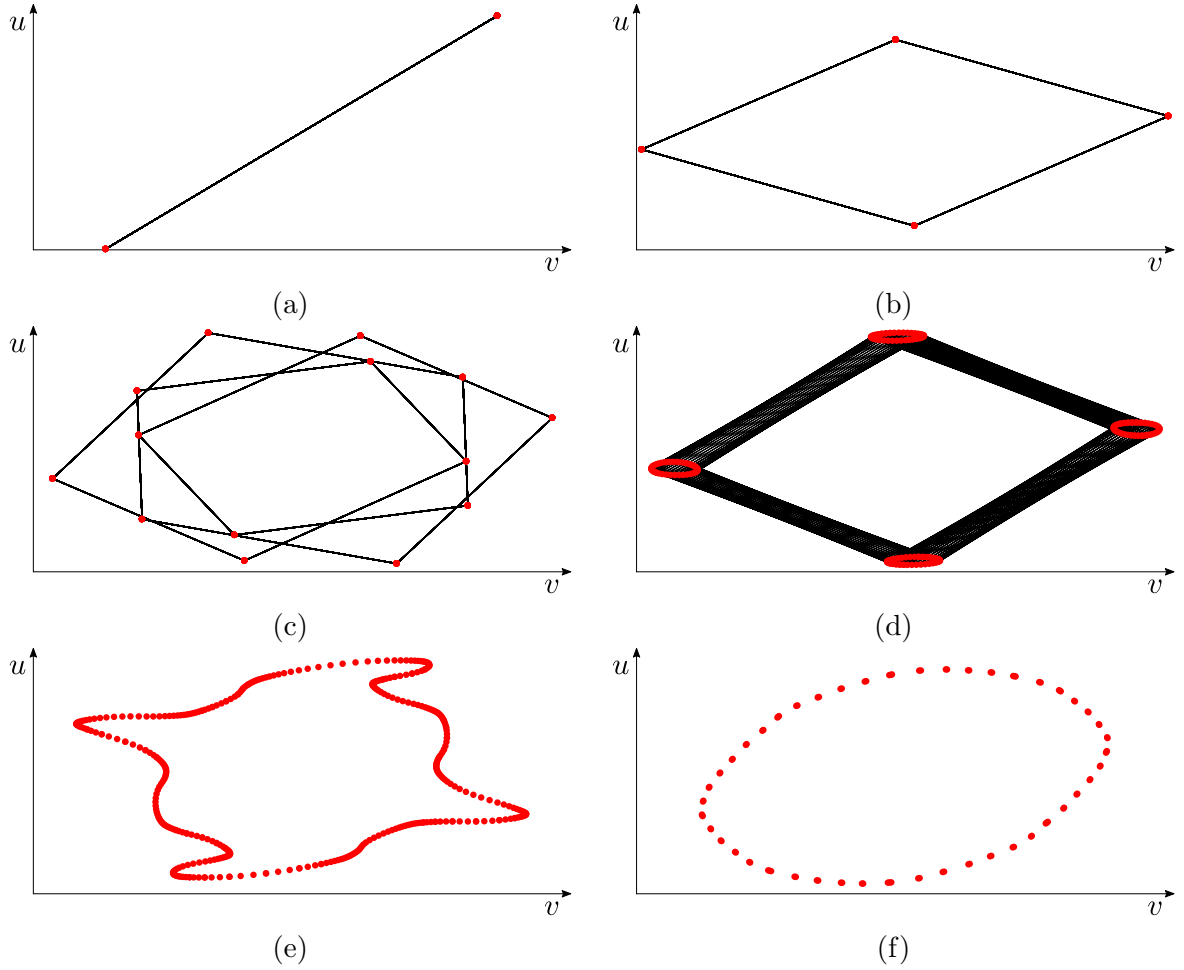


Figure 5.5. Projections of various trajectories (at integer time moments) of the hybrid system (5.13) onto  $(v, u)$  plane. The system contains one stop operator (5.14) (representing one agent). Parameters of equations (5.13) are given in the format  $a, b = (b_1, b_2), c = (c_1, c_2, c_3)$ .

- (a) 2-periodic orbit for  $a = 0.617, b = (0.429, 2.78), c = (1.16, 5.5, 0.566)$ .
- (b) 4-periodic orbit for  $a = 1.0, b = (0.075, 3.54), c = (0.95, 1.2, 0.15)$ .
- (c) 14-periodic orbit for  $a = 1.0, b = (0.075, 3.54), c = (0.95, 1.2, 0.19)$ .
- (d) A quasi-periodic orbit of the 4-th iterate of the map for  $a = 1.0, b = (0.075, 3.54), c = (0.96, 1.3, 0.18)$ .
- (e) A quasi-periodic orbit for  $a = 1.0, b = (0.075, 3.54), c = (0.95, 1.5, 0.18)$ .
- (f) A quasi-periodic orbit for  $a = 0.61, b = (0.428, 2.78), c = (0.9, 4.2, 0.57)$ .

### 5.3 Multi-agent model

Just as traders in financial markets process the same information differently and make decisions which they consider prudent by their judgment, so do economic agents. Agents process and interpret the same piece of information differently based on their individual perceptions and expectations. While a pessimist may quickly make a decision when inflation is at a point on a day, an optimist may adopt the wait-and-see attitude with the hope that inflation may decline or stagnate for the next few days. In addition, these agents may also receive and process imperfect information [29, 30] from various sources. This phenomenon of agents interpreting perfect (or imperfect) and using information differently depending on their convictions suggests that the agent's expectation, which is modeled by the play operator could be replaced by an aggregate expectation of multiple agents, modeled by the PI operator [63, 111]. Figure 2.6 illustrates how the expectations of individual agents are generated by the PI operator.

Let us now consider model (2.25) – (2.27) with multiple play operators ( $m > 1$ ). To simplify the problem, and also to emphasize the role of multiple stop operators (the PI model), we set the coefficient  $c_3$  of the Taylor rule to zero as in Chapter 4. Hence, we consider the system (4.1), (4.2) coupled with the relationship (2.26) between  $p_t$  and  $v_t$ :

$$p_t = \sum_{i=1}^t \mu_i \mathcal{P}_{\alpha_i}[v_t, p_0^i] = v_t - \sum_{i=1}^m \mu_i \mathcal{S}_{\alpha_i}[v_t, s_0^i], \quad (5.25)$$

where

$$\sum_{i=1}^m \mu_i = 1. \quad (5.26)$$

The PI operator (5.25) replaces the simple play operator (4.3) considered in Chapter 4.

The implicit system (4.1), (4.2), (5.25) with multiple agents can be converted into an explicit form using the technique described in Section 2.3. The explicit system

$$z_t = Az_{t-1} + \hat{\mathcal{K}}[c \cdot z_{t-1} + \hat{\xi}_t]d + N\xi_t, \quad (5.27)$$

which is similar to its counterpart (4.5), but includes a PI operator  $\hat{\mathcal{K}}$  with rescaled thresholds  $\gamma_i$  and weights  $\kappa_i$  (see Section 2.3 for details; note that  $\hat{\mathcal{K}} = \mathcal{K}^{-1}$ );  $\xi_t, \hat{\xi}_t$  denote the noise terms. Equation (5.27) is a PWL system in  $\mathbb{R}^{m+2}$ .

The stability properties of the equilibrium states of system (5.27) with multiple agents are similar to the stability properties considered above in Section 4.5. In particular, if we consider the system without external noise for  $c_1 > 1$ , then the set of equilibrium states is globally stable, and every trajectory converges to an equilibrium state.

In the simulations of this section, we classify economic agents into three categories, strongly, moderately, and weakly sensitive to inflation rate variations (hence  $m = 3$ ), by assigning thresholds  $\alpha_1 < \alpha_2 < \alpha_3$ , respectively, to these groups, see Figure 2.6. Further, the contribution of each group to the aggregate expectation of inflation carries equal weight,  $\mu_i = 1/3$ .

Numerical results that we obtained for model (4.1), (4.2), (5.25) with three agents are qualitatively similar to the results obtained for the model with one agent, see Figures 5.6 – 5.13, which are counterparts of Figures 4.3 – 4.9, respectively. The parameter regime for these two set of Figures are in Table 4.1.

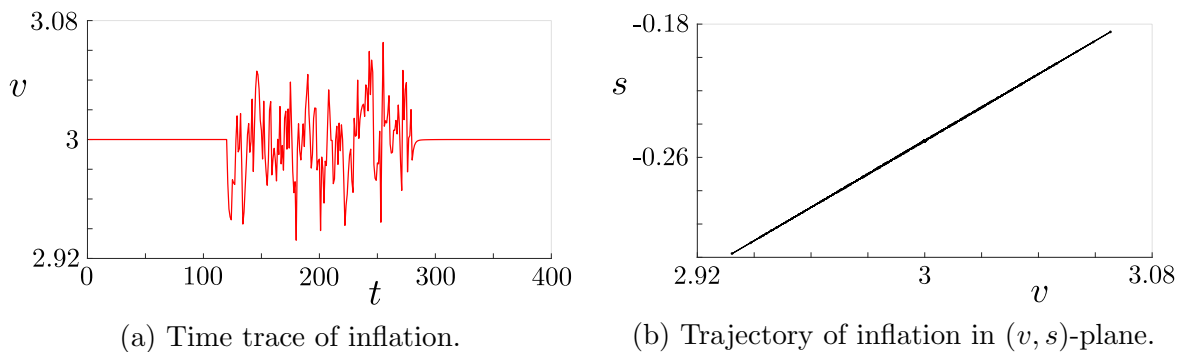


Figure 5.6. Trajectory of system (5.27) with 3 agents near an equilibrium state when none of the agents achieves an extreme sentiment (cf. Figure 4.3(a,d)).

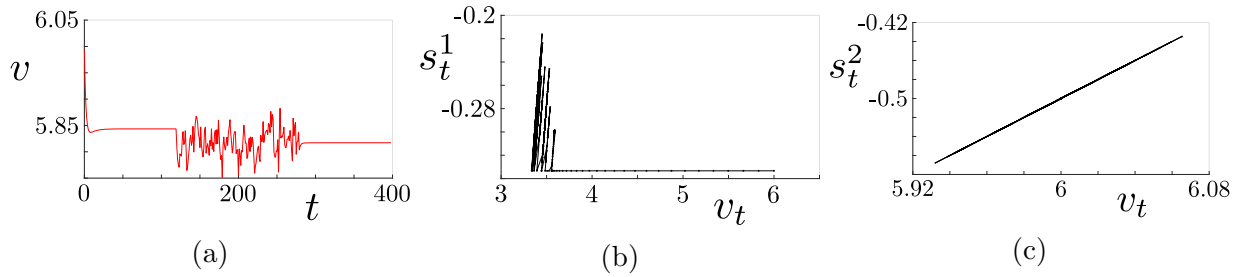


Figure 5.7. Trajectory of the system with 3 agents when the most sensitive agent reaches an extreme sentiment and the two less sensitive agents don't (cf. Figure 4.3(b,e)). (a) Time trace of inflation. A change of the equilibrium state occurs. (b) Trajectory in  $(v, s)$ -plane for  $\alpha = \frac{1}{3}$ . (c) Trajectory in  $(v, s)$ -plane for  $\alpha = \frac{2}{3}$  and  $\alpha = 1$ .

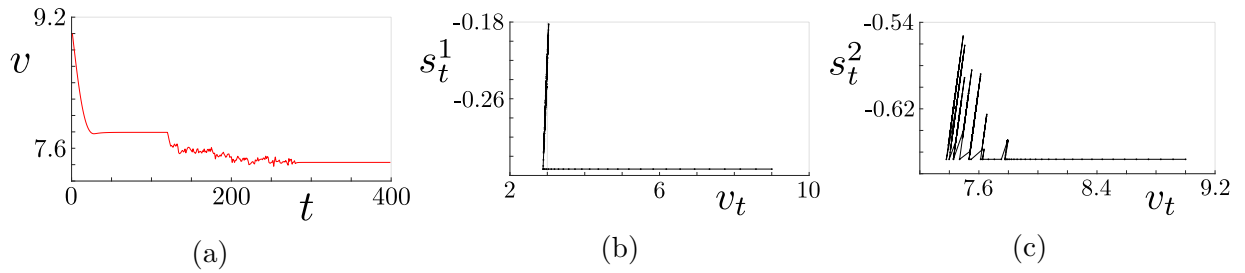


Figure 5.8. Trajectory of the system with 3 agents with the most sensitive agent and the moderately sensitive agent having an extreme sentiment at the initial (equilibrium) point (cf. Figure 4.3(c,d)). (a) Time trace of inflation. (b) Trajectory in  $(v, s)$ -plane for  $\alpha = \frac{1}{3}$ . (c) Trajectory in  $(v, s)$ -plane for  $\alpha = \frac{2}{3}$ . Trajectory of least sensitive agent (i.e.,  $\alpha = 1$ ) is similar to Figure 5.7(c).

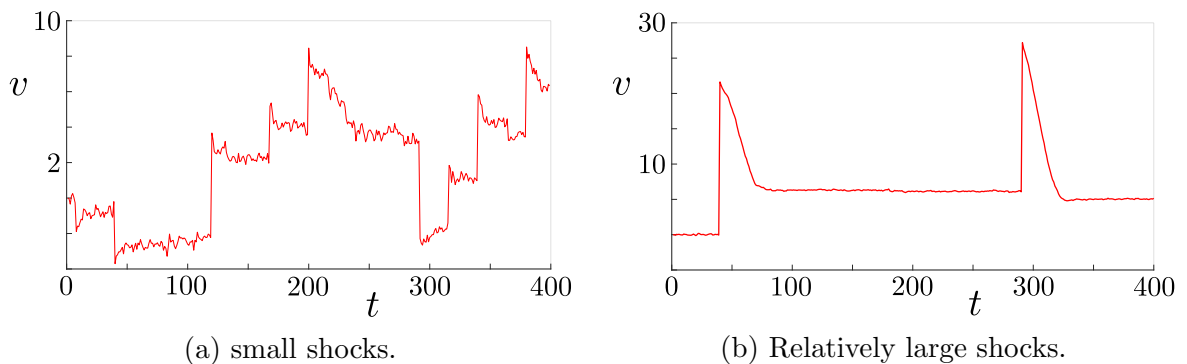


Figure 5.9. Changes of the equilibrium state in the model with 3 agents due to shocks (cf. Figures 4.4, 4.5).

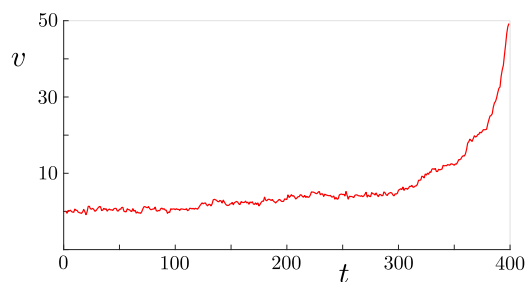
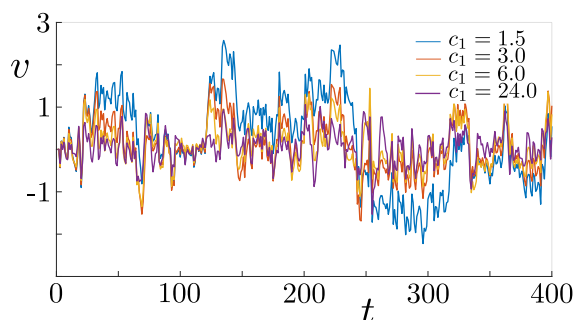
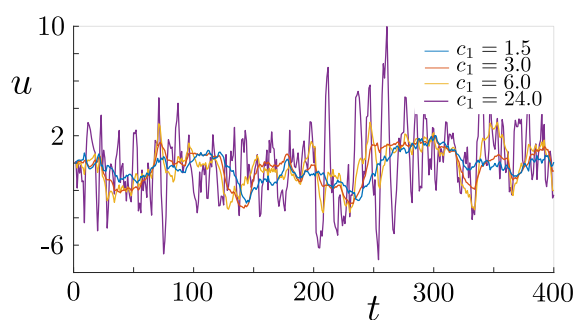


Figure 5.10. The run-away inflation scenario in the model with three agents in the case  $c_1 < 1$  (cf. Figure 4.6).

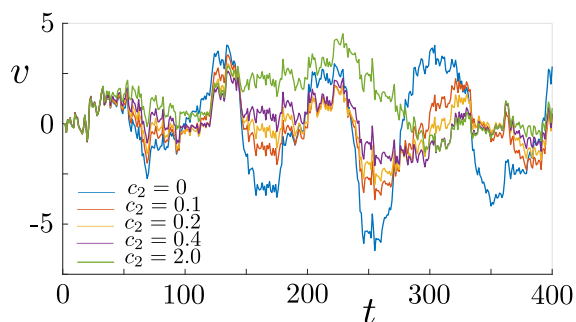


(a) Inflation rate,  $v_t$ .

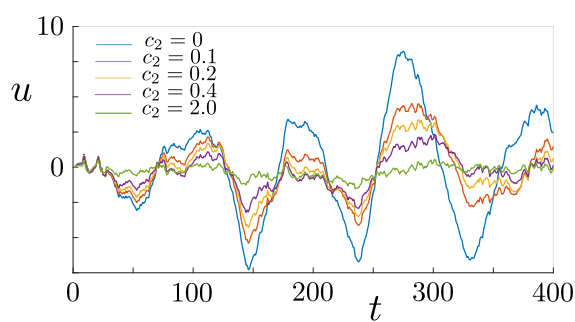


(b) Output gap,  $u_t$ .

Figure 5.11. Trade-off between inflation rate and output gap volatility in the model with 3 agents as the inflation targeting parameter  $c_1$  in the Taylor rule is varied (cf. Figure 4.7).



(a) Inflation rate,  $v_t$ .



(b) Output gap,  $u_t$ .

Figure 5.12. Trade-off between inflation rate and output gap volatility in the model with 3 agents as the output gap targeting parameter  $c_2$  in the Taylor rule is varied (cf. Figure 4.8).

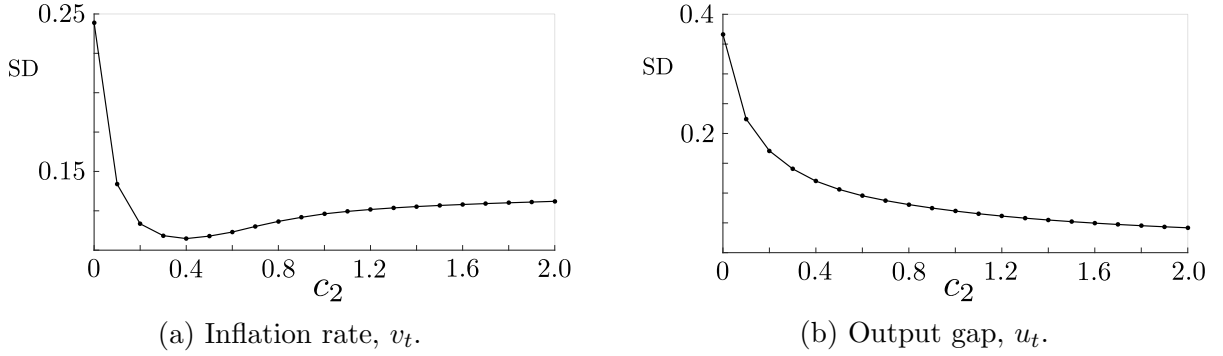


Figure 5.13. Measure of the effect of  $c_2$  on the volatility of  $v_t$  and  $u_t$  with standard deviation (SD) (cf. Figure 4.9).

#### 5.4 Sticky Central Bank model

The Central Bank policy can presumably exhibit stickiness too. To explore this scenario, in this section, we again consider system (4.1) but replace the Taylor rule (4.2) with the relation

$$w_t = \mathcal{P}_\sigma[c_1 v_t + c_2 u_t] \tag{5.28}$$

involving the play operator. At the same time, for the sake of simplicity, and in order to isolate the effect of stickiness in the Central Bank response on the system, we remove the play operator from equations (4.1) thus assuming that the aggregate expectation of inflation equals to the current actual inflation rate,  $p_t = v_t$ ; this corresponds to setting  $\alpha = 0$  in equations (4.1) – (4.3). In this case,

$$\begin{cases} u_t = u_{t-1} - a(w_t - v_t) + \varepsilon_t, \\ v_t = v_{t-1} + \frac{b_2}{1-b_1} u_t + \eta_t. \end{cases} \tag{5.29}$$

It would be interesting to consider the model with both sticky inflation expectation and sticky Central Bank response, however this is beyond the scope of this dissertation.

System (5.28), (5.29) can be written in the form (4.5) with

$$s_t = \mathcal{S}_\sigma[c_1 v_t + c_2 u_t],$$



the matrix  $A$  defined by (4.6), vector  $d$  and matrix  $N$  defined by

$$d = \begin{pmatrix} \frac{a(1-b_1)}{(1-b_1)(1+ac_2)+ab_2(c_1-1)} \\ \frac{ab_2}{(1-b_1)(1+ac_2)+ab_2(c_1-1)} \end{pmatrix},$$

$$N = \begin{pmatrix} \frac{1-b_1}{(1-b_1)(1+ac_2)+ab_2(c_1-1)} & \frac{a(1-b_1)(1-c_1)}{(1-b_1)(1+ac_2)+ab_2(c_1-1)} \\ \frac{b_2}{(1-b_1)(1+ac_2)+ab_2(c_1-1)} & \frac{(1-b_1)(1+ac_2)}{(1-b_1)(1+ac_2)+ab_2(c_1-1)} \end{pmatrix}.$$

The inversion technique presented in Subsection 2.3 can be easily adapted to convert the implicit system (5.28), (5.29) into a well-defined explicit system provided that

$$1 - b_1 - ab_2 > 0. \quad (5.30)$$

(see Appendix A.6). Hence, we assume that this condition is satisfied.

Equilibrium states of system (5.28), (5.29) with zero noise terms form the segment

$$(u_*(s_*), v_*(s_*)) = \left(0, \frac{s_*}{c_1 - 1}\right), \quad s_* \in [-\sigma, \sigma]. \quad (5.31)$$

Notice that the output gap value is zero for all the equilibrium states, while the equilibrium of inflation rate ranges over an interval of values.

The linearization  $z_t - z_*(s_*) = B(z_{t-1} - z_*(s_*))$  of this system at any equilibrium point with  $s_* \in (-\sigma, \sigma)$  has the matrix

$$B = \begin{pmatrix} \frac{1-b_1}{1-b_1-ab_2} & \frac{a(1-b_1)}{1-b_1-ab_2} \\ \frac{b_2}{1-b_1-ab_2} & \frac{1-b_1}{1-b_1-ab_2} \end{pmatrix}.$$

Since

$$\det B = \frac{1 - b_1}{1 - b_1 - ab_2} > 1,$$

all these equilibrium states are *unstable*. Therefore, all the equilibrium states with  $s_* \in (-\sigma, \sigma)$  are unstable for any set of parameter values. That is, stickiness in the Taylor rule leads to destabilization of equilibrium states.

On the other hand, for large values of  $z_t = (u_t, v_t)^\top$ , the system can be approximated by equation (4.15), which is exponentially stable (as shown in Appendix A.3). This ensures the *permanence* property of system (5.28), (5.29) in the sense that, in the absence of noise, all trajectories converge to a bounded domain  $\Omega$  surrounding the segment of equilibrium states and, upon entering this domain, remain there. In the presence of noise, a trajectory wanders in a vicinity of  $\Omega$  most of the time, and returns to this vicinity after a large fluctuation or perturbation.

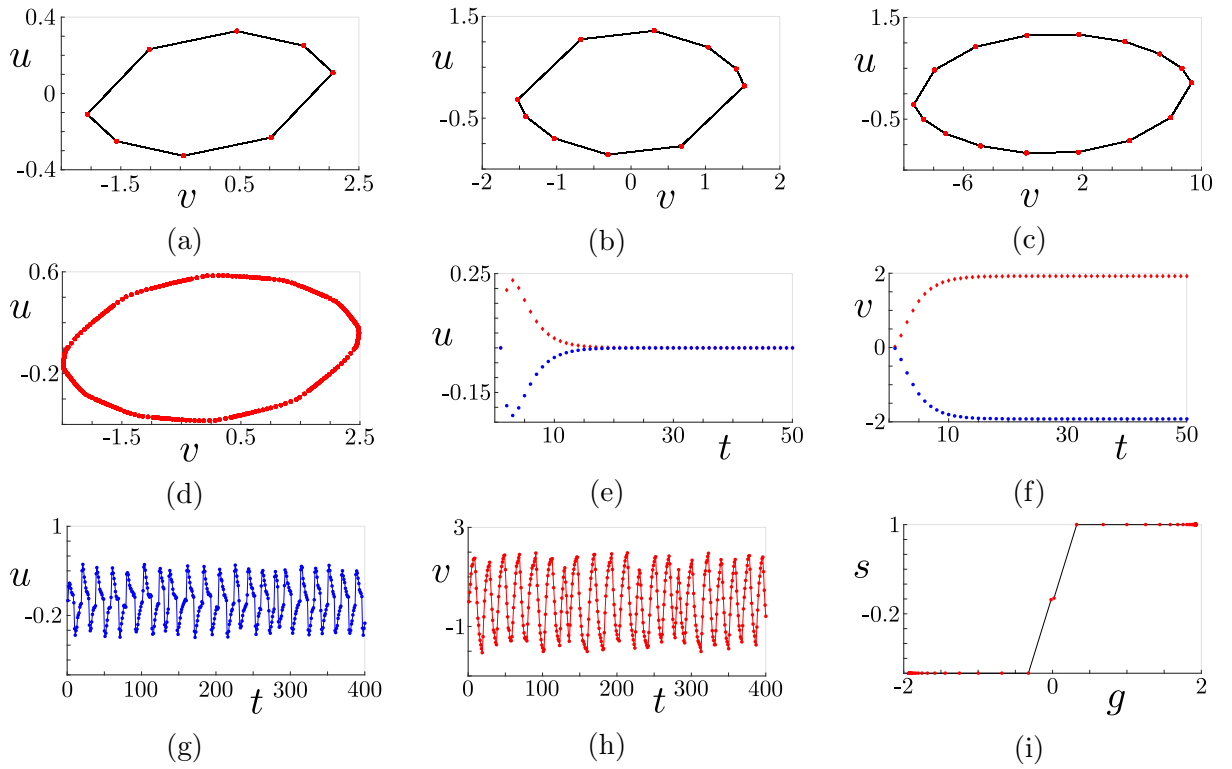


Figure 5.14. An attractor of system (5.28), (5.29) for several parameter sets. (a-c) A periodic orbit (with period 8, 10, 16, respectively) shown on the  $(u, v)$  plane for the system without noise. (d) A quasi-periodic orbit. (e,f) Time trace of  $u_t$  and  $v_t$  converging to equilibrium points of the system for trajectories with different initial points. (g,h) Time trace of  $u_t$  and  $v_t$  for trajectories of the system with noise for the same parameters as in (e,f). (i) Trajectories of (e,f) in  $(g, s)$ -space; the two equilibrium states correspond to  $s_* = \pm\sigma$ .

Figure 5.14 shows a few shapes of the attractor of system (5.28), (5.29) obtained for different sets of parameter values. The attractor belongs to  $\Omega$ . The size of the domain  $\Omega$  is

controlled by the parameter  $\sigma$  of the sticky Taylor rule (5.28). This size can be estimated using the Lyapunov function introduced in section 4.6.

## CHAPTER 6

### CONCLUSIONS

In our work, we propose and rigorously analyzed several variants of a simple macroeconomic model with sticky inflation expectations. Perhaps surprisingly, although the model is nonlinear it can be considered as a hybrid linear system and analyzed using linear tools. This led us to the analysis of dynamics of piecewise linear systems by methods of the theory of piecewise smooth systems and systems with hysteresis operators.

For such a simple model, defined via a single (and conceptually quite elementary) change from a standard one, the sticky play operator introduces surprisingly complicated, subtle yet realistic phenomena into the dynamics. Some of the more detailed conclusions of our simulations may be model-specific but, based on the mathematics presented and additional numerical simulations with more complex variants of the model, we believe at least the following two qualitative features to be generic and robust.

Firstly, the presence of an entire continuum of equilibria rather than a unique one (or even finite numbers of them as occurs in many New-Keynesian models). This causes permanence and path dependence at a deep level. It should be noted that in more sophisticated models, with more variables and more play operators, the set of possible equilibria may be extremely complicated with the possibility of ‘cascades’ where one play operator starting to drag causes others to do so (the analogy with earthquakes made in the Introduction then becomes even closer).

Secondly, the existence of different modes depending upon whether particular play operators are currently ‘stuck’ or ‘dragged’ – in our case the ‘inner’ and ‘outer’ modes. If some modes are less stable than others (in our main model the outer mode is less stable than the inner one) then a large enough shock may move the system far away from the set of equilibria that the route back to an equilibrium is both long and unpredictable. It may even move the system into an unstable regime – in this case runaway inflation – without any change in

the system parameters. Both of these features are highly significant not just because they correspond closely to actual economic events but they have implications for forecasting and policy prescriptions too.

Our choice of inflation expectations as the candidate for an initial investigation was influenced by the work of De Grauwe [29] on a different type of boundedly rational expectation formation process in a simple DSGE model. However, play operators are also a viable candidate for modeling other sticky economic variables at both the micro- and macro-economic levels. To demonstrate this, in one of the variants of the model we used one to represent sticky responses by the Central Bank.

The modeling approach presented above can also be considered as a ‘stress’ test of the usual rational expectations assumption in the underlying DSGE model. By introducing a boundedly rational ‘perturbation’ into the rationality assumptions we can test the structural stability of the original model. Or to put it another way we are also investigating the robustness of the modeling assumptions rather than just the solutions within the model. We believe that such a modeling philosophy has intrinsic merit and can provide valuable insights.

The models presented in the last chapter demonstrate that there are various ways in which this work can be extended, in particular to systems with multiple agents and multiple play operators. Although it has not been relevant to this work, play and stop operators, when combined appropriately [62] can have a remarkably simple aggregated response, even when connected via a network. This allows for (almost)-analytic solutions even when cascades and rapid transitions between states are occurring and will be the subject of future work.

## APPENDIX

### A.1 Derivation of equations (4.5) – (4.9)

Here we show how to obtain the explicit system (5.3) – (4.9) from model (4.1) – (4.3). To this end, we substitute the equation for  $w_t$  into the equation for  $u_t$  and obtain

$$(1 + ac_2)u_t = u_{t-1} - ac_1v_t + ap_t + \varepsilon_t.$$

Next, we substitute this equation into the equation for  $v_t$  and simplify to obtain

$$\vartheta v_t - \phi p_t = b_2 u_{t-1} + (1 - b_1)(1 + ac_2)v_{t-1} + b_2 \varepsilon_t + (1 + ac_2)\eta_t, \quad (\text{A.1})$$

where

$$\vartheta = 1 + ac_2 + ab_2c_1, \quad \phi = b_1(1 + ac_2) + ab_2.$$

Since  $p_t = v_t - s_t$ , equation (A.1) can be rewritten as

$$\beta v_t + s_t = f_t \quad (\text{A.2})$$

with  $\beta$  and  $f_t$  defined by (4.8), (4.9). Therefore,  $v_t = \beta^{-1}(f_t - s_t)$ , which combined with (4.8), (4.9) gives

$$v_t = \frac{b_2}{\phi\beta}u_{t-1} + \frac{(1 - b_1)(1 + ac_2)}{\phi\beta}v_{t-1} - \frac{1}{\beta}s_t + \frac{b_2}{\phi\beta}\varepsilon_t + \frac{1 + ac_2}{\phi\beta}\eta_t. \quad (\text{A.3})$$

Subsequently, substituting equation (A.3) into equation (A.1) gives

$$\begin{aligned} u_t &= \frac{ab_2(1 - c_1) + \phi\beta}{\phi\beta(1 + ac_2)}u_{t-1} + \frac{a(1 - c_1)(1 - b_1)}{\phi\beta}v_{t-1} \\ &\quad + \frac{a(c_1 - 1 - \beta)}{\beta(1 + ac_2)}s_t + \frac{\phi\beta + ab_2(1 - c_1)}{\phi\beta(1 + ac_2)}\varepsilon_t \\ &\quad + \frac{a(1 - c_1)}{\phi\beta}\eta_t \end{aligned} \quad (\text{A.4})$$

Therefore, (4.1) becomes (4.5).

## A.2 Jury's stability criterion

Jury's stability criterion is the discrete time counterpart of the Routh-Hurwitz stability criterion, which is used to test the stability of linear continuous time systems.

Given the characteristic polynomial of a linear discrete time dynamical system  $x_t = Dx_{t-1}$  of order  $n$ ,

$$P(\lambda) = a_n \lambda^n + a_{n-1} \lambda^{n-1} + \cdots + a_1 \lambda + a_0, \quad (\text{A.5})$$

where  $a_n > 0$ , define

$$b_k = \begin{vmatrix} a_0 & a_{n-k} \\ a_n & a_k \end{vmatrix}, \quad c_k = \begin{vmatrix} b_0 & b_{n-k-1} \\ b_{n-1} & b_k \end{vmatrix}, \quad d_k = \begin{vmatrix} c_0 & c_{n-k-2} \\ c_{n-2} & c_k \end{vmatrix}, \quad \cdots \quad (\text{A.6})$$

The necessary and sufficient conditions for the characteristic equation to have all the roots inside the open unit circle are given as:

1.  $P(1) > 0$ ,
2.  $(-1)^n P(-1) > 0$ ,
3.  $a_n > |a_0|$ ,
4.  $\begin{cases} |b_0| > |b_{n-1}|, \\ |c_0| > |c_{n-2}|, \\ |d_0| > |d_{n-3}|, \\ \dots \end{cases}$

Condition 4 is required only when the degree of the polynomial is  $n > 2$ .

## A.3 Proof of Lemma 4.1 (local stability analysis of system (4.1) – (4.3))

The characteristic polynomial of the matrix (4.14) in the linearization (4.13) at an equilibrium point is

$$P_B(\lambda) = \lambda^2 - \lambda \left( \frac{2 + ac_2 - b_1(1 + ac_2)}{1 + a(b_2c_1 + c_2)} \right) + \frac{1 - b_1}{1 + a(b_2c_1 + c_2)}.$$

Applying Jury's stability criterion (cf. section A.2) to the characteristic polynomial gives the following set of inequalities:

$$\begin{aligned} P_B(1) &= 1 - \frac{2 + ac_2 - b_1(1 + ac_2)}{1 + a(b_2c_1 + c_2)} + \frac{1 - b_1}{1 + a(b_2c_1 + c_2)} > 0, \\ P_B(-1) &= 1 + \frac{2 + ac_2 - b_1(1 + ac_2)}{1 + a(b_2c_1 + c_2)} + \frac{1 - b_1}{1 + a(b_2c_1 + c_2)} > 0, \\ 1 &> \frac{1 - b_1}{1 + a(b_2c_1 + c_2)}. \end{aligned}$$

It is easy to see that all the three inequalities above are satisfied for any set of parameters

$$a > 0, \quad 0 < b_1 < 1, \quad b_2 > 0, \quad c_1 > 0, \quad c_2 \geq 0,$$

hence every equilibrium state  $z_*(s_*)$  with  $|s_*| < \alpha$  is asymptotically stable.

Now, consider system (4.15) without stickiness. The characteristic polynomial of the matrix  $A$  is

$$P_A(\lambda) = \lambda^2 - \lambda \left( \frac{(1 - b_1)(2 + ac_2)}{(1 - b_1)(1 + ac_2) + ab_2(c_1 - 1)} \right) + \frac{1 - b_1}{(1 - b_1)(1 + ac_2) + ab_2(c_1 - 1)}.$$

Applying Jury's stability criterion to this characteristic polynomial gives the following set of inequalities:

$$\begin{aligned} P_A(1) &= 1 - \frac{(1 - b_1)(2 + ac_2)}{(1 - b_1)(1 + ac_2) + ab_2(c_1 - 1)} + \frac{1 - b_1}{(1 - b_1)(1 + ac_2) + ab_2(c_1 - 1)} > 0, \\ P_A(-1) &= 1 + \frac{(1 - b_1)(2 + ac_2)}{(1 - b_1)(1 + ac_2) + ab_2(c_1 - 1)} + \frac{1 - b_1}{(1 - b_1)(1 + ac_2) + ab_2(c_1 - 1)} > 0, \\ 1 &> \frac{1 - b_1}{(1 - b_1)(1 + ac_2) + ab_2(c_1 - 1)}. \end{aligned}$$

Taking into account the constraints  $0 < b_1 < 1$ ,  $a > 0$ ,  $b_2 > 0$ ,  $c_2 \geq 0$  and  $\beta > 0$ , these conditions result in the relationship

$$c_1 > 1.$$

Note that system  $z_t = Az_{t-1}$  is the linearization of sticky system (4.5) at infinity, which describes recovering of the sticky system towards near equilibrium dynamics after a large perturbation. Hence, the stability condition  $c_1 > 1$  for  $A$  agrees with the global stability criterion obtained in Section 4.4.



#### A.4 The effect of parameters on stability properties

Here we provide some numerical analysis of the effect of parameters on stability properties of the equilibrium states of system (4.1) – (4.3). Stronger stability generally means smaller volatility and longer times of persistence of a specific equilibrium. We evaluate local stability using the maximum absolute value,  $|\lambda_{i,e}|$ , of eigenvalues of the linearized system at an equilibrium point. This means that we evaluate stability to relatively small noise. The subscripts  $e$  and  $i$  refer to the system without stickiness ( $\alpha = 0$ ) and with stickiness ( $\alpha = 1$ ), respectively.

The model contains five parameters,  $a$ ,  $b_1$ ,  $b_2$ ,  $c_1$  and  $c_2$ . Figure A.1 showing the dependence of  $|\lambda_{i,e}|$  on the parameter  $a$  implies that the system with stickiness is more stable than the system without stickiness. Other parameter values are taken from Table 4.1. Interestingly, system with stickiness becomes more stable with increasing  $a$ , while this dependence for the non-sticky system is non-monotone since  $|\lambda_e|$  has a minimum at  $a \approx 0.8$ .

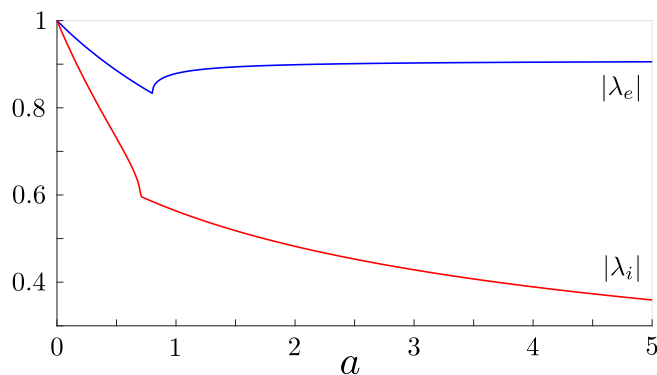


Figure A.1. Variation of  $|\lambda_i|$  and  $|\lambda_e|$  with  $a$ . Other parameters are taken from Table 4.1.

The range of output gap equilibrium values is proportional to the ratio of parameters  $b_1$  and  $b_2$  according to (4.12). Figure A.2 presents the dependence of  $|\lambda_{i,e}|$  on these parameters. System with stickiness is more stable than its non-sticky counterpart for  $b_1 < 0.9$ , but becomes less stable than the non-sticky system as  $b_1$  approaches 1 (in the latter case, the future inflation rate is defined predominantly by expectations). The dependence of  $|\lambda_{i,e}|$  on

$b_2$  and the dependence of  $|\lambda_e|$  on  $b_1$  is monotone (stronger stability for larger  $b_{1,2}$ ), while the dependence of  $|\lambda_i|$  on  $b_2$  is non-monotone. The strongest stability is achieved by the sticky system for some intermediate value of  $b_1$  between 0 and 1.

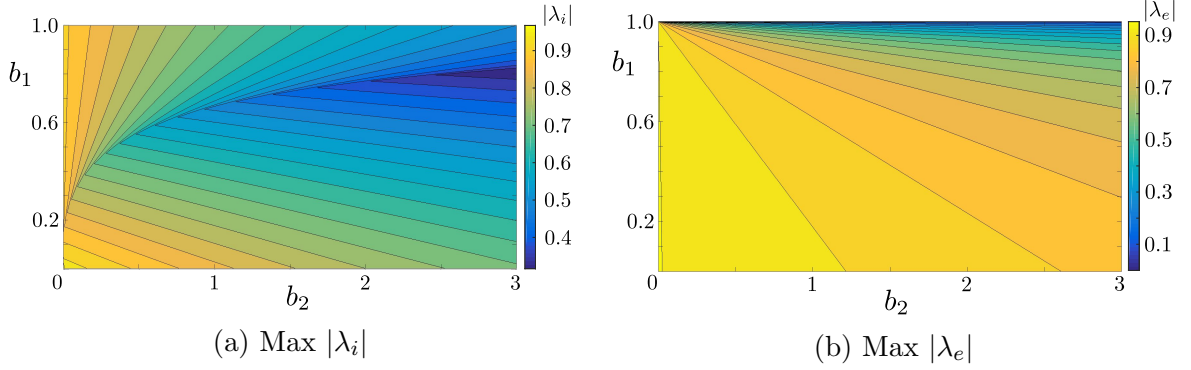


Figure A.2. Dependence of  $|\lambda_i|$  and  $|\lambda_e|$  on  $b_1, b_2$ . Other parameters are taken from Table 4.1.

Parameters  $c_1$  and  $c_2$  control the range of inflation rate equilibrium values according to (4.12). This range contracts when  $c_1$  increases (for  $c_1 > 1$ ) and expands when  $c_2$  increases. Figure A.3 shows that the sticky system is generally more stable than the non-sticky one. Both systems become more stable with increasing  $c_1$  (stronger inflation targeting in Taylor's rule), see Figures A.3 and A.4. The dependence of  $|\lambda_i|$  on  $c_2$  demonstrates some slight non-monotonicity for large  $c_2$  values, see Figure A.4(b). The non-monotonicity of  $|\lambda_i|$  with  $c_2$  is much more pronounced with the minimum achieved for a certain value of  $c_2$  depending on  $c_1$ , see Figures A.3(b) and A.4(b). This minimum corresponds to strongest stability and, in this sense, optimizes the Central Bank policy. In Figure A.3(b), the strongest stability is achieved on the 'parabolic' line.

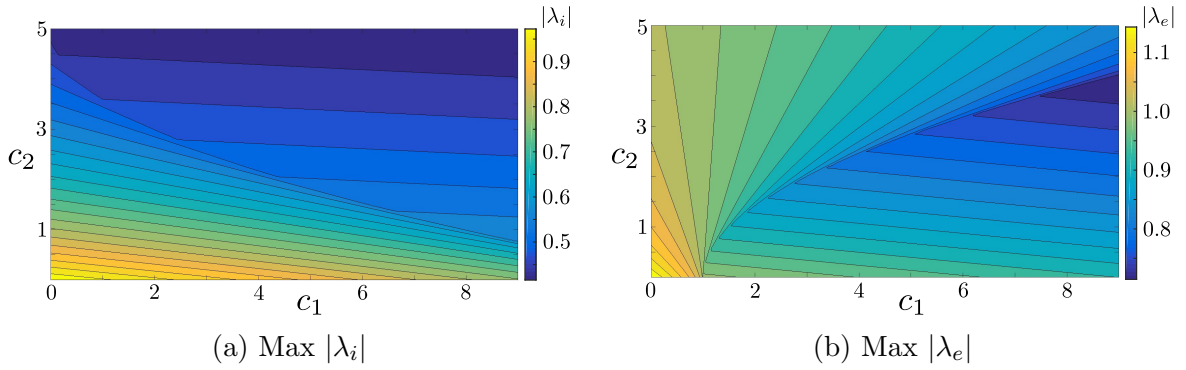
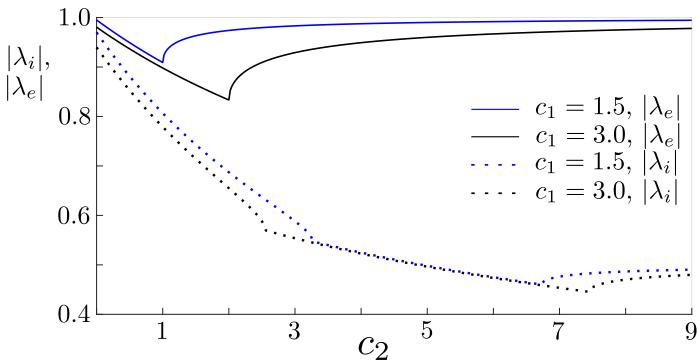
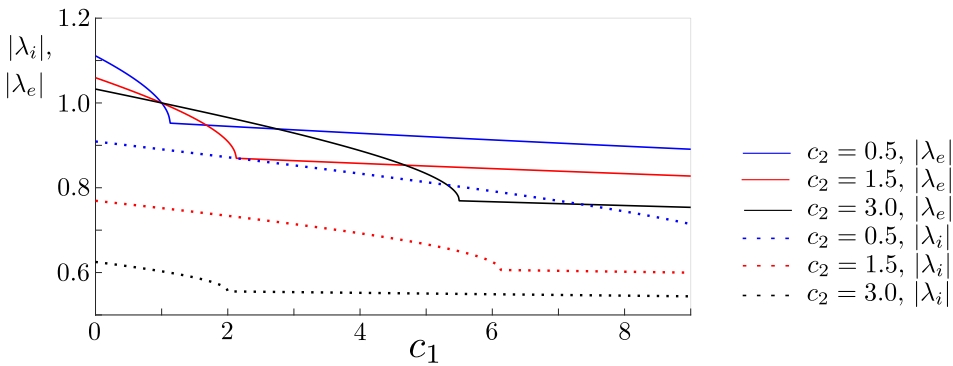


Figure A.3. Dependence of  $|\lambda_i|$  and  $|\lambda_e|$  on  $c_1$  and  $c_2$ . Other parameters are taken from Table 4.1.



(a) Various  $c_2$  values.



(b) Various  $c_1$  values.

Figure A.4. Cross sections of the plots shown in Figure A.3 for various  $c_1$  and (b)  $c_2$  values.

## A.5 Derivations of the explicit form for model (5.1), (5.2)

Finally, we show how to obtain equation (5.3) from model (5.1), (5.2). To this end, we substitute the equation for  $w_t$  into the equation for  $u_t$  and obtain

$$(1 + ac_2)u_t = ap_t - ac_1v_t + u_{t-1} - ac_3w_{t-1} + ac_1v^* - a\zeta_t + \varepsilon_t.$$

Next, we substitute the resulting equation into the equation for  $v_t$  and simplify to obtain

$$\begin{aligned} \vartheta v_t + \phi p_t &= b_2u_{t-1} + (1 - b_1)(1 + a_2c_2)v_{t-1} - ab_2c_3w_{t-1} \\ &+ ab_2c_1v^* + b_2\varepsilon_t + (1 + ac_2)\eta_t - ab_2\zeta_t, \end{aligned} \quad (\text{A.7})$$

where

$$\vartheta = 1 + ac_2 + ab_2c_1, \quad \phi = b_1(1 + ac_2) + ab_2.$$

Using  $p_t = v_t - s_t$ , (A.7) becomes

$$\beta v_t + s_t = f_t. \quad (\text{A.8})$$

with  $\beta$  and  $f_t$  defined by (5.6) and (5.7), respectively, for  $v^* = 0$ . Further, from equation (A.8), we obtain

$$\begin{aligned} v_t &= \frac{b_2}{\Delta}u_{t-1} + \frac{(1 - b_1)(1 + ac_2)}{\Delta}v_{t-1} - \frac{ab_2c_3}{\Delta}w_{t-1} - \frac{ab_2 + b_1(1 + ac_2)}{\Delta}s_t \\ &+ \frac{b_2}{\Delta}\varepsilon_t + \frac{1 + ac_2}{\Delta}\eta_t - \frac{ab_2}{\Delta}\zeta_t, \end{aligned} \quad (\text{A.9})$$

where  $\Delta = (1 - b_1)(1 + ac_2) + ab_2(c_1 - 1)$

Substituting  $w_t$  into the equation for  $u_t$  in (5.1) gives

$$(1 + ac_2)u_t = u_{t-1} - ac_1v_t - ac_3w_{t-1} - a\zeta_t + ap_t + \varepsilon_t.$$

Substituting equation (A.9) into this equation results in

$$\begin{aligned} u_t &= \frac{1 - b_1}{\Delta}u_{t-1} + \frac{a(1 - b_1)(1 - c_1)}{\Delta}v_{t-1} + \frac{a(b_1 - 1)c_3}{\Delta}w_{t-1} + \frac{a(b_1c_1 - 1)}{\Delta}s_t \\ &+ \frac{1 - b_1}{\Delta}\varepsilon_t + \frac{a(1 - c_1)}{\Delta}\eta_t + \frac{a(b_1 - 1)}{\Delta}\zeta_t. \end{aligned} \quad (\text{A.10})$$

Finally, substituting (A.9) and (A.10) into the equation for  $w_t$  in (5.1) gives

$$\begin{aligned}
w_t = & \frac{(1-b_1)c_2 + b_2c_1}{\Delta}u_{t-1} + \frac{(1-b_1)(c_1 + ac_2)}{\Delta}v_{t-1} + \frac{(1-b_1-ab_2)c_3}{\Delta}w_{t-1} \\
& - \frac{(b_1 + ab_2)c_1 + ac_2}{\Delta}s_t + \frac{(1-b_1)c_2 + b_2c_1}{\Delta}\varepsilon_t + \frac{c_1 + ac_2}{\Delta}\eta_t \\
& + \frac{1-b_1-ab_2}{\Delta}\zeta_t.
\end{aligned} \tag{A.11}$$

Therefore system (5.1), (5.2) is equivalent to (5.3) – (5.7).

### A.6 Derivations of the explicit form for system (5.28), (5.29)

In order to convert system (5.28), (5.29) with sticky Central Bank response to the explicit form, we replace the variable  $u_t$  with the variable  $g_t = c_1v_t + c_2u_t$  and obtain

$$g_t = (c_1 + ac_2)v_t + g_{t-1} - c_1v_{t-1} - ac_2\mathcal{P}_\sigma[g_t] + c_2\varepsilon_t, \tag{A.12}$$

$$v_t = \frac{c_2(1-b_1)}{b_2c_1 + c_2(1-b_1)}v_{t-1} + \frac{b_2}{b_2c_1 + c_2(1-b_1)}g_t + \frac{c_2(1-b_1)}{b_2c_1 + c_2(1-b_1)}\eta_t. \tag{A.13}$$

Furthermore, substituting (A.13) into (A.12) gives

$$\rho g_t + \kappa\mathcal{P}_\sigma[g_t] = f_t \tag{A.14}$$

with

$$\begin{aligned}
\rho &= \frac{c_2(1-b_1-ab_2)}{b_2c_1 + c_2(1-b_1)}, & \kappa &= ac_2, \\
f_t &= g_{t-1} - c_1v_{t-1} + \frac{c_2(1-b_1)(c_1 + ac_2)}{b_2c_1 + c_2(1-b_1)}(v_{t-1} + \eta_t) + c_2\varepsilon_t.
\end{aligned}$$

Using the fact that  $\rho > 0$  due to (5.30), we can invert (A.14) to obtain

$$g_t = \frac{1}{\rho} \left( f_t - \frac{\kappa}{\rho + \kappa} \mathcal{P}_{\rho\sigma}[f_t] \right).$$

This equation together with (A.13) define the explicit system for (5.28), (5.29).

## REFERENCES

- [1] Adjemian, S., H. Bastani, M. Juillard, F. Mihoubi, G. Perendia, M. Ratto, and S. Villemot (2011). Dynare: Reference manual, version 4. Technical report, Dynare Working Paper.
- [2] Al-Bender, F., W. Symens, J. Swevers, and H. Van Brussel (2004). Theoretical analysis of the dynamic behavior of hysteresis elements in mechanical systems. *International Journal of Non-Linear Mechanics* 39(10), 1721–1735.
- [3] Al Janaideh, M. and P. Krejčí (2011). An inversion formula for a prandtl–ishlinskii operator with time dependent thresholds. *Physica B: Condensed Matter* 406(8), 1528–1532.
- [4] Al Janaideh, M. and P. Krejčí (2013). Inverse rate-dependent prandtl–ishlinskii model for feedforward compensation of hysteresis in a piezomicropositioning actuator. *IEEE/ASME Transactions on mechatronics* 18(5), 1498–1507.
- [5] Aljanaideh, O. (2009). *A stop operator-based prandtl-ishlinskii model for compensation of smart actuator hysteresis effects*. Ph. D. thesis, Concordia University.
- [6] Amable, B., J. Henry, F. Lordon, and R. Topol (1995). Weak and strong hysteresis: an application to foreign trade. *ECONOMIC NOTES-SIENA-*, 353–374.
- [7] Anderson, S. P., A. De Palma, J.-F. Thisse, and C. F. Manski (1993). Discrete choice theory of product differentiation. *Journal of Economic Literature* 31(4), 1972.
- [8] Arnold, M., N. Begun, P. Gurevich, E. Kwame, H. Lamba, and D. Rachinskii (2017). Dynamics of discrete time systems with a hysteresis stop operator. *SIAM Journal on Applied Dynamical Systems* 16(1), 91–119.
- [9] Ball, L. (2009). Hysteresis in unemployment: Old and new evidence. *The National Bureau of Economic Research Working Paper* 14818, 1–35.
- [10] Belke, A., M. Göcke, and M. Günther (2012). Exchange rate bands of inaction and play-hysteresis in German exports-sectoral evidence for some OECD destinations. *Metroeconomica* 64(1), 152–179.
- [11] Bernardo, M., C. Budd, A. R. Champneys, and P. Kowalczyk (2008). *Piecewise-smooth dynamical systems: theory and applications*, Volume 163. Springer Science & Business Media.
- [12] Bick, A. (2010). Threshold effects of inflation on economic growth in developing countries. *Economics Letters* 108(2), 126–129.

- [13] Brock, W. A. and C. H. Hommes (1997). A rational route to randomness. *Econometrica: Journal of the Econometric Society*, 1059–1095.
- [14] Brokate, M., C. Carstensen, and J. Valdman (2004). A quasi-static boundary value problem in multi-surface elastoplasticity: Part 1—analysis. *Mathematical Methods in the Applied Sciences* 27, 1697–1710.
- [15] Brokate, M., A. V. Pokrovskii, D. Rachinskii, and O. Rasskazov (2006). Differential equations with hysteresis via a canonical example. In I. Mayergoyz and G. Bertotti (Eds.), *The Science of Hysteresis*, Volume 1, pp. 125–291. Elsevier, Academic Press.
- [16] Brokate, M. and J. Sprekels (1996). *Hysteresis and Phase Transitions*. Springer Series in Computational Mathematics. Springer Berlin Heidelberg.
- [17] Calvo, G. A. (1983). Staggered prices in a utility-maximizing framework. *Journal of monetary Economics* 12(3), 383–398.
- [18] Carlstrom, C. T., T. S. Fuerst, and M. Paustian (2015). Inflation and output in new keynesian models with a transient interest rate peg. *Journal of Monetary Economics* 76, 230–243.
- [19] Christiano, L. J., M. Trabandt, and K. Walentin (2010). Dsge models for monetary policy analysis. Technical report, National Bureau of Economic Research.
- [20] Colander, D., P. Howitt, A. Kirman, A. Leijonhufvud, and P. Mehrling (2008). Beyond DSGE models: toward an empirically based macroeconomics. *The American Economic Review* 98(2), 236–240.
- [21] Cross, R. (2014). Unemployment: natural rate epicycles or hysteresis? *European Journal of Economics and Economic Policies: Intervention* 11(2), 136–148.
- [22] Cross, R., M. Grinfeld, H. Lamba, and T. Seaman (2007). Stylized facts from a threshold-based heterogeneous agent model. *The European Phys. Journal B* 57, 213–218.
- [23] Cross, R., H. McNamara, L. Kalachev, and A. Pokrovskii (2013). Hysteresis and post walrasian economics. *Discrete and Continuous Dynamical Systems B* 18, 377–401.
- [24] Cross, R., H. McNamara, A. Pokrovskii, and D. Rachinskii (2008). A new paradigm for modelling hysteresis in macroeconomic flows. *Physica B* 403, 231–236.
- [25] Cross, R., H. McNamara, and A. V. Pokrovskii (2012). Memory of recessions. *Journal of Post Keynesian Economics* 34(3), 413–430.

- [26] Darby, J., R. Cross, and L. Piscitelli (2005). Hysteresis and unemployment: A preliminary investigation. In G. Bertotti and I. Mayergoyz (Eds.), *The Science of Hysteresis*, Volume Chapter 8, pp. 667–698. Elsevier.
- [27] Davino, D., P. Krejčí, A. Pimenov, D. Rachinskii, and C. Visone (2016). Analysis of an operator-differential model for magnetostrictive energy harvesting. *Communications in Nonlinear Science and Numerical Simulation* 39, 504–519.
- [28] Davino, D., P. Krejčí, and C. Visone (2013). Fully coupled modeling of magnetomechanical hysteresis through ‘thermodynamic’ compatibility. *Smart Mater. Structures* 22, 095009.
- [29] De Grauwe, P. (2012). Booms and busts in economic activity: A behavioral explanation. *Journal of Economic Behavior & Organization* 83(3), 484–501.
- [30] Driscoll, J. C. and S. Holden (2014). Behavioral economics and macroeconomic models. *Journal of Macroeconomics* 41, 133–147.
- [31] Edge, R. M., M. T. Kiley, and J.-P. Laforte (2010). A comparison of forecast performance between federal reserve staff forecasts, simple reduced-form models, and a dsge model. *Journal of Applied Econometrics* 25(4), 720–754.
- [32] Eleuteri, M., J. Kopfova, and P. Krejčí(2015). A new phase field model for material fatigue in an oscillating elastoplastic beam. *Discrete and Continuous Dynamical Systems A* 35(6), 2465–2495.
- [33] Ewing, J. A. (1885). Experimental research in magnetism. *Philos. Trans. R. Soc. of London* 176, 523–640.
- [34] Fisher, I. (2006). *Mathematical investigations in the theory of value and prices, and appreciation and interest*. Cosimo, Inc.
- [35] Fournier-Prunaret, D., P. Chargé, and L. Gardini (2011). Border collision bifurcations and chaotic sets in a two-dimensional piecewise linear map. *Communications in Nonlinear Science and Numerical Simulation* 16(2), 916–927.
- [36] Francu, J. (2001). Homogenization of diffusion equation with scalar hysteresis operator. *Mathematica Bohemica* 126(2), 363–377.
- [37] Fränzle, M. (1999). Analysis of hybrid systems: An ounce of realism can save an infinity of states. In *Computer Science Logic*, pp. 126–139. Springer.
- [38] Friedman, G., S. McCarthy, and D. Rachinskii (2014). Hysteresis can grant fitness in stochastically varying environment. *PLoS ONE* 9(7), e103241.



- [39] Frimpong, J. M. and E. F. Oteng-Abayie (2010). When is inflation harmful? estimating the threshold effect for Ghana. *American Journal of Economics and Business Administration* 2(3), 232.
- [40] Gandolfo, G. (1997). *Economic dynamics: study edition*. Springer Science & Business Media.
- [41] Gardini, L., D. Fournier-Prunaret, and P. Chargé (2011). Border collision bifurcations in a two-dimensional piecewise smooth map from a simple switching circuit. *Chaos: An Interdisciplinary Journal of Nonlinear Science* 21(2), 023106.
- [42] Gills, B. K. (2013). *Globalization in crisis*. Routledge.
- [43] Göcke, M. and L. Werner (2015). Play hysteresis in supply or in demand as part of a market model. *Metroeconomica* 66(2), 339–374.
- [44] Goldin, C. D. and F. D. Lewis (1975). The economic cost of the american civil war: Estimates and implications. *The Journal of Economic History* 35(02), 299–326.
- [45] Grinfeld, M., R. Cross, and H. Lamba (2009). Hysteresis and economics-taking the economic past into account. *IEEE Control Systems* 29(1), 30–43.
- [46] Gu, G.-Y., L.-M. Zhu, and C.-Y. Su (2014). Modeling and compensation of asymmetric hysteresis nonlinearity for piezoceramic actuators with a modified prandtl–ishlinskii model. *IEEE Transactions on Industrial Electronics* 61(3), 1583–1595.
- [47] Gurevich, P. and D. Rachinskii (2015). Pattern formation in parabolic equations containing hysteresis with diffusive thresholds. *J. Math. Anal. Appl.* 424(2), 1103–1124.
- [48] Gurevich, P. and D. Rachinskii (2016). Asymptotics of sign-changing patterns in hysteretic systems with diffusive thresholds. *Asymptotic Analysis* 96(1), 1–22.
- [49] Harris, R. S. (2005). Pressure-volume curves of the respiratory system. *Respiratory care* 50(1), 78–99.
- [50] Hiskens, I. A. and M. A. Pai (2000). Trajectory sensitivity analysis of hybrid systems. *IEEE Transactions on Circuits and Systems I: Fundamental Theory and Applications* 47(2), 204–220.
- [51] Hoppensteadt, F. and W. Jäger (1980). Pattern formation by bacteria. In *Biological growth and spread*, pp. 68–81. Springer.
- [52] Ishlinskii, A. Y. (1944). Some applications of statistical methods to describing deformations of bodies. *Izv AN SSSR Techn Ser* 9, 583–590.

- [53] Kaldor, N. (1972). The Irrelevance of Equilibrium Economics. *The Economic Journal* 82(4), 1237–55.
- [54] Kaltenbacher, B. and P. Krejčí (2016). A thermodynamically consistent phenomenological model for ferroelectric and ferroelastic hysteresis. *ZAMM· Z. Angew. Math. Mech* 96(7), 874–891.
- [55] Keen, B. D. (2009). Output, inflation, and interest rates in an estimated optimizing model of monetary policy. *Review of Economic Dynamics* 12(2), 327–343.
- [56] Khan, M. and A. S. Senhadji (2001). Threshold effects in the relationship between inflation and growth. *IMF Staff Papers* 48(1), 1–21.
- [57] Kopfova, J. (2006). Hysteresis in biological models. In *Journal of Physics: Conference Series*, Volume 55, pp. 130–134. IOP Publishing.
- [58] Krasnosel’skii, M. A. and A. V. Pokrovskii (1989). *Systems with Hysteresis*. Springer.
- [59] Krejčí, P. (1996). *Hysteresis, Convexity and Dissipation in Hyperbolic Equations*. GAKUTO International series. Gattōtoscho.
- [60] Krejčí, P., J. OKane, A. Pokrovskii, and D. Rachinskii (2012). Properties of solutions to a class of differential models incorporating preisach hysteresis operator. *Physica D: Nonlinear Phenomena* 241(22), 2010–2028.
- [61] Krejčí, P. and V. Recupero (2014). Bv solutions of rate independent differential inclusions. *Mathematica Bohemica* 139(4), 607–619.
- [62] Krejčí, P., H. Lamba, S. Melnik, and D. Rachinskii (2014). Analytical solutions for a class of network dynamics with mechanical and financial applications. *Phys. Rev. E* 90, 032822.
- [63] Krejčí, P., H. Lamba, S. Melnik, and D. Rachinskii (2015). Kurzweil integral representation of interacting prandtl-ishlinskii operators. *Discrete and Continuous Dynamical Systems B* 20(9), 2949–2965.
- [64] Krejčí, P. and J. Sprekels (2007). Elastic-ideally plastic beams and prandtl-ishlinskii hysteresis operators. *Math. Meth. Appl. Sci.* 30, 2371–2393.
- [65] Kremer, S., A. Bick, and D. Nautz (2013). Inflation and growth: new evidence from a dynamic panel threshold analysis. *Empirical Economics* 44(2), 861–878.
- [66] Kuhnen, K. (2003). Modeling, identification and compensation of complex hysteretic nonlinearities. a modified prandtl-ishlinskii approach. *European Journal of Control* 9, 407–418.

- [67] Kunze, M. and M. D. P. M. Marques (2000). An introduction to moreau sweeping process. In B. Brogliato (Ed.), *Impacts in Mechanical Systems. Analysis and Modelling*, pp. 1–60. Springer.
- [68] Lamba, H. (2010). A queueing theory description of fat-tailed price returns in imperfect financial markets. *Eur. Phys. J. B* 77, 297–304.
- [69] Lamba, H. (2014). Implausible equilibrium solutions in economics and finance. Available at SSRN 2408013.
- [70] Lamba, H. and T. Seaman (2008). Market statistics of a psychology-based heterogeneous agent model. *Int. J. of Theoretical and Applied Finance* 11, 717–737.
- [71] Mankiw, N. G. (2006). The macroeconomist as scientist and engineer. *The Journal of Economic Perspectives* 20(4), 29–46.
- [72] Mankiw, N. G. (2010). *Macroeconomics* (Seventh ed.). Worth Publishers.
- [73] Mankiw, N. G. and R. Reis (2002, nov). Sticky information versus sticky prices: A proposal to replace the new keynesian phillips curve. *The Quarterly Journal of Economics* 117(4), 1295–1328.
- [74] Mayergoyz, I. (2003). *Mathematical Models of Hysteresis and Their Applications*. Elsevier.
- [75] Mielke, A. (2012). Generalized prandtl–ishlinskii operators arising from homogenization and dimension reduction. *Physica B: Condensed Matter* 407(9), 1330–1335.
- [76] Mirowski, P. (1991). *More heat than light: Economics as social physics, physics as nature’s economics*. Cambridge University Press.
- [77] Moreau, J. (2011). On unilateral constraints, friction and plasticity. In G. Capriz and G. Stampacchia (Eds.), *New Variational Techniques in Mathematical Physics, Lectures given at a Summer School of the Centro Internazionale Matematico Estivo (C.I.M.E.) held in Bressanone (Bolzano), Italy, June 17-26, 1973*, pp. 171–322. Springer.
- [78] Moreau, J. J. (1977). Evolution problem associated with a moving convex set in a hilbert space. *Journal of differential equations* 26(3), 347–374.
- [79] Muth, J. (1961). Rational expectations and the theory of price movements. *Econometrica* 6.
- [80] Nicollin, X., A. Olivero, J. Sifakis, and S. Yovine (1993). An approach to the description and analysis of hybrid systems. *Hybrid Systems*, 149–178.

- [81] Noori, H. R. (2014). *Hysteresis phenomena in biology*. Springer.
- [82] Phillips, A. W. (1950). *Mechanical models in economic dynamics*. London School of Economics and Political Science.
- [83] Pimenov, A., T. C. Kelly, A. Korobeinikov, M. J. O’Callaghan, and D. Rachinskii (2016). Memory and adaptive behavior in population dynamics: anti-predator behavior as a case study. *Journal of Mathematical Biology*, 1–27.
- [84] Pimenov, A., T. C. Kelly, A. Korobeinikov, M. J. A. O’Callaghan, A. Pokrovskii, and D. Rachinskii (2012). Memory effects in population dynamics: spread of infectious disease as a case study. *Mathematical Modelling of Natural Phenomena* 7, 1–30.
- [85] Platzer, A. (2010). *Logical analysis of hybrid systems: proving theorems for complex dynamics*. Springer Science & Business Media.
- [86] Prandtl, L. (1928). Ein gedankenmodell zur kinetischen theorie der festen krper. *Journal of Applied Mathematics and Mechanics* 8, 85106.
- [87] Preisach, F. (1935). Über die magnetische nachwirkung. *Zeitschrift für Physik A Hadrons and Nuclei* 94(5), 277–302.
- [88] Åström, K. J. (1995). Oscillations in systems with relay feedback. In K. J. Åström, G. C. Goodwin, and P. R. Kumar (Eds.), *Adaptive Control, Filtering, and Signal Processing*, Volume 74 of *The IMA Volumes in Mathematics and its Applications*, pp. 1–25. Springer New York.
- [89] Rios, L. A., D. Rachinskii, and R. Cross (2017a). A model of hysteresis arising from social interaction within a firm. In *Journal of Physics: Conference Series*, Volume 811, pp. 012011. IOP Publishing.
- [90] Rios, L. A., D. Rachinskii, and R. Cross (2017b). On the rationale for hysteresis in economic decisions. In *Journal of Physics: Conference Series*, Volume 811, pp. 012012. IOP Publishing.
- [91] Rizos, D. D. and Fassois, S. D. (2009). Friction identification based upon the lugre and maxwell slip models. *IEEE Transactions on control systems technology* 17(1), 153–160.
- [92] Robinson, J. (1974). History versus equilibrium. *Indian Economic Journal* 21(3), 202.
- [93] Ruderman, M. (2015). Presliding hysteresis damping of lugre and maxwell-slip friction models. *Mechatronics* 30, 225–230.

- [94] Ruderman, M., F. Hoffmann, and T. Bertram (2009). Modeling and identification of elastic robot joints with hysteresis and backlash. *IEEE Trans. on Industrial Electronics* 56, 3840–3847.
- [95] Ruderman, M. and D. Rachinskii (2017). Use of prandtl-ishlinskii hysteresis operators for coulomb friction modeling with presliding. *Journal of Physics: Conference Series* 811(1), 012013.
- [96] Rychlik, I. (1987). A new definition of the rainflow cycle counting method. *International Journal of Fatigue* 9(2), 119–121.
- [97] Salje, E. K. H. and K. A. Dahmen (2014). Crackling noise in disordered materials. *Annu. Rev. Condens. Matter Phys.* 5(1), 233–254.
- [98] Sayyaadi, H. and M. R. Zakerzadeh (2012). Position control of shape memory alloy actuator based on the generalized prandtl–ishlinskii inverse model. *Mechatronics* 22(7), 945–957.
- [99] Sbordone, A. M., A. Tambalotti, K. Rao, and W. K. (2010). Policy analysis using dsge models: An introduction. *Economic policy review* 16(2), 23–43.
- [100] Schelling, T. C. (1971). Dynamic models of segregation. *Journal of mathematical sociology* 1(2), 143–186.
- [101] Sethna, J. P., K. Dahmen, S. Kartha, J. A. Krumhansl, B. W. Roberts, and J. D. Shore (1993). Hysteresis and hierarchies: Dynamics of disorder-driven first-order phase transformations. *Phys. Rev. Lett.* 70, 3347–3350.
- [102] Sethna, J. P., K. A. Dahmen, and O. Perkovic (2005). Random-field ising models of hysteresis. In G. Bertotti and I. Mayergoyz (Eds.), *The Science of Hysteresis*, Volume 2, pp. 107–168. Elsevier.
- [103] Setterfield, M. (1997). Should economists dispense with the notion of equilibrium? *Journal of post Keynesian economics* 20(1), 47–76.
- [104] Simpson, D. J. W. and J. D. Meiss (2008). Neimark–sacker bifurcations in planar, piecewise-smooth, continuous maps. *SIAM Journal on Applied Dynamical Systems* 7(3), 795–824.
- [105] Sushko, I. and L. Gardini (2008). Center bifurcation for two-dimensional border-collision normal form. *International Journal of Bifurcation and Chaos* 18(04), 1029–1050.
- [106] Sushko, I. and L. Gardini (2010). Degenerate bifurcations and border collisions in piecewise smooth 1d and 2d maps. *International Journal of Bifurcation and Chaos* 20(07), 2045–2070.

- [107] Taylor, J. B. (1994). The inflation-output variability trade-off revisited. *Federal Reserve Bank of Boston Conference Series 38*, 21–38.
- [108] Torres, J. L. (2015). *Introduction to Dynamic Macroeconomic General Equilibrium Models* (Second ed.). Vernon Art & Science, Incorporated.
- [109] Vinayagathan, T. (2013). Inflation and economic growth: A dynamic panel threshold analysis for asian economies. *Journal of Asian Economics 26*, 31–41.
- [110] Visintin, A. (1994). *Differential Models of Hysteresis*. Springer.
- [111] Visintin, A. (1996). Mathematical models of hysteresis. In *Modelling and Optimization of Distributed Parameter Systems Applications to engineering*, pp. 71–80. Springer.
- [112] Visintin, A. (2005). Mathematical models of hysteresis. In G. Bertotti and I. Mayergoyz (Eds.), *The Science of Hysteresis*, Volume Chapter 1, pp. 1–123. Elsevier.

## CURRICULUM VITAE

# Eyram Kwame

August 1, 2017

### Contact Information:

Department of Mathematical Sciences      Email: [eyram.kwame@utdallas.edu](mailto:eyram.kwame@utdallas.edu)  
The University of Texas at Dallas  
800 W. Campbell Rd.  
Richardson, TX 75080-3021, U.S.A.

### Educational History:

PhD, Mathematics, The University of Texas at Dallas,  
Richardson, Texas, U.S.A., 2017

*Dynamics of macroeconomics models with hysteresis operators*  
PhD Dissertation

Mathematical Sciences Department, The University of Texas at Dallas  
Advisor: Prof. Dmitrii Rachinskii

MS, Industrial and Environmental Modelling, University of Bristol,  
Bristol, UK, 2005

*Modelling Micro-Electro Mechanical Systems (MEMS) power generator*  
Masters Degree Thesis

Department of Mathematics, University of Bristol  
Advisor: Prof. Alan Champneys

BS, Mathematics, Kwame Nkrumah University of Science and Technology (KNUST),  
Kumasi, Ghana, 2003

### Employment History:

Teaching Assistant, The University of Texas at Dallas, January 2014 – August 2017  
Lecturer, Regional Maritime University, Accra, Ghana, July 2006 – August 2012

### Professional Memberships:

Society of Industrial and Applied Mathematics (SIAM), 2012–present  
American Mathematical Society (AMS), 2012–present